

DNA-GRAFTED SUPRAMOLECULAR POLYMERS: DESIGN, SYNTHESIS,
SELF-ASSEMBLY AND POTENTIAL APPLICATIONS

Inauguraldissertation
der Philosophisch-naturwissenschaftlichen Fakultät
der Universität Bern

vorgelegt von
Yuliia Vyborna
von der Ukraine

Leiter der Arbeit
Prof. Dr. Robert Häner
Department Chemie und Biochemie der Universität Bern

DNA-GRAFTED SUPRAMOLECULAR POLYMERS: DESIGN, SYNTHESIS,
SELF-ASSEMBLY AND POTENTIAL APPLICATIONS

Inauguraldissertation
der Philosophisch-naturwissenschaftlichen Fakultät
der Universität Bern

vorgelegt von
Yulia Vyborna
von der Ukraine

Leiter der Arbeit
Prof. Dr. Robert Häner
Department Chemie und Biochemie der Universität Bern

von der Philosophisch-naturwissenschaftlichen Fakultät angenommen

Bern, February 09, 2018

Der Dekan:
Prof. Dr. G. Colangelo

ACKNOWLEDGEMENTS

After four challenging years of hard work, I am finishing the most interesting part of my research work that I described in this thesis. On this occasion, I would like to emphasize that the completion of this work could only be possible thanks to the direct or indirect involvement of many former and current colleagues.

With sincere and utmost appreciation I would like to thank my supervisor Prof. Dr. Robert Häner. You gave me a lot of confidence, inspiration and space for creative ideas. I learned many things from you about chemistry, writing good papers and choosing a scientific strategy. Finally, I want to thank you for your help in my orientation to the next step and wish all success in new projects.

Also, I would like to thank all current and former members of Häner's group. It was a pleasure to work with you and to learn from you.

I would like to thank the esteemed members of my defense committee. Thank you for reading my manuscript and making the journey to Bern for my defense.

It takes a lot of effort to keep a research department running, and therefore I would like to thank all highly capable staff members of the Department of Chemistry and Biochemistry of the University of Bern.

My deepest appreciation belongs to my family who put their faith in me, supported and encouraged to learn and to do better.

TABLE OF CONTENTS

Table of Contents	
CHAPTER 1. General Introduction	3
1.1 Supramolecular polymers	3
1.2 DNA-based supramolecular self-assemblies	9
1.2.1 DNA in modern nanotechnology	9
1.2.2 DNA as a scaffold for the arrangement of synthetic molecules.....	13
1.2.3 Synthetic molecules as scaffolds for DNA arrangement.....	15
1.3 Aim of the study	23
CHAPTER 2. DNA-Grafted Supramolecular Polymers – Helical Ribbon Structures Formed by Self-Assembly of Pyrene-DNA Chimeric Oligomers...	25
2.1 Introduction.....	26
2.2 Results and discussions	27
2.2.1 DNA-pyrene conjugates based on 1,6-modified pentynyl pyrene..	27
2.2.2 DNA-pyrene conjugates based on 2,7-modified pentynyl pyrene..	49
2.3 Conclusions.....	53
2.4 Experimental section	53
CHAPTER 3. Pathway diversity in the self-assembly of DNA-grafted supramolecular polymers	59
3.1 Introduction.....	60
3.2 Results and discussions	61
3.3 Conclusions.....	68
3.4 Experimental section	68
CHAPTER 4. From Ribbons to Networks: Hierarchical Organization of DNA-Grafted Supramolecular Polymers	71
4.1 Introduction.....	72
4.2 Results and discussions	72
4.2.1 Effect of AT base pairs on the self-assembly via blunt-ended interactions	80

4.2.2 Effect of nucleobase mismatches on the formation of the networks	82
4.2.3 Effect of Py7b10/a10 ratio on the hierarchical organization.	84
4.2.4 Reversibility of networks upon addition of b10 (separator strand)..	86
4.2.5 Network formation from ribbons composed of 27Py7b10	89
4.2.6 Self-assembly pathway in a three-component system which involves blunt-end stacking.....	90
4.3 Conclusions	93
4.4 Experimental section	94
CHAPTER 5. Potential Applications of DNA-Grafted Supramolecular Polymers.....	95
5.1 Introduction.....	96
5.2 Results and discussions	97
5.2.1 FRET Analysis	97
5.2.2 Arrangement of gold nanoparticles	98
5.3 Conclusions	100
5.4 Experimental section	100
CHAPTER 6. General Conclusions.....	103
BIBLIOGRAPHY	106
APPENDICES	132

CHAPTER 1. GENERAL INTRODUCTION

1.1 SUPRAMOLECULAR POLYMERS

Exploring non-covalent interactions in functional molecular systems is a fascinating topic. Over the past few decades, this research direction has become one of the mainstream and paradigm shifting concepts in materials science. In the pioneering work, Lehn described intermolecular supramolecular bonds as “chemistry beyond the molecule”.¹ This definition reflects the prevailing notion that in contrast to covalent bonds supramolecular interactions connect monomeric units by dynamic, programmable and highly reversible non-covalent bonds.^{2,3} The major types of these interactions are hydrogen and halogen bonding,^{4,5} π - π stacking,⁶ metal-ligand binding⁷ and host-guest interactions (Figure 1-1).⁸

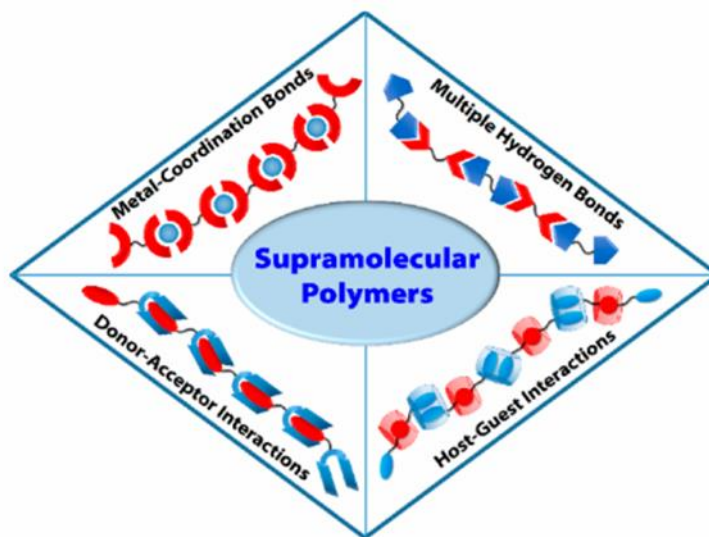


Figure 1-1. Some of the types of interactions in supramolecular assemblies. The image is taken from ref.³

During the last two decades, the research in supramolecular chemistry changed our understanding of the polymerization mechanisms occurring in non-covalent systems, giving rise to a new field of supramolecular polymers. To provide further insight into the growth of the supramolecular polymers,

Meijer and coworkers concluded that it is possible to classify different types of supramolecular polymerization processes using their thermodynamic parameters. According to this classification, supramolecular polymerization can occur as an isodesmic, cooperative and ring-chain mediated process (Figure 1-2).⁹ An isodesmic mechanism is characterized by an equal association constant for each self-assembly step. Thus, the growth of aggregates occurs gradually. In sharp contrast, a cooperative mechanism consists of two regimes that have different equilibrium constants. During the first nucleation stage, energetically unfavorable nucleus-size small aggregates are formed.

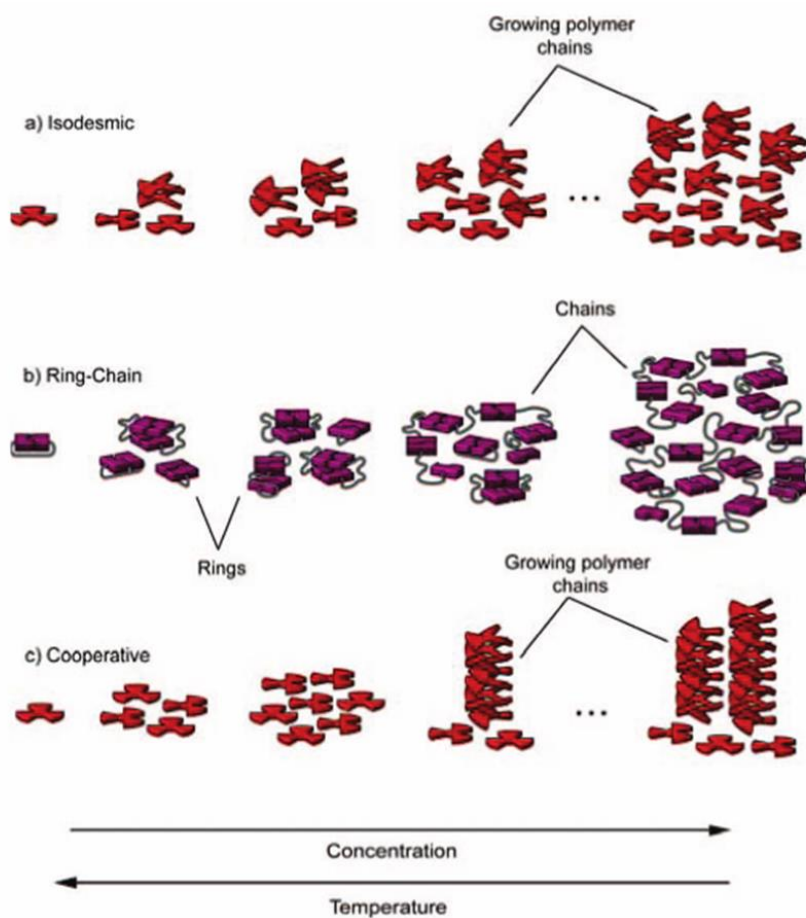


Figure 1-2. Schematic representation of supramolecular polymer growth by three types of self-assembly mechanisms. The image is taken from ref.⁹

This process is followed by a more thermodynamically favorable elongation step. During the ring-chain mediated regime, ditopic ligands capable of

assembling at two sites undergo ring-chain supramolecular polymerization where the growth of the polymer occurs in equilibrium with cyclization.

Similar to the products of chemical reactions, supramolecular polymers could be formed either under thermodynamic or kinetic control. Supporting this idea, Mattia and Otto defined three distinct regimes of the self-assembly in organic materials: equilibrium assemblies, kinetically trapped and far-from-equilibrium systems (Figure 1-3).¹⁰ Thermodynamically favorable assemblies are formed under equilibrium conditions and characterized by persistent stability. The aggregation governed by the kinetics of the system results in the metastable state of the supramolecular polymers that upon time or supplying energy may undergo re-assembly into thermodynamically stable structures. The formation of kinetically trapped states often happens when the initial monomer can polymerize into various structures via multiple self-assembly pathways (pathway complexity). Thus, the morphology and properties of these metastable aggregates largely depend on the preparation procedure. For example, the team led by Sugiyasu has recently shown the controlled kinetic self-assembly of the porphyrin molecules into either fibers or sheets using seeding method and mechanical agitation (Figure 1-4).¹¹ Following their procedure, a high level of control over the self-assembly similar to living polymerization mechanism was achieved.

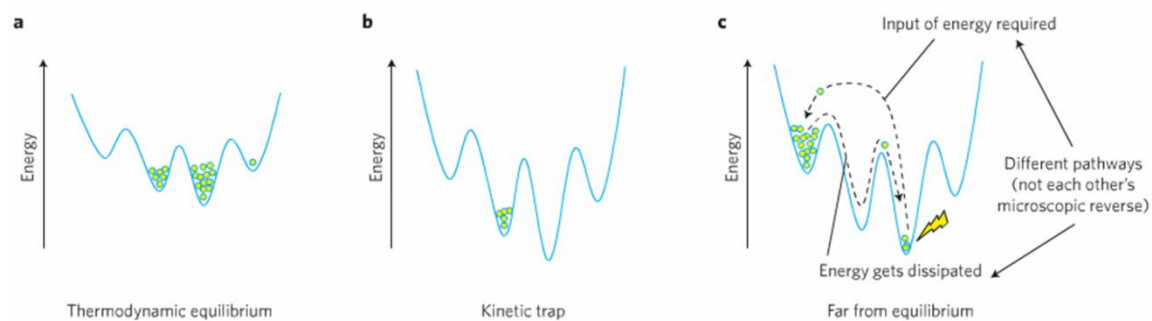


Figure 1-3. Thermodynamic regimes of the supramolecular self-assembly. The image is taken from ref.¹⁰

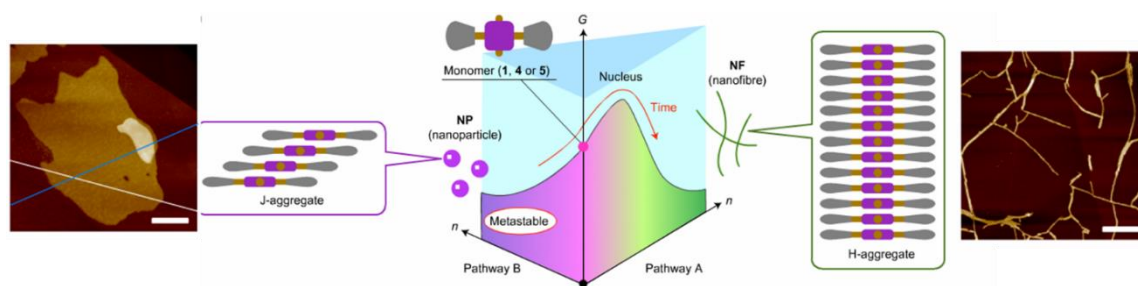


Figure 1-4. Self-assembly energy landscapes and the AFM images of the resulting porphyrin aggregates. The image is taken from ref. ¹¹

The third type of assemblies, far-from-equilibrium systems, remains in its state only upon a constant supply of energy. Otherwise, such systems are shifted to thermodynamically stable or kinetically trapped states due to the dissipation of energy. These far-from-equilibrium systems have received considerable attention during the last few years. Figure 1-5 highlights an excellent example of such systems. Using a system with only a few simple molecular compounds, Eelkema and coworkers demonstrated dynamic self-assembly of the synthetic molecules into filament structures driven by chemical fuel. After the consumption of fuel, the dissipative reaction took place and fibers were dissolved over time.¹²

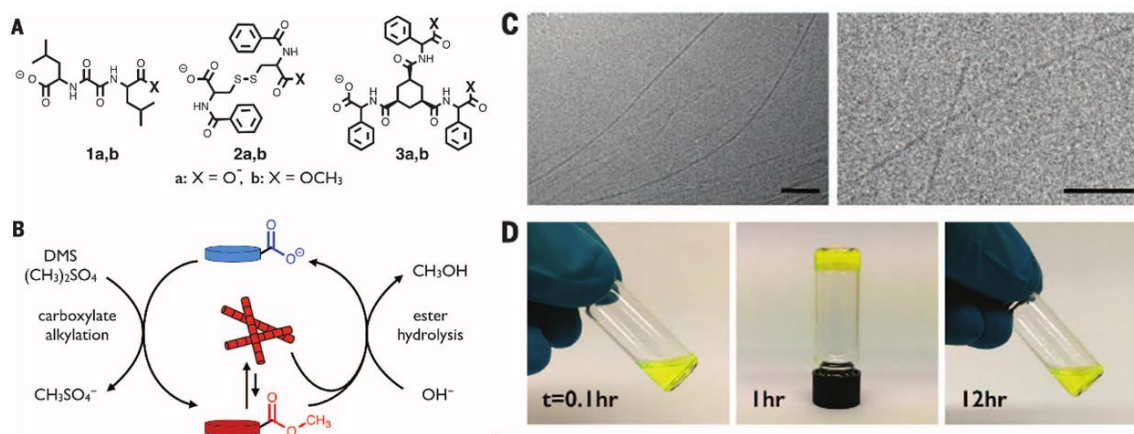


Figure 1-5. Chemical structures of the monomers (A), reaction cycle (B), microscopic illustrations (C) and images (D) of the chemically-fueled self-assemblies. The images are taken from ref.¹²

The benefits of exploiting supramolecular bonds are apparent, and materials made of supramolecular polymers are becoming valuable for numerous applications in nanotechnology, molecular electronics, and biomimicry.^{13,14} With hundreds of examples of supramolecular structures now presented and the number growing daily, a few examples may suffice to illustrate recent development in this broad topic.

The development of materials capable of self-repairing a damaged site is currently one of the most exciting areas in supramolecular polymers.^{15,16} Recently, Wu and co-workers have reported on supramolecular polymers comprised of hydrogen-bonded poly(glycerol sebacate)-graft-ureido-pyrimidinone (PGS-U).¹⁷ The shape-memory material made of this polymer exhibits self-healing properties responding to the external stimuli such as temperature and pressure (Figure 1-6).

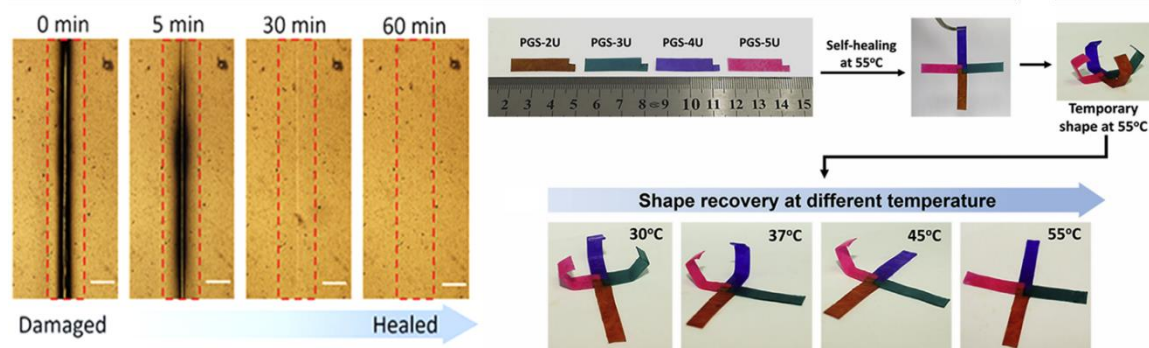


Figure 1-6. Optical microscope images of damaged and healed PGS-U samples at 55 °C for a different time and recovery of the PGS-U arms with 3D temporary shapes into their initial shapes step-by-step with the increase of temperature. The image is taken from ref.¹⁷

Sensing applications are yet another interesting line of research in supramolecular polymers.^{18,19} The use of non-covalent polymers as a stimuli-responsive system was studied in particular by Sessler and coworkers,²⁰ who reported a chemoresponsive system comprised of bis-2,5,7-trinitro-dicyanomethylene-fluorene-4-carboxylate which can be used for the detection of nitroaromatic explosives and anions (Figure 1-7 A).

Finally, supramolecular polymers were employed as drug-delivery vehicles in many systems. An important example of a biocompatible and biodegradable nanomaterial was published by Meijer and co-workers.²¹ The authors demonstrated the intracellular transport of cargo (siRNA) electrostatically attached to the backbone of the fibrous structure formed from co-assembled neutral and cationic PEGylated benzenetricarboxamides (Figure 1-7 B).

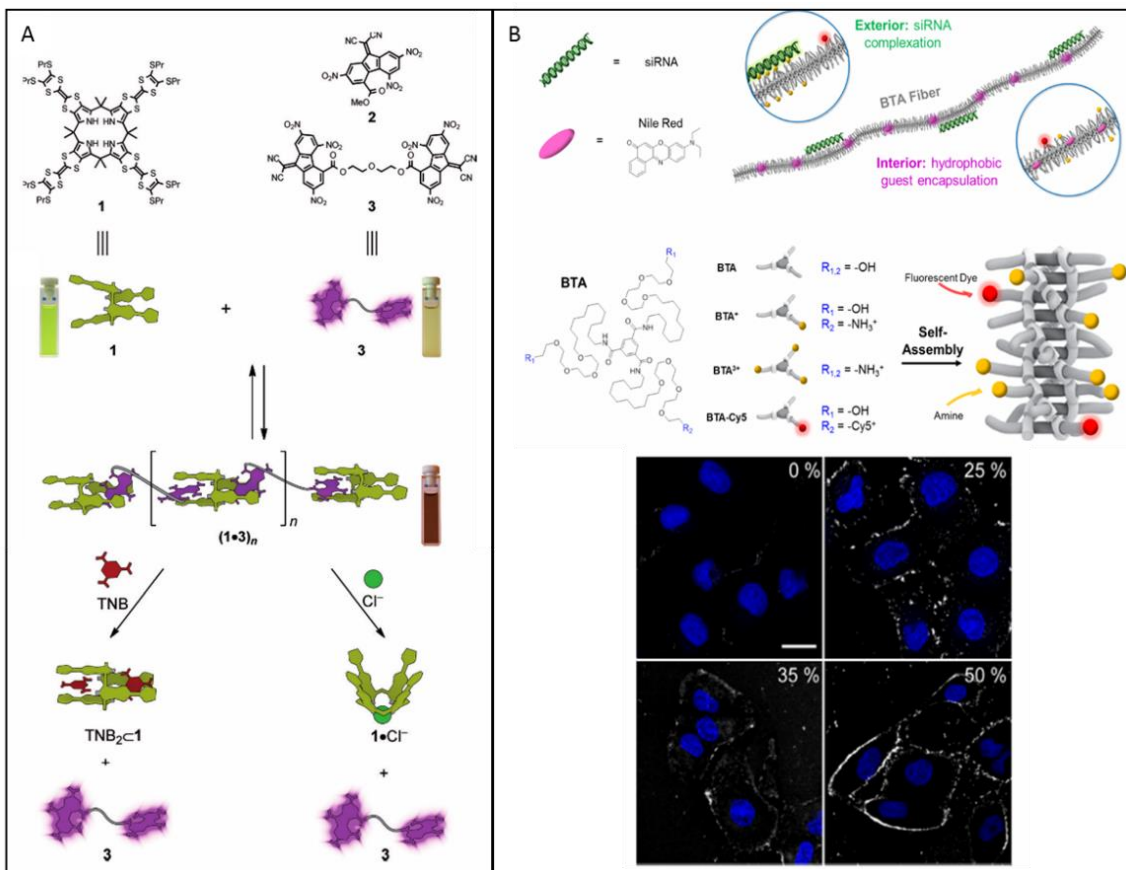


Figure 1-7. A: Graphical illustration of the self-assembly and consequent disruption of chemoresponsive system in response to nitroaromatic compound and chloride ion. B: Schematic representation of the delivery system and confocal microscopy images of the cells. The images are taken from ref.^{20,21}

Finally, these examples demonstrate a myriad of ways in which modern nanotechnology integrates supramolecular interactions in novel functional materials. Emerging strategies and applications are created at an increasing pace. Particularly exciting results originate from water-soluble

supramolecular polymers.^{22,23} It becomes apparent since water plays a crucial role in all biochemical processes and offers enormous opportunities as a solvent for supramolecular assembly. The ability to form hydrogen bonds and sustain hydrophobic interactions is remarkable for novel applications. For instance, the properties of DNA as a material inspired numerous research directions. A concise description of several elegant and inventive applications of DNA becomes the subject of the next section.

1.2 DNA-BASED SUPRAMOLECULAR SELF-ASSEMBLIES

1.2.1 DNA in modern nanotechnology

Nature uses self-assembly to create the most sophisticated systems known to mankind – living organisms. In this regard, DNA remains an outstanding example of natural technology. One of the most intriguing properties of DNA is its self-recognition behavior. An extremely precise Watson-Crick base pairing between nucleobases drives two single-stranded DNA to assemble into the double helix (Figure 1-8).

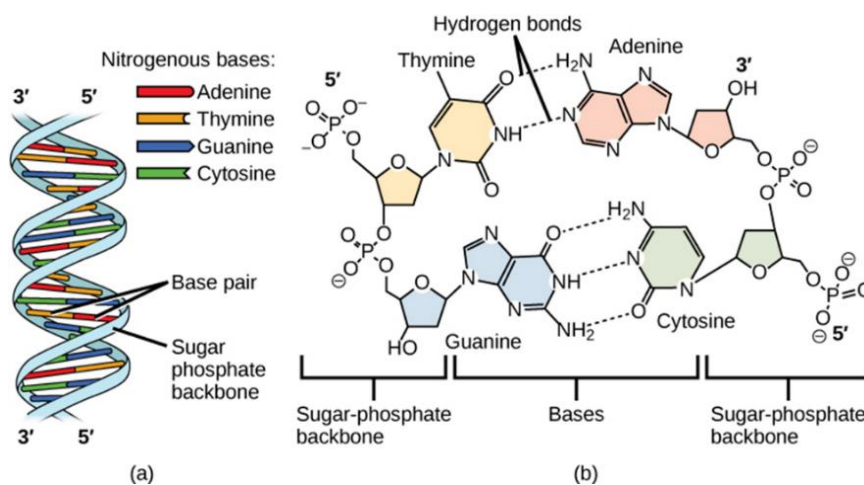


Figure 1-8. The schematic illustration of DNA double helix and complementarity of base pairing.

These properties greatly extend the scope of DNA as an efficient information storage and transfer material. In recent years, DNA became

extensively used as a building block for the spatial organization of organic molecules into complex architectures due to several reasons.

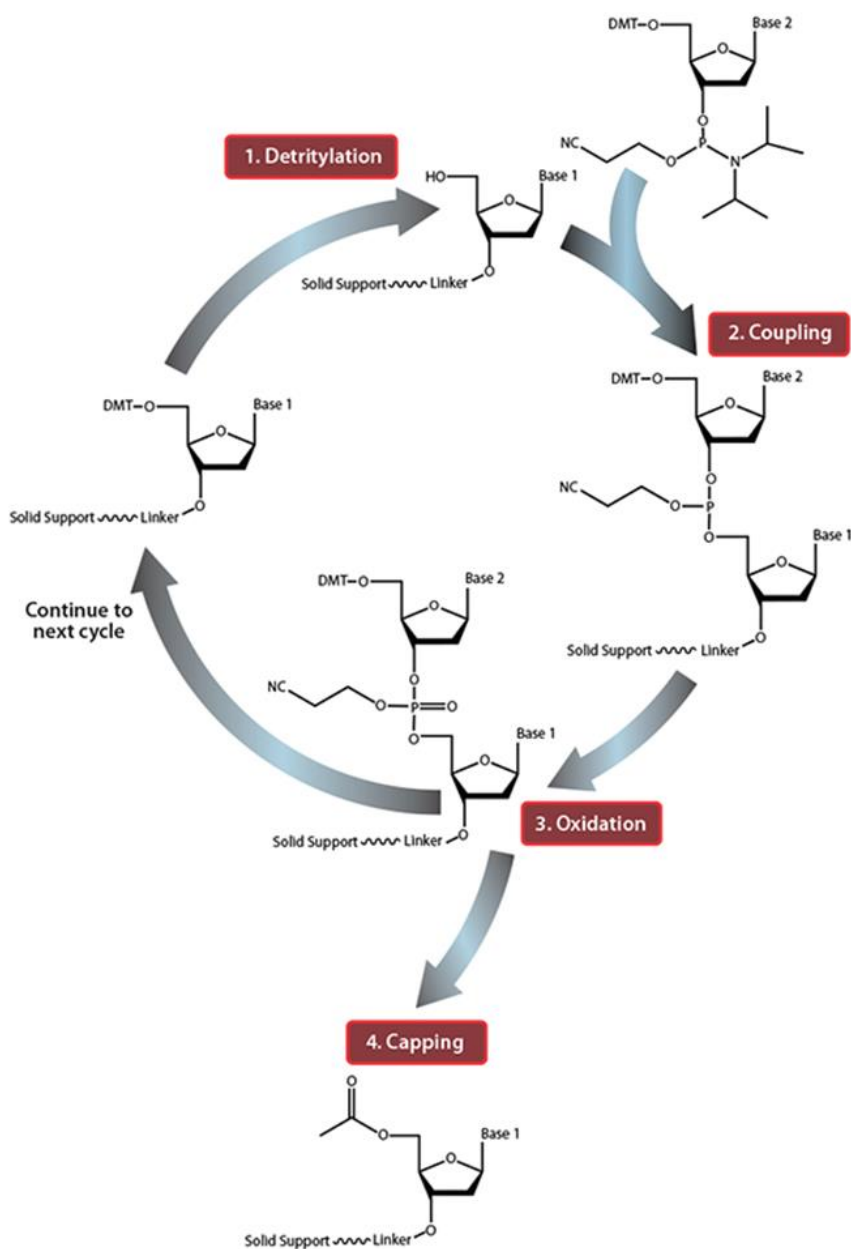


Figure 1-9. The schematic illustration of solid-phase oligonucleotide synthesis.

First, technological advances made DNA synthesis convenient and inexpensive. Thus, solid-phase phosphoramidite chemistry is widely used for the oligonucleotide synthesis (Figure 1-9).²⁴ A molecule designed for the

incorporation in the oligomer chain is protected with dimethoxytrityl and phosphoramidite groups. The synthesis occurs as a cycle of consecutive activation, coupling, oxidation and deprotection steps (Figure 1-9). This approach offers high control over the length and composition of the resulting oligomer and polymer strands. Moreover, various oligomers and polymers comprising non-nucleoside units become easily accessible via this method..²⁵⁻

31

Second, the predictable self-assembly of DNA offers reliable design principles and a high level of control over resulting constructs.³² Using a set of sticky ends and branched junctions, meticulously designed DNA strands could be arranged into the most spatially intricate nanostructures. It is noteworthy that there is an increasing amount of self-assembled DNA systems which find widespread applications beyond DNA's natural role^{33,34}, e.g. sensing,³⁵ nanoelectronics,³⁶ catalysis,³⁷ nanomachines.³⁸ Nowadays, virtually any desired structure could be made from the set of DNA strands generated by software, for example the one created by Bathe and coworkers (Figure 1-10).³⁹ A general protocol is rather straightforward: the scaffold strand (strand from bacteria of a several thousand nucleotides) and shorter staple strands are mixed and annealed to allow for hybridization of the complementary fragments, resulting in the desired architecture. This approach, pioneered by Rothemund, is known as a DNA origami technique.^{40,41} It provides an opportunity to create more and more complex architectures on nanometer and micrometer scale.

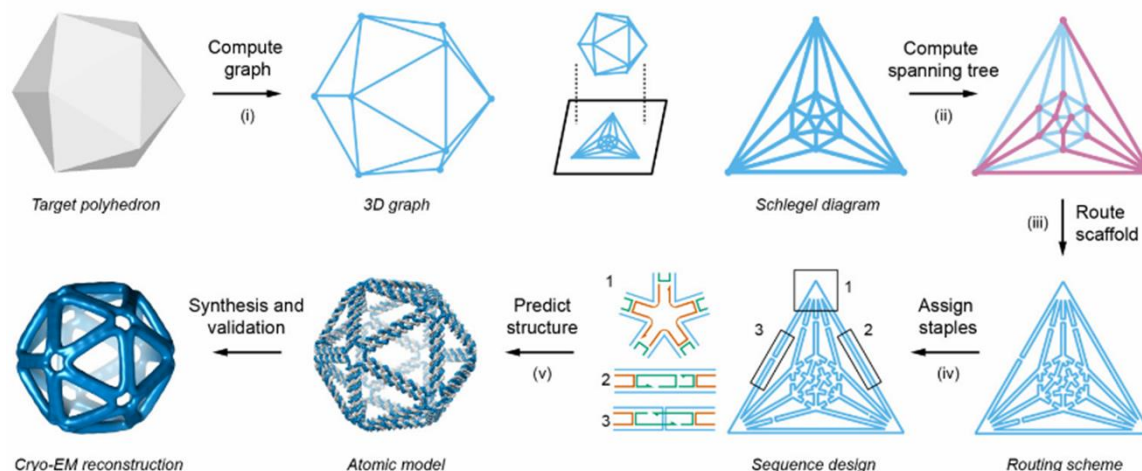


Figure 1-10. Top-down sequence design procedure from DNA origami structure for desired geometry. The image is taken from ref.³⁹

Although most of the researchers tend to utilize canonical base pairing in DNA nanostructures, blunt-end interactions are yet another attractive unorthodox force that drives the assembly between nucleobases (Figure 1-11 A). The strategy of nucleobase stacking between the termini of the DNA duplex is particularly valuable for the hierarchical assembly of the multiunit DNA origami structures.^{42,43} Among others, the use of blunt-end stacking was studied by Dietz and co-workers, who reported DNA origami building blocks sculpted to bind selectively at specific places due to their shape-complementary geometry.⁴⁴ Mimicking proteins' shape-recognition behavior, the DNA origami building blocks stack together as designed, enhancing the tunability and directionality of the blunt-end interactions. Helping to overcome the size limitation of the DNA origami technique, macro binding between separate DNA origami compartments enables the preparation of larger constructs with dynamic properties (Figure 1-11 B).⁴⁴

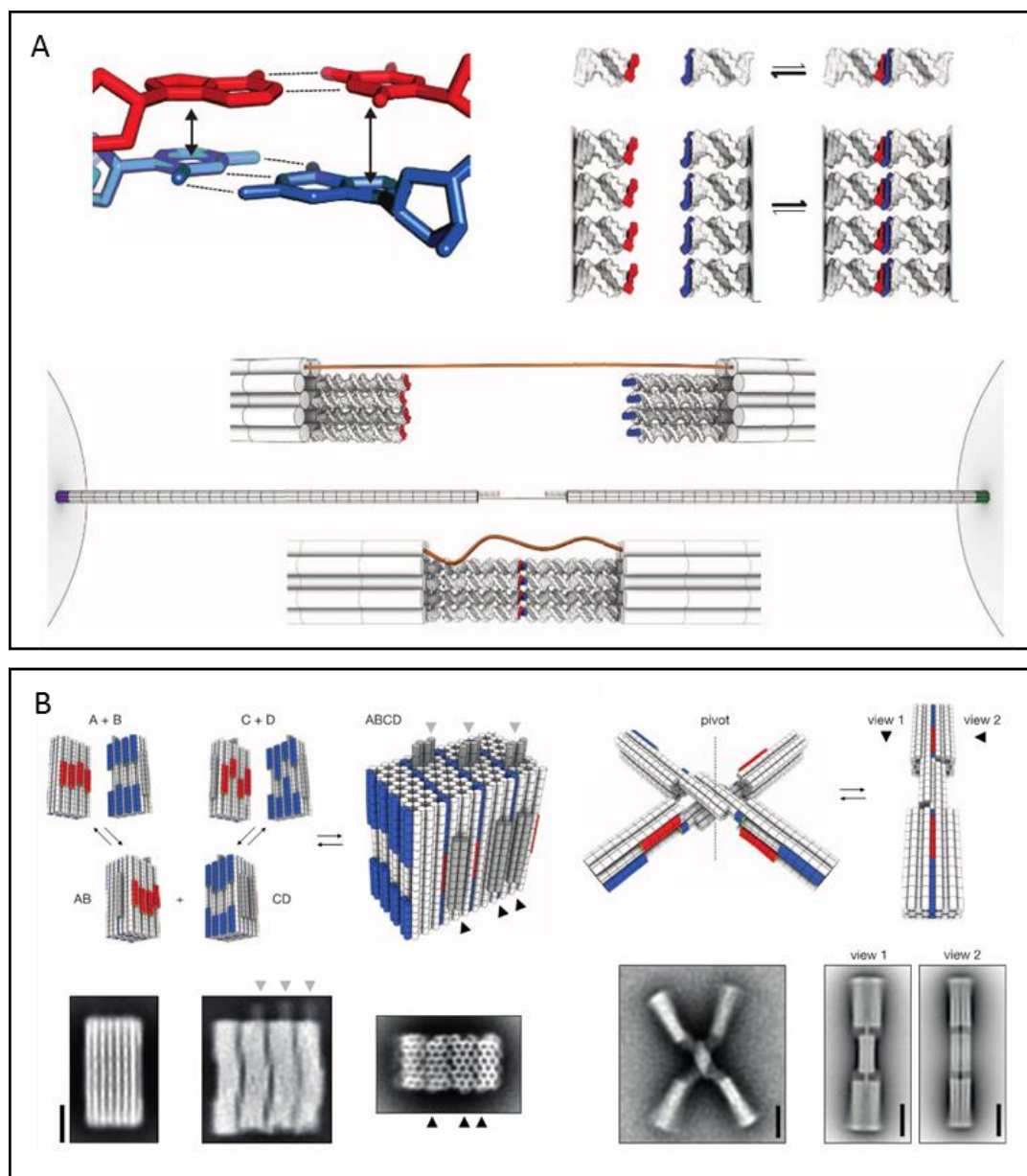


Figure 1-11. A: The schematic illustration of the DNA blunt-end interactions. B: Schematic representation and corresponding TEM images of the dynamic DNA origami constructs formed via blunt-ended stacking between shape-complementary moieties. The images are taken from ref.^{43,44}

1.2.2 DNA as a scaffold for the arrangement of synthetic molecules

In nature, a templating approach operates abundantly at different scales – from bulk biomineralization to ultraprecise DNA self-organization on scaffold proteins. The programmable self-assembly of DNA itself can be turned into a

benefit for the directed arrangement of non-nucleoside molecular blocks.⁴⁵⁻⁴⁷ The self-recognition properties of DNA are especially promising in the established areas of materials science and biotechnology. In this regard, using base-pairing interactions is the main focus of DNA-guided arrangement of the functional moieties such as aromatic molecules, metallic nanoparticles, proteins and etc.⁴⁸⁻⁵⁰

Häner and co-workers used DNA for the creation of multichromophore arrays with a precision hardly achievable by other approaches. Introducing non-nucleoside chromophores often led to the increased stability of hybrid double strands.⁵¹⁻⁵³ A large number of chromophores were successfully arranged exploiting the DNA scaffolding strategy for the diverse applications in photophysics,⁵⁴ optoelectronics⁵⁵ and sensing^{56,57}.

Gold nanoparticles were arranged in a regular manner on ever more sophisticated DNA scaffolds ranging from octahedral to toroidal structures.⁵⁸⁻⁶⁰ Recently, Ke and coworkers prepared honeycomb DNA origami structures for precise patterning of gold nanoparticles that serve as plasmonic metamaterials (Figure 1-12 A).⁶¹

Another example of templated arrangement has been proposed by the team lead by Lin. They reported on hollow DNA origami structures for the controlled shaping of liposomes using a DNA-mediated assembly that mimics the cytoskeleton's membrane shaping function (Figure 1-12 B).⁶² The shape of the resulting liposomes can be effectively controlled by the geometry of the DNA scaffold.

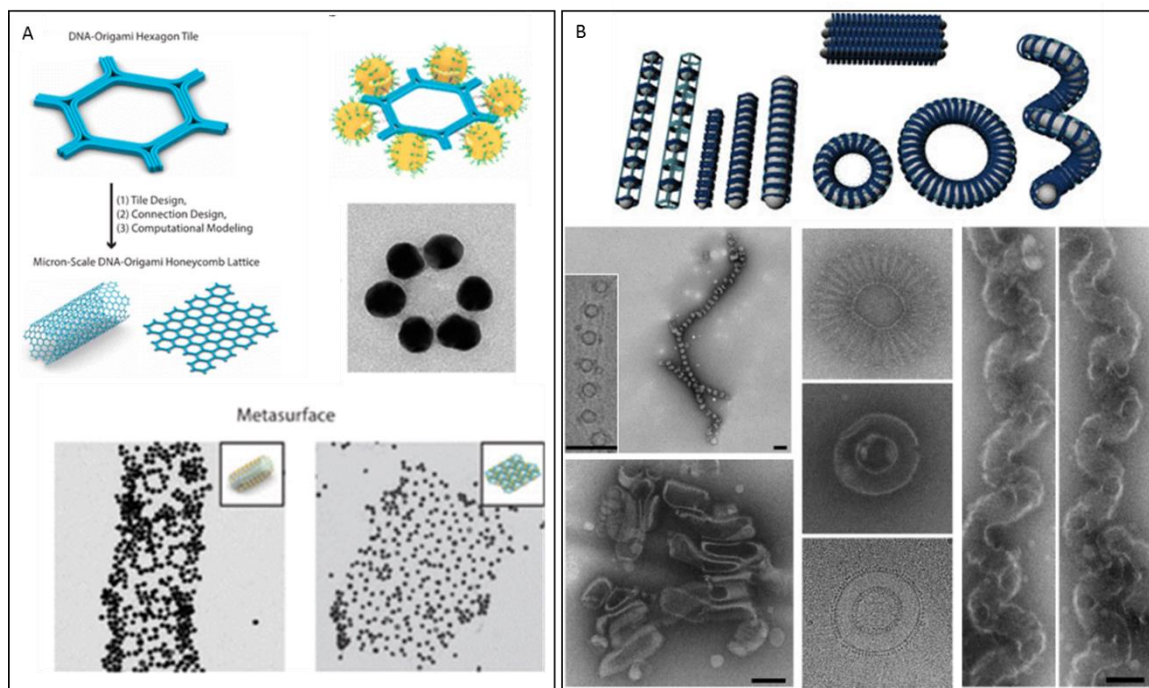


Figure 1-12. A: Schematic illustration and TEM images of gold nanoparticles arrangement on the honeycomb lattice and tube. B: Schematic illustration and TEM images of liposomes' arrays on different templates. The images are taken from ref. ^{61,62}

1.2.3 Synthetic molecules as scaffolds for DNA arrangement

As indicated previously, the conjugation of DNA strands to functional entities with a specific set of optical, mechanical or biological properties allows engineering of sophisticated DNA-containing architectures. Such hybrids are regarded as one of the most potential biocompatible functional platforms. Besides the DNA-guided assemblies discussed above, DNA block copolymers can be successfully used for the preparation of nanoparticles, side-chain polymers and non-covalent architectures with grafted oligonucleotides.^{63,64} Being arranged on the scaffold, protruding oligonucleotides serve as an active motif for the hierarchical assembly and stimuli-responsive switches.

The systems comprised of closely spaced DNA single strands benefit from unique properties that depend on the length of DNA, the density of the oligonucleotide package and ionic strength in solution.^{65,66} It was observed that

hybridization between complementary grafted DNA strands occurs through an exceptionally sharp temperature transition in contrast to this process in solution.⁶⁷ A more cooperative behavior of the assembly/disassembly processes for crowded systems is associated with a high local counterion concentration. Subsequently, higher ionic strength results in the increased melting temperatures and stability of duplexes. The length of oligonucleotides also influences the efficiency of binding.⁶⁸ While the transitions become sharper with the increase of the oligonucleotide length, the risk of hybridization between adjacent strands as well as self-hybridization obstructs the attractive forces between complementary strands. The sensitivity and tunability of the oligonucleotide interactions in DNA-grafted systems further finds numerous applications.

One of the most critical requirement for applications remains the ability to control the architecture of the target structure. A team led by Mirkin proposed a method for the crystallization of DNA-nanoparticles into well-defined polyhedra mimicking atomic crystallization (Figure 1-13 A).⁶⁹ They used temperature as a trigger for the assembly, cooling the system over several days. Mediated by DNA hybridization, the assembly of conjugates results in shape-controlled crystal structures.

DNA nanoparticles, in the form of brush polymers and inorganic systems, were employed in drug delivery and sensing.^{70,71} For example, Raeesi *et al.* reported on drug-delivery system based on core-satellite gold nanoparticle assemblies (Figure 1-13 B).⁷² These nanostructures were loaded with a hydrophobic drug, doxorubicin, which intercalates into the DNA linkers. The strategy proposed by the authors enables photo- and thermally driven drug release. The loading capacity and stability of the structures can be controlled by the length of DNA sequences.

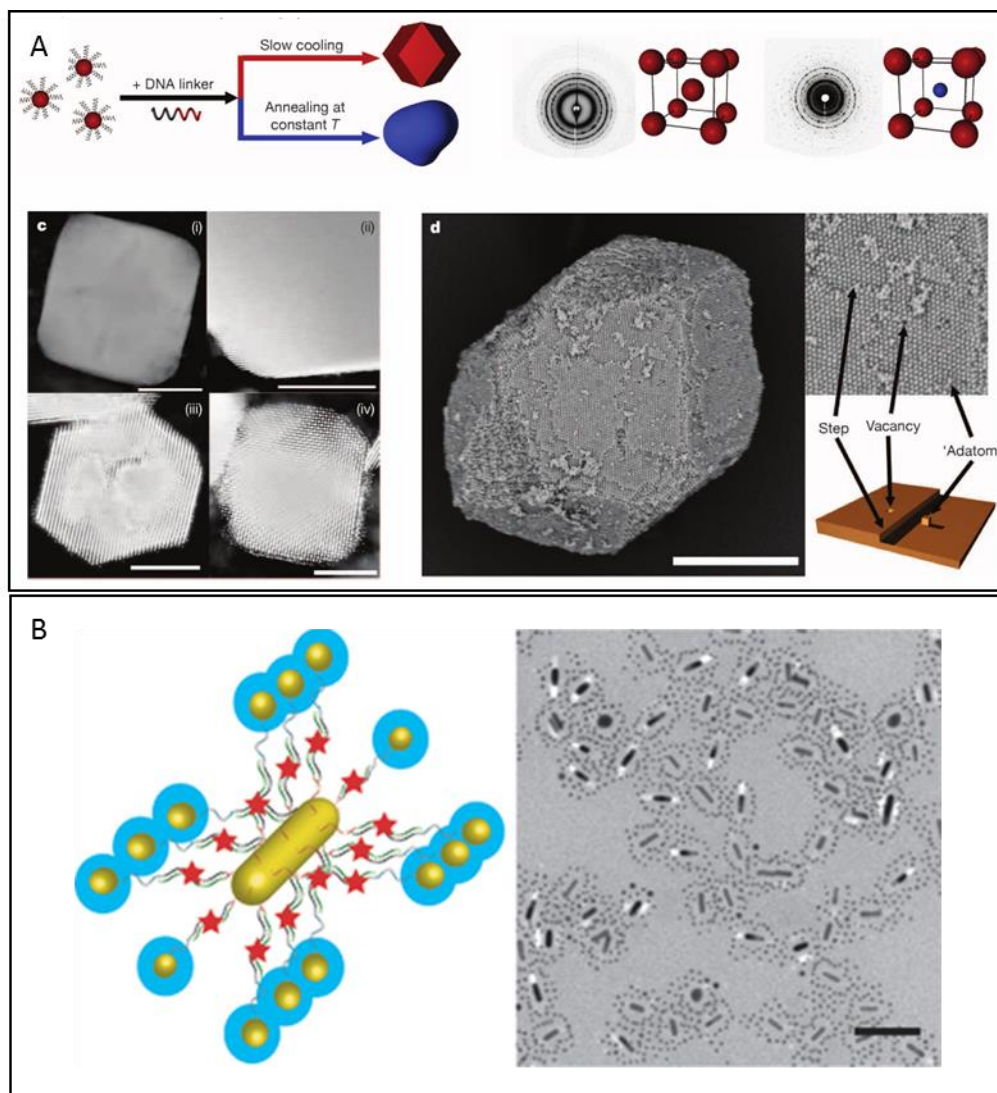


Figure 1-13. A: SAXS data; TEM and SEM images for DNA-nanoparticle superlattices prepared by slow-cooling technic. B: Doxorubicin-loaded gold nanoparticle superstructure. The images are taken from ref.^{69,72}

Utilizing the same strategy for controlled assembly via DNA hybridization, the self-organization of nanopolymersomes was presented by the groups of Meier and Palivan.⁷³ Hollow spherical nanocompartments functionalized by DNA single strands were assembled into defined clusters preserving their initial morphology (Figure 1-14 A). Similarly, the DNA-mediated assembly of liposomes has been reported by several groups.^{74,75} For example, the interconnection of lipophilic vesicles for the subsequent fusion was

DNA-grafted polymers are yet another promising material for the drug delivery systems, therapeutic applications, and DNA diagnostics.⁷⁷ Such materials are characterized by chemical stability, physical flexibility and high mechanical strength. In addition, they benefit from the dynamic nature of DNA that are aligned along the polymer chains and readily available for hybridization.

The behavior of isolated DNA-grafted polymer wires, as well as their controlled positioning and further manipulations, were extensively studied in the group of Gothelf. Figure 1-15 shows a DNA-brush polymer deposited on the surface of DNA origami sheets.⁷⁸ The deposition is mediated by DNA hybridization that offers high control over the orientation of the wires and further conformational switches.⁷⁹ Furthermore, Gothelf and coworkers reported on energy transfer between two separate conjugated polymer chains as well as quenching effect as the result of hybridization with the complementary strand modified with the quencher.⁷⁸ These results demonstrate the addressability of the grafted DNA chains and the potential utility of the DNA-grafted polymers as molecular wires.

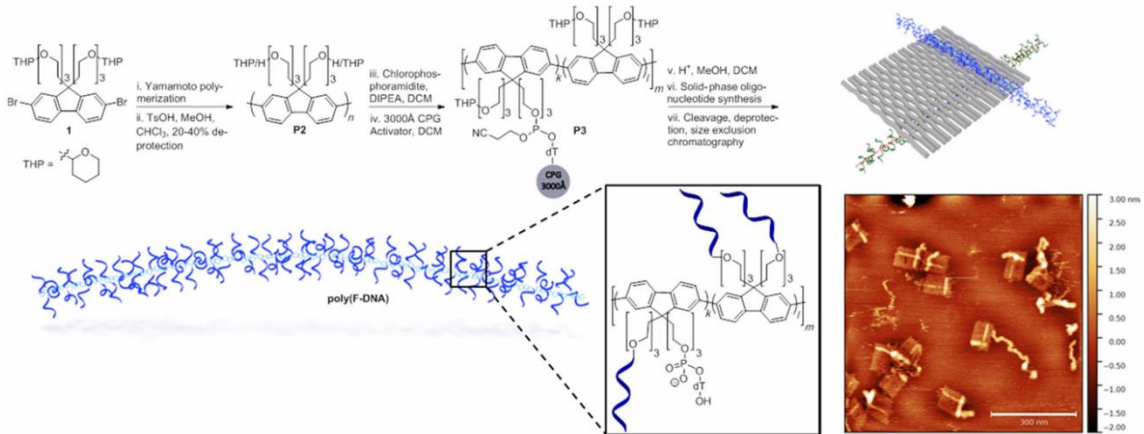


Figure 1-15. Synthesis of a DNA-grafted polymer; schematic illustration and AFM image of the deposited DNA-polymer conjugates on the surface of DNA origami. The image is taken from ref.⁷⁸

DNA is commonly used as a linker for polymer chains driving the formation of networks, hybrid hydrogels.^{80,81} On the other hand, DNA serves as a stimuli-responsive motif that can be triggered by pH, temperature, metal ions, etc., and used for the preparation of responsive systems based on hydrogels.⁸² Recently, Willner and coworkers have reported on DNA-acrylamide hydrogel microcapsules for the controlled drug release.⁸³ The release occurred upon pH change that caused a DNA linker to switch its conformation to an i-motif unlocking the capsules (Figure 1-16).

DNA-polymer hybrid materials formed by covalent bonds lack several remarkable characteristics such as tunability and reversibility of interactions, self-organization, and the ability to self-heal disintegrated domains. To overcome these limitations, non-covalent interactions between DNA-conjugated building blocks can be used. One of the interesting strategies used for the preparation of these functional materials resides in the self-assembly of DNA amphiphiles. The aggregation of hydrophobic moieties connected to oligonucleotides results in the formation of DNA-grafted non-covalently bonded scaffolds in water. Depending on the hydrophobic-hydrophilic balance, the morphology of these scaffolds varies from spherical to worm-like micellar structures. For example, drug-cored micellar nanostructures of different morphologies were reported by Tan et al. (Figure 1-17 A) The self-assemblies comprised of camptothecin-conjugated oligonucleotide amphiphiles exhibit light responsiveness, enabling controllable drug release.⁸⁴

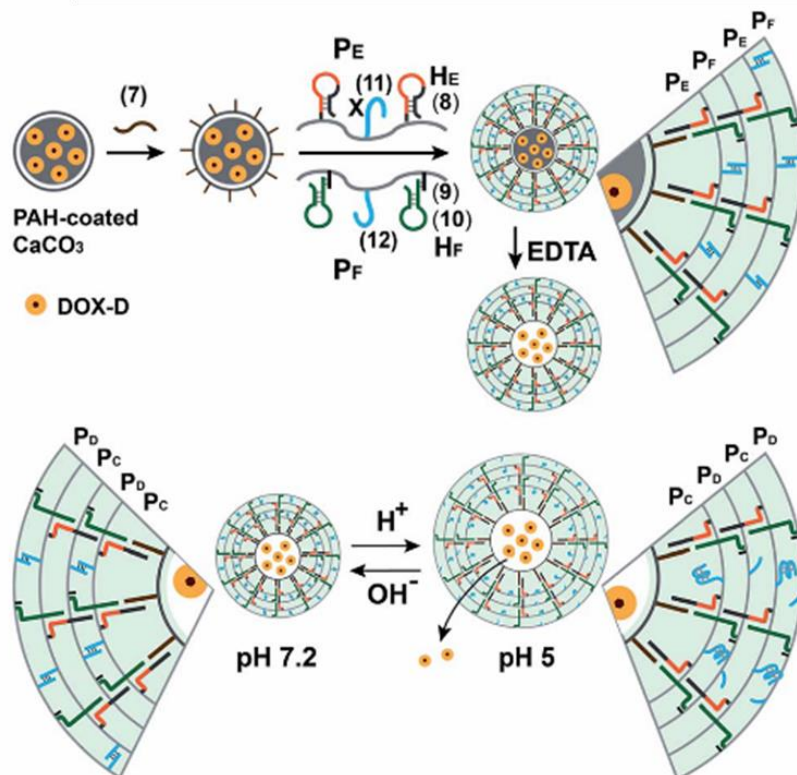


Figure 1-16. The schematic illustration of the preparation of DNA-acrylamide hydrogel microcapsules and controlled the pH-triggered release of the drug doxorubicin. The image is taken from ref.⁸³

Reversible labeling of the DNA-grafted supramolecular polymers by gold-nucleotide conjugates was demonstrated by Noteborn et al.⁸⁵ The write-erase process was accomplished via hybridization between complementary DNA using a strand-displacement method (Figure 1-17 B).

In the last example depicted here, Wu et al. described the system for the controlled association of *E. coli* based on supramolecular DNA-dendron polymers (Figure 1-17 C).⁸⁶ The association occurred through mannose recognition sites, which were attached to the fibers via DNA hybridization.

The examples of the non-covalent DNA-grafted polymers are limited and mostly presented by micellar structures. The controlled arrangement of the molecules into defined structure for the dense arrangement of the DNA remains a formidable challenge.

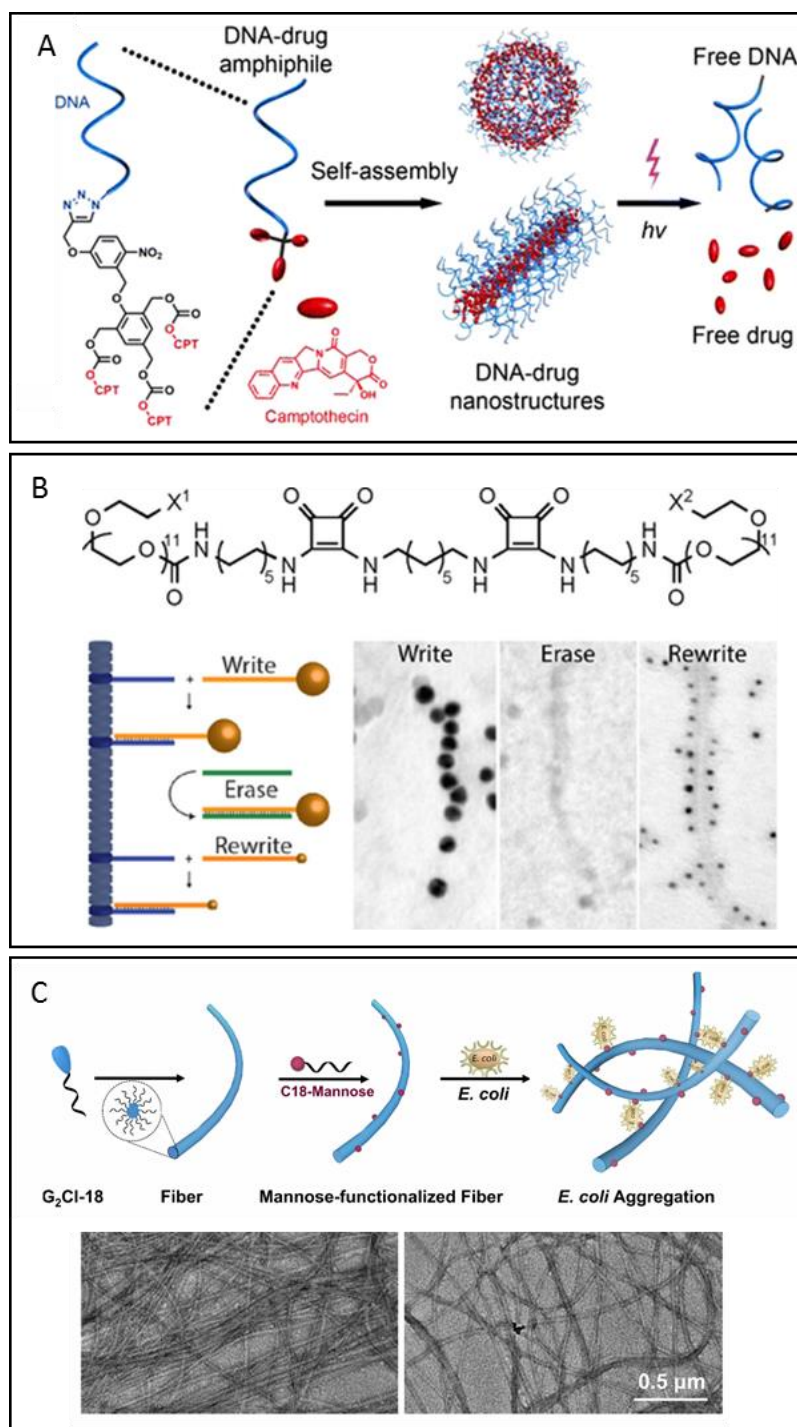


Figure 1-17. A: Schematic illustration of the self-assembly and light-triggered release of the camptothecin-nucleotide amphiphiles. B: Schematic illustration and TEM images of the squaraimide-based DNA-grafted supramolecular polymers and write/erase labeling by gold nanoparticles. C: Illustration of the formation of the Dendron-DNA supramolecular polymers and association of *E. coli* and corresponding TEM images. The images are taken from ref. ⁸⁴⁻⁸⁶

1.3 AIM OF THE STUDY

The self-assembly of natural polyphosphodiester yields unique biomaterials from relatively simple building blocks, emphasizing the importance of hierarchical organization and precision of sequences on their properties. Future developments in the field of polyphosphodiester synthesis can help to shift focus from polyamides as self-assembling molecules and thus expand the existing toolbox of biocompatible, environmentally friendly functional systems.⁸⁷⁻⁹⁰ Surprisingly, despite recent advances in synthetic polyphosphodiesters,⁹¹⁻⁹³ there is an almost unexplored area of their supramolecular polymerization – a key step in transferring a chemical structure into properties and functions.⁹⁴ Reports on the self-assembly of polyphosphodiesters appear in different research fields, including DNA/RNA nanotechnology,⁹⁵⁻⁹⁸ bioconjugated^{77,78,99} and supramolecular polymers.¹⁰⁰⁻¹⁰⁵ Knowledge in the areas is somehow disconnected, hampering the development and discovery of new applications. In each case, the self-assembly properties remain key to the functions and are determined by potential noncovalent interactions (hydrogen bonding, hydrophobic effect and stacking) and environmental factors.

Our efforts are mainly directed to the non-covalent synthesis and studying the properties of DNA-grafted supramolecular polymers. Such interest is largely inspired by the intrinsic properties of supramolecular polymers^{13,106,107}, such as their dynamics and stimuli-responsiveness, and recent advances in functional DNA nanoparticles.^{108,109}

CHAPTER 2. DNA-GRAFTED SUPRAMOLECULAR POLYMERS –
HELICAL RIBBON STRUCTURES FORMED BY SELF-ASSEMBLY OF
PYRENE-DNA CHIMERIC OLIGOMERS

ABSTRACT

The controlled arraying of DNA strands on adaptive polymeric platforms remains a challenge. Here, we present the non-covalent synthesis of DNA-grafted, linear supramolecular polymers from short chimeric oligomers. The oligomers are composed of an oligopyrenotide strand attached to the 5'-end of an oligodeoxynucleotide. Supramolecular polymerization of the oligomers in aqueous medium leads to the formation of one-dimensional (1D) helical ribbon structures. Hydrophobic and stacking interactions of intramolecularly folded pyrenes are the driving force behind the development of the DNA-grafted polymers. Atomic force and transmission electron microscopy show rod-like polymers of several hundred nanometers length. The temperature-controlled formation of the polymers is completely reversible and follows a nucleation-elongation mechanism. DNA-grafted polymers of the type described herein will serve as models for the development of structurally and functionally diverse supramolecular platforms with applications in materials science and diagnostics.

Part of this work has been published:

Y. Vyborna, M. Vybornyi, A. V. Rudnev and R. Häner, *Angew. Chemie Int. Ed.*, 2015, **54**, 7934–7938.

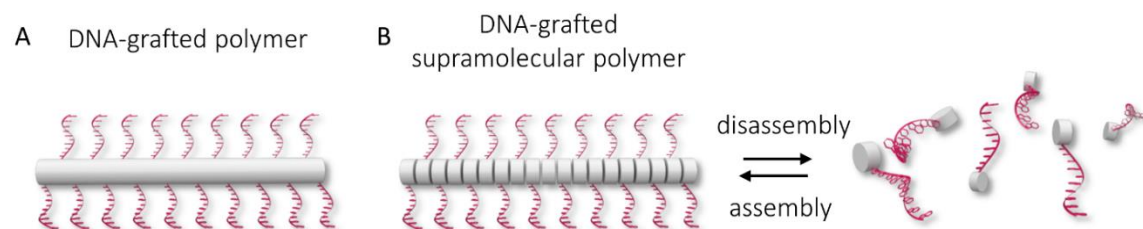
Y. Vyborna, M. Vybornyi and R. Häner, *Chem. Commun.* 2017, **53**, 5179-5181.

Y. Vyborna, S. Altunbas, M. Vybornyi and R. Häner, *Chem. Commun.* 2017, accepted, DOI: 10.1039/C7CC07511A .

2.1 INTRODUCTION

DNA plays an important role in modern nanotechnology.^{77,108,110–119} The merging of organic entities, such as polymers,¹²⁰ lipid chains^{100,121} or aromatic molecules^{25,45,122–128} with canonical DNA motifs allows the design and engineering of supramolecular architectures with special optical, mechanical or biological properties.^{129–134} While the self-assembly behavior of the resulting DNA conjugates is still controlled by base pairing interactions,¹³⁵ the overall structural and functional properties of the hybrid materials can be directed by the conjugated moieties.^{49,136–138} In DNA-grafted polymers⁶⁴ (Scheme 2-1. A) oligonucleotides are arranged in a comb-like fashion on a polymer backbone.

Scheme 2-1. A: Schematic representation of a DNA-grafted polymer. B: DNA-grafted supramolecular polymer.



DNA polymer hybrids were shown to adapt morphologically distinct shapes that are influenced by environmental factors.¹³⁹ Not surprisingly, such polymers find interest as materials for various applications including drug delivery or DNA sensing¹⁴⁰ and it is highly desirable to enhance further the functional diversity of both, the DNA and the polymer parts.^{139,141–143} Supramolecular polymers are formed by non-covalent interactions^{107,144} and, thus, bear additional responsiveness towards external stimuli in comparison to covalent polymers. In this chapter, we describe the formation of DNA-grafted supramolecular polymers (Scheme 2-1 B). We show that pyrene-DNA chimeric oligomers self-assemble into ribbon-like helical structures in an aqueous medium.

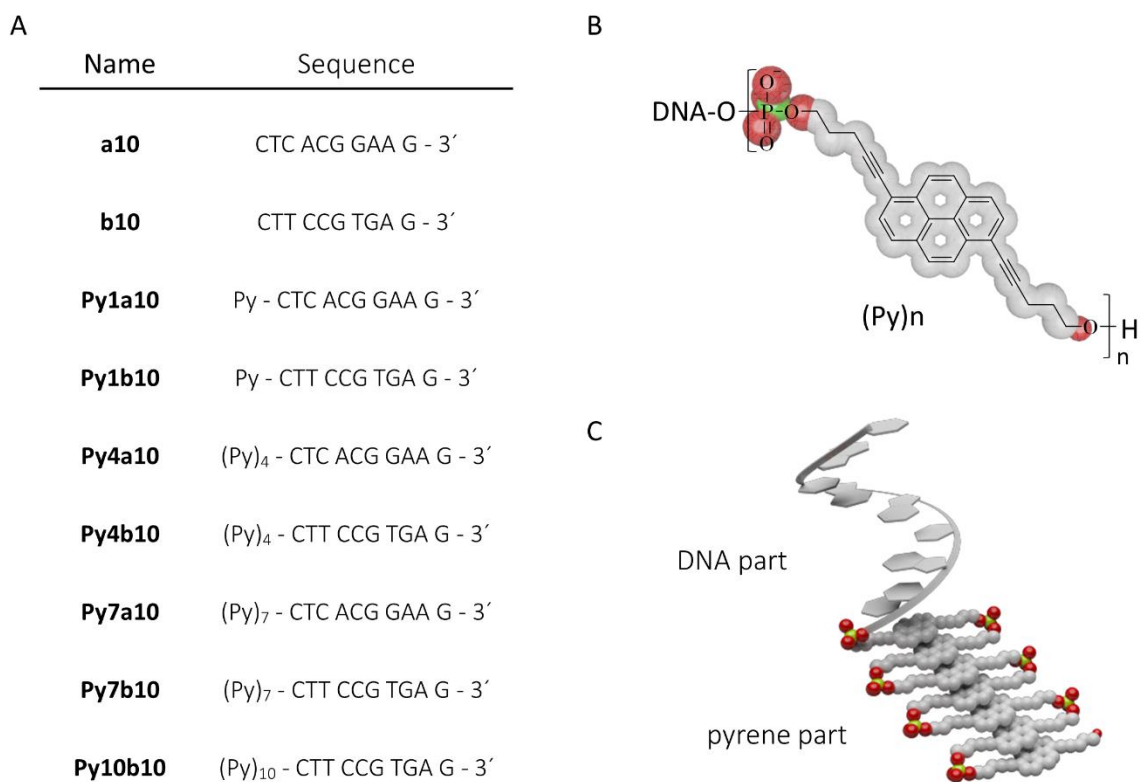
2.2 RESULTS AND DISCUSSIONS

2.2.1 DNA-pyrene conjugates based on 1,6-modified pentynyl pyrene

2.2.1.1 Dependence of the self-assembly on the length of the pyrene chain

The chimeric pyrene-DNA oligomers^{102,145,146} used in this study were prepared by solid phase synthesis according to published procedures¹⁴⁷ and are summarized in Scheme 2-2. The oligomers are composed of an identical DNA strand (10 nucleotides) and a 5'-linked pyrene part of variable length (0, 1, 4, 7 or 10 units). Individual 1,6-bis-pentynyl pyrene units are connected by phosphodiester groups. The non-modified DNA sequences **a10** and **b10** are complementary.

Scheme 2-2. A: the list of the DNA hybrid sequences used in this study; B: chemical structure of the phosphodiester-linked pyrene units; C: model for the pyrene-DNA chimeric oligomer. Pyrene units are arranged in a stair-like fashion; negatively charged phosphodiester groups are located on the edges of the pyrene stack. The appended oligonucleotide is arbitrarily shown as a right-handed single strand.



All oligomers were found to be soluble at elevated temperatures ($>80^{\circ}\text{C}$) in an aqueous medium (100 mM NaCl, 10 mM sodium phosphate buffer, pH 7). Upon cooling of 2 μM solution of oligomers containing pyrenes, the self-assembly of polymers takes place. The polymerization process is readily followed by UV/vis-absorption. The simultaneous formation of an H-band at 335 nm ($S_0 \rightarrow S_1$) and a J-band at 305 nm ($S_0 \rightarrow S_2$) was observed for the self-assemblies of **Py7a10**, **Py7b10** and 1:1 mixture of these oligomers **Py7a10/Py7b10** (Figure 2-1, Figure 2-2). In contrast, oligomers **Py1a10**, **Py1b10**, **Py4a10** and **Py4b10**, which have a lower number of pyrene units present in the oligomer, did not show a similar spectroscopic pattern (Figure 2-2).

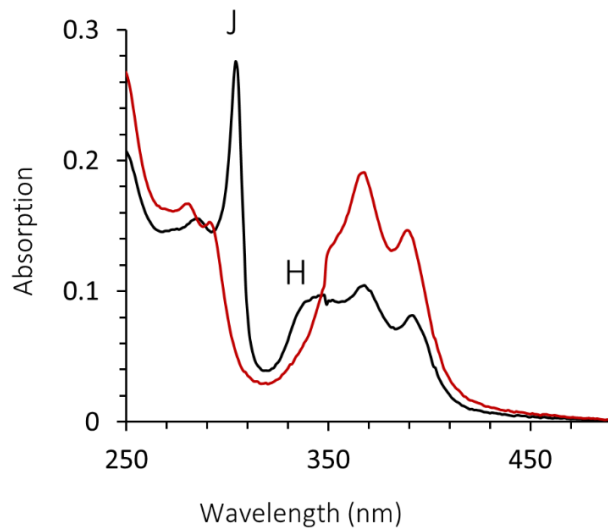


Figure 2-1. UV/vis spectra of **Py7a10** at 90°C (red) and 20°C (black). Conditions: oligomer concentration 2 μM , 10 mM phosphate buffer, pH = 7, 100 mM sodium chloride.

These characteristic shifts are reminiscent of previous observations made with 1,6-linked pyrene trimers and are explained by a stair-like folding of pyrene oligomers.^{148,149} The stair-like folding of the seven pyrenes present in oligomers **Py7a10** or **Py7b10** is illustrated in Scheme 2-2 C. The folded oligopyrenes consist of a layer of pyrenes that are flanked by the negative charges of the phosphodiester groups located on the edges of the stack.

Subsequent aggregation of individual oligomers leads to the formation of supramolecular polymers.

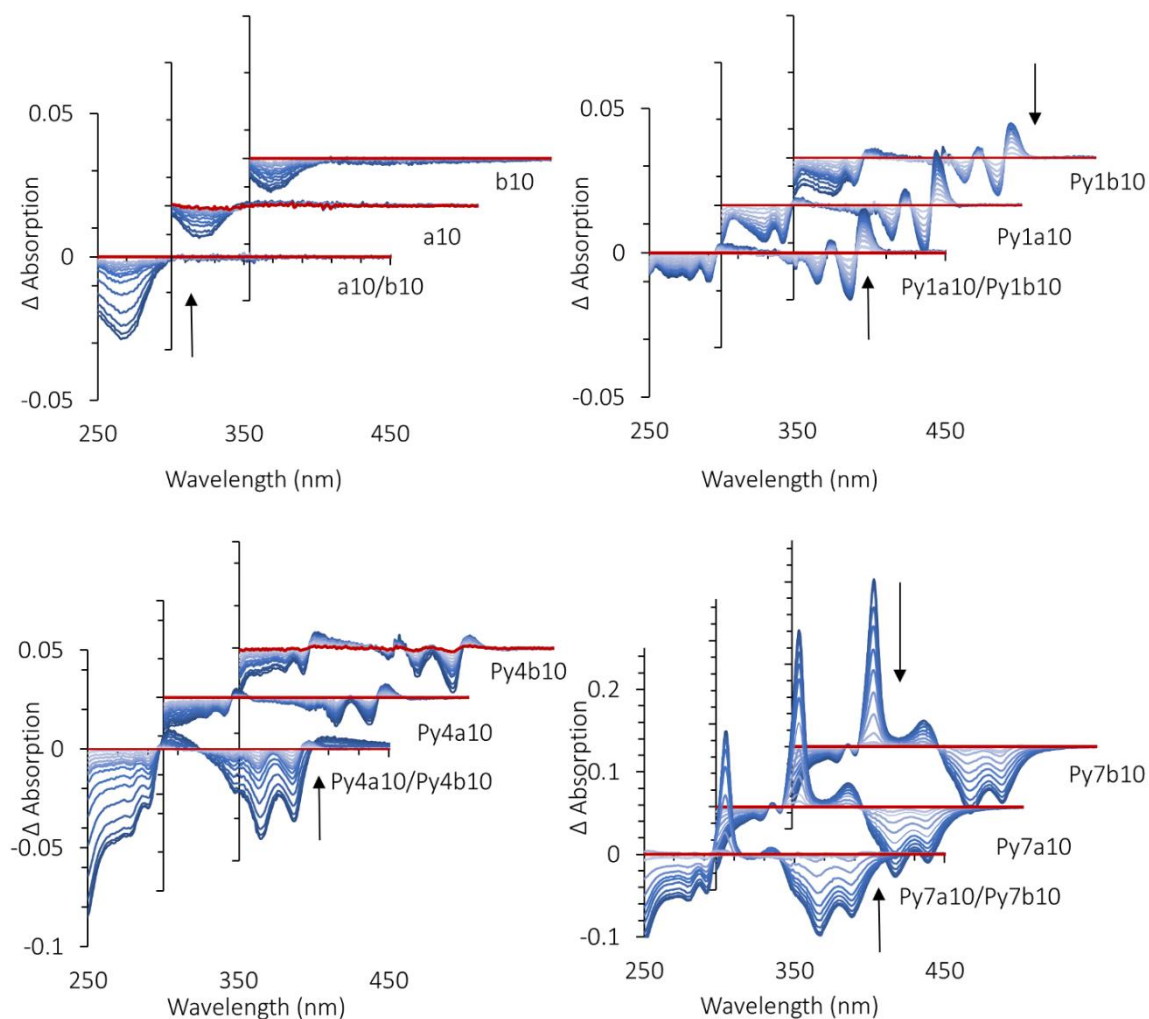


Figure 2-2. Temperature-dependent changes (Δ Absorption = Abs. T° - Abs. 90°) in the absorption spectra; the direction of arrows indicates increasing temperature (20°C \rightarrow 90°C). Conditions: oligomer concentration 2 μ M, 10 mM phosphate buffer, pH = 7, 100 mM sodium chloride.

Investigation of the samples after cooling to room temperature by atomic force microscopy (AFM) on APTES-modified mica surface reveals the formed polymers. Oligomers **Py1a10**, **Py1b10**, **Py4a10** and **Py4b10** assembled into small nm-scale spherical objects (Figure 2-4). Whereas, the polymers made of strands comprising seven pyrenes exhibit a one-dimensional (1D) shape (Figure 2-5). They appear as rod-like objects, which are highly uniform

concerning their thickness (2.5 ± 0.2 nm) (Figure 2-3). Clusters of individual ribbons could occasionally be observed. The cross-section analysis (Figure 2-3 B) of an accidental overlay of two ribbons indicates that such an overlap leads to a doubling of the thickness measured. Moreover, laterally-connected ribbons may be found, but their fraction is rather small.

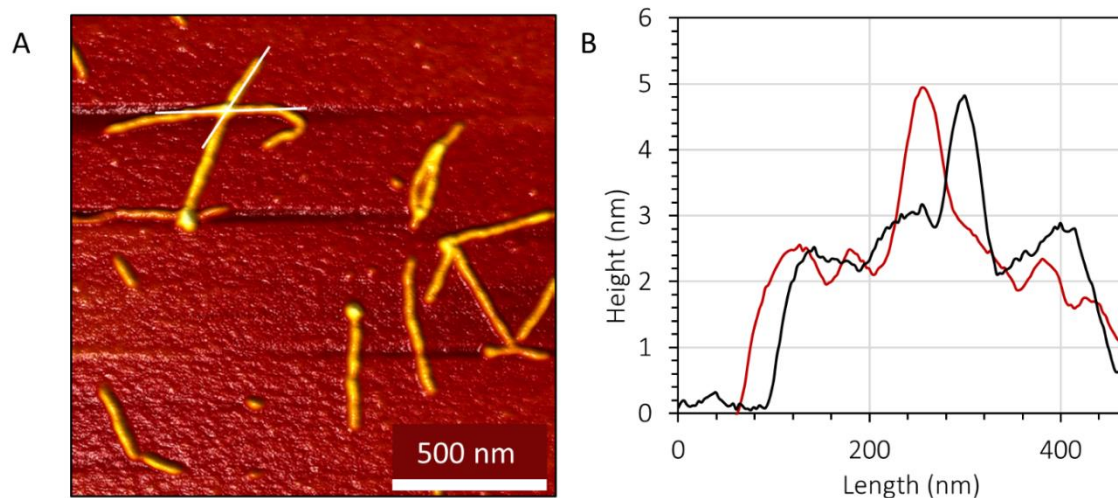


Figure 2-3. AFM image (A) and cross-section analysis (B) of the self-assemblies of **Py7a10/Py7b10**. Conditions: 10 μ M total strand concentration, 10 mM phosphate buffer, 250 mM sodium chloride.

The length of the nanoribbons considerably depends on the ionic strength of the solution and the overall concentration of the monomers. For example, the self-assembly of 0.2 μ M solution of DNA amphiphiles in 100 mM NaCl media leads to the formation of non-defined aggregates (Figure 2-5 A). Upon increasing the NaCl concentration to 250 mM and the strand concentration to 5 μ M, the length of the aggregates gradually increased to 500 nm.

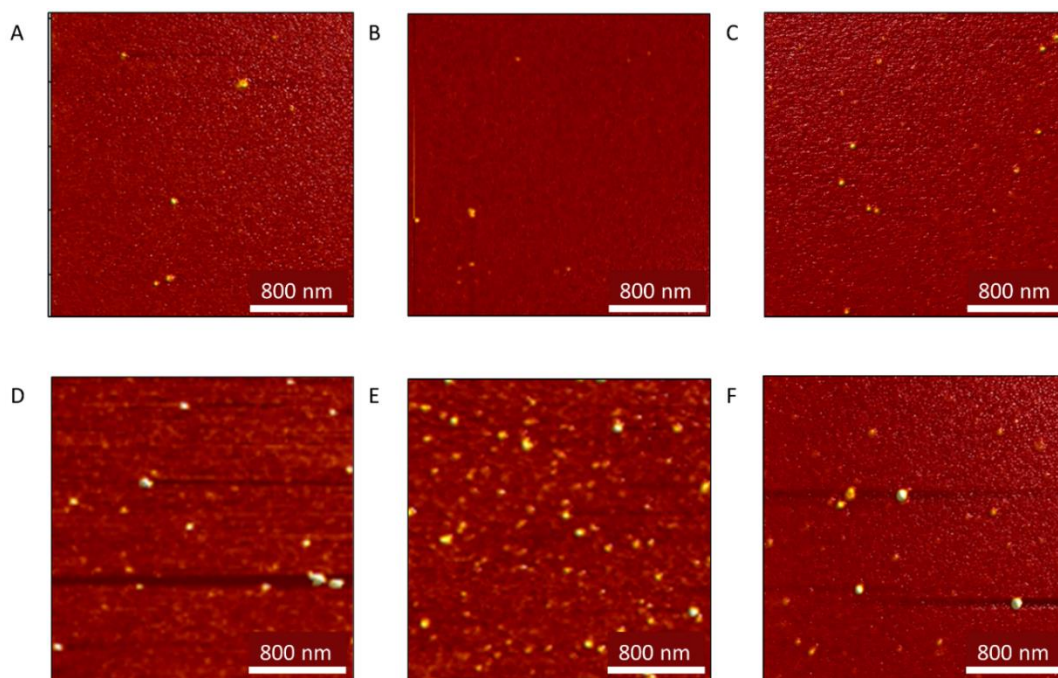


Figure 2-4. AFM images of the self-assemblies of 2 μM oligonucleotides **Py1a10/Py1b10** (A), **Py1a10** (B), **Py1b10** (C), **Py4a10/Py4b10** (D), **Py4a10** (E), **Py4b10** (F) in 100 mM NaCl, 10 mM phosphate buffer (pH=7).

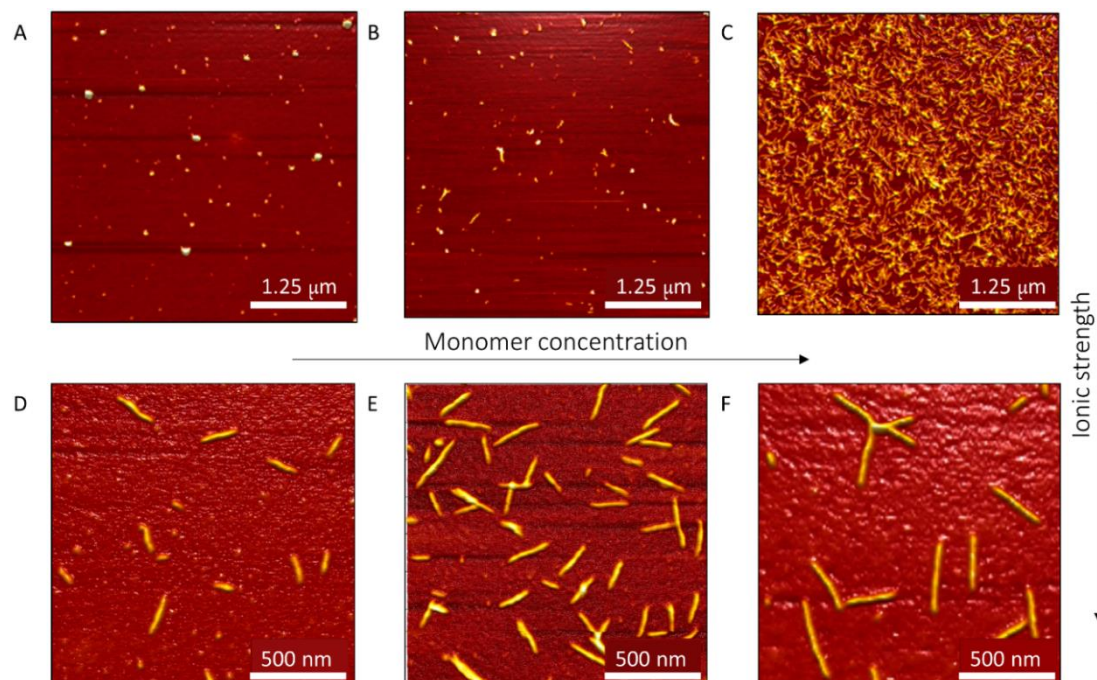


Figure 2-5. AFM images of the self-assemblies of **Py7a10** in 100 mM (A-C) and 250 mM (D-F) NaCl, 10 mM phosphate buffer (pH=7). The overall concentration of the monomers: 0.2 μM (A, D), 1 μM (B, E) and 5 μM (C, F).

Remarkably, the same type of polymers is also formed from a solution containing a 1:1-mixture of oligomers **Py7a10** and **Py7b10** (Figure 2-6 A, D). These observations indicate that the interaction between the pyrene segments outweighs the base pairing interactions between the complementary DNA strands.

Interestingly, the 1D polymers formed from oligomers **Py7a10** and/or **Py7b10** exhibit an apparent helical structure. The helical pitch can be determined by tracking the thickness of the objects along their contour (Figure 2-7).

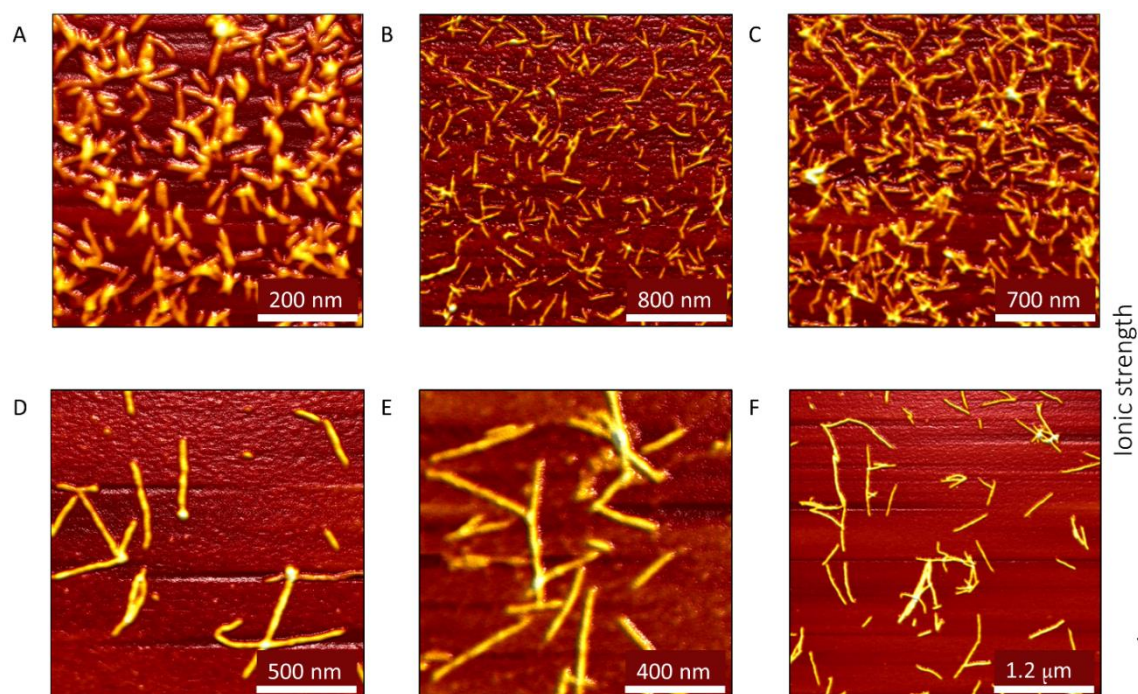


Figure 2-6. AFM images of the self-assemblies of 10 μM of **Py7a10/Py7b10** (A, D), **Py7a10** (B, E) and **Py7b10** (C, F) in 100 mM (A-C) and 250 mM (D-F) NaCl, 10 mM phosphate buffer (pH=7).

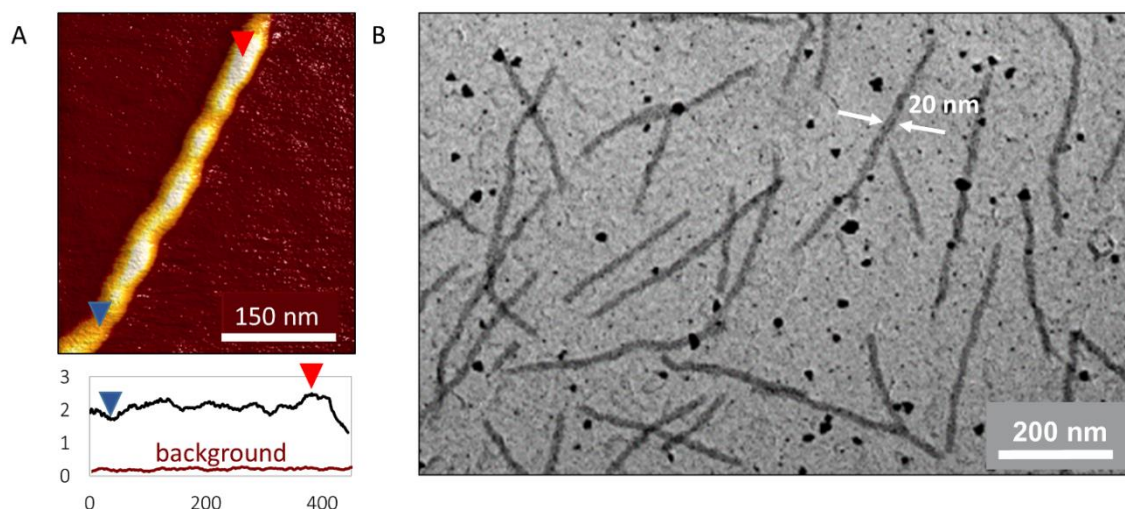


Figure 2-7. AFM (A) and TEM (B) images of supramolecular polymers formed from 10 μM of **Py7a10/Py7b10**. (A bottom: trace of polymer height profile). Conditions: 10 mM phosphate buffer, pH 7, 250 mM NaCl.

Statistical evaluation of the peak-to-valley profiles renders an average pitch value of 50 ± 15 nm (Figure 2-8). Transmission electron microscopy (TEM) was used as an additional tool to visualize the DNA-grafted supramolecular polymers on the surface (Figure 2-7). The TEM images of the **Py7a10/Py7b10** self-assemblies provide further evidence that the aggregates exist as helical ribbons. The ribbons appear on the carbon-coated copper grid as elongated 1D objects with a width of 19 ± 2 nm.

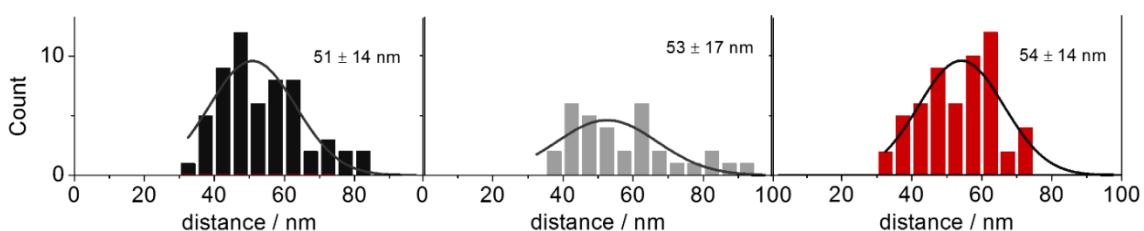
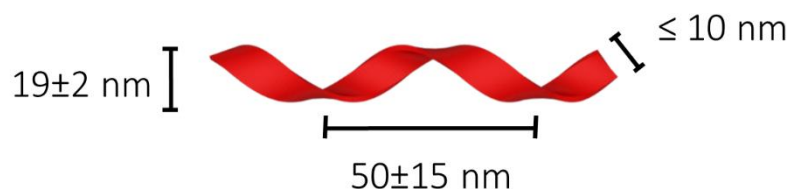


Figure 2-8. Distribution of the distance between pitches of the supramolecular polymers **Py7a10** (black), **Py7a10/Py7b10** (gray), **Py7b10** (red) in 250 mM NaCl.

Scheme 2-3. Proposed schematic illustration of the dimensions of the self-assemblies.



The handedness of the formed aggregates cannot be distinguished clearly by AFM. The objects are relatively small compared to the radius of curvature at the apex of the tip and can appear to have artificially-induced handedness. As an additional method to determine the helicity of the structures, CD experiments were performed. However, they demonstrated a weak chiroptical response in a pyrene part (Figure 2-9). These results could originate from the increased flexibility of the ribbons. Therefore, the claims on relative helicity could be wrongly interpreted by the techniques used.

The polymerization process of **Py7a10** and a 1:1-mixture of **Py7a10/Py7b10** was investigated in more detail by temperature-dependent UV/vis studies. Figure 2-10 shows the degree of polymerization (α_{agg}) as monitored by the development of the J-band (305 nm). A substantial hysteresis is present (~ 12 °C at $\alpha_{agg}=0.5$) between melting and annealing curves. To minimize kinetic effects, the heating/cooling curves were recorded using a low-temperature gradient (0.1 °C/min). Further time-dependent isothermal UV-vis measurements did not reveal any significant changes in the spectroscopic and morphological properties of the supramolecular assemblies.

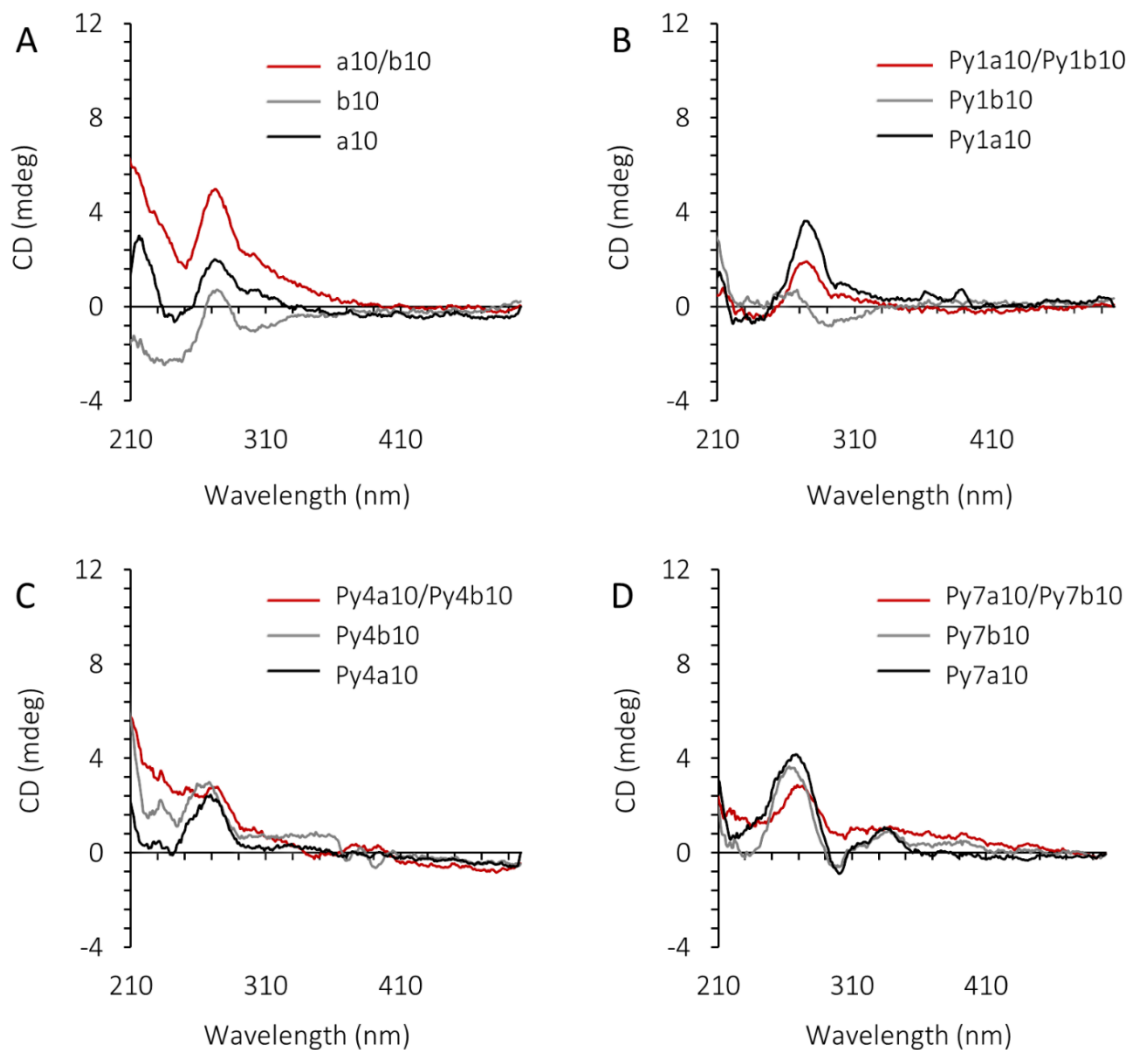


Figure 2-9. CD spectra of the 2 μM single and binary component aggregates in 100 mM NaCl, 10 mM phosphate buffer at 20 $^{\circ}\text{C}$.

The shapes of the curves for both, single- and binary-component system, are similar and exhibit the typical features of a cooperative nucleation-elongation mechanism. The cooling curves were fitted to the described theoretical model.¹⁵⁰ The derived elongation temperature (T_e) is approximately 51 ± 1 $^{\circ}\text{C}$ for both systems under the conditions used (see Experimental Section). Upon increasing ionic strength of the solution, the elongation temperature is also increased (Figure 2-25 Experimental Section).

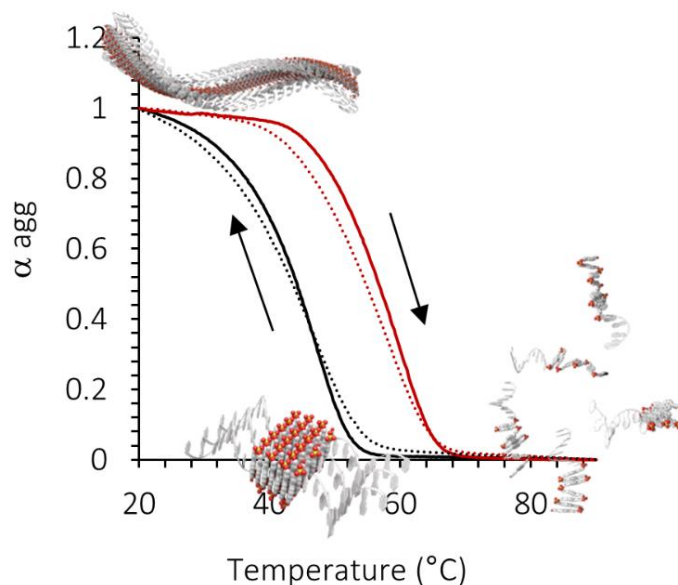
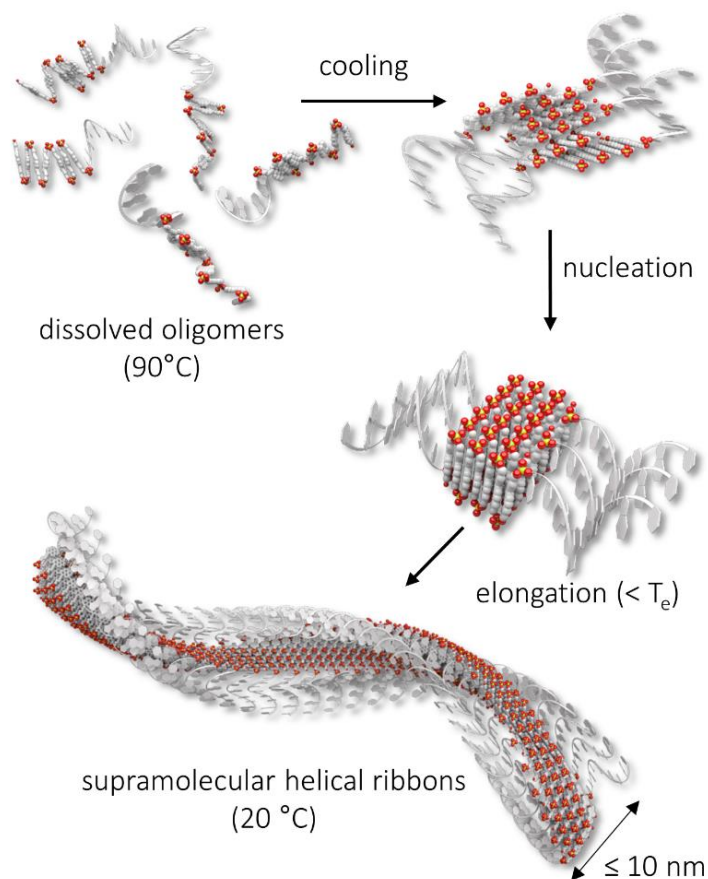


Figure 2-10. Heating (red) and cooling (black) curves recorded with a solution of **Py7a10** (dotted) or a 1:1-mixture of **Py7a10/Py7b10** (solid); the direction of arrows indicates a change of temperature. Conditions: 2 μM total strand concentration, 10 mM phosphate buffer, 100 mM sodium chloride; temperature gradient: 0.1 $^{\circ}\text{C}/\text{min}$.

The proposed model for the formation of DNA-grafted supramolecular polymers by cooperative self-assembly is illustrated in Scheme 2-4. At elevated temperatures, oligomeric molecules (**Py7a10** and/or **Py7b10**) exist as molecularly dissolved chains. Upon cooling, the oligomers tend to self-assemble to form small aggregates. The interaction between individual strands is driven by hydrophobic and stacking interactions of pyrene residues. Further cooling leads to the formation of nuclei that serve as templates for elongation of polymers. Fitting the curves according to the nucleation-elongation theory allows an estimation of the number (N) of oligomers required to form a nucleus. For both types of systems, the number of oligomers required to form the nucleus is ~ 7 (Figure 2-22 and Figure 2-23 Experimental Section). The continued addition of oligomers to the nuclei occurs in a cooperative manner and leads to the formation of the helical ribbon structures.

Scheme 2-4. Illustration of the formation of DNA-grafted supramolecular polymers from chimeric DNA-pyrene oligomers via a nucleation-elongation process.



Importantly, nucleation occurs at temperatures considerably higher than the melting temperature T_m of the DNA hybrid formed of the two complementary oligodeoxynucleotides **a10/b10** ($T_m = 37^\circ\text{C}$, Figure 2-24 Experimental Section). Furthermore, spectroscopic and microscopic properties of single- and double-component mixtures (i.e. polymers formed from **Py7a10** or **Py7b10** alone or a 1:1-mixture of both) are minor. These results provide further strong evidence that the formation of the supramolecular polymers is mainly driven by intermolecular interactions between the pyrene segments and interactions between the nucleotide segments – even canonical base pairing interactions – play a minor role. On the other hand, the stability of the

polymers is also strongly dependent on the length of the pyrene stretch. When the number of pyrenes is reduced, such as in oligomers **Py1a10**, **Py1b10**, **Py4a10** or **Py4b10**, no polymers of comparable length or shape can be observed by microscopic methods. This is paralleled by UV/vis data as shown in Figure 2-11. Oligomers containing four instead of seven pyrenes exhibit only an ill-defined J-band upon changing the temperature from 90 °C to 20 °C. If only a single pyrene is appended to the oligonucleotide, the J-band is not observed at all.

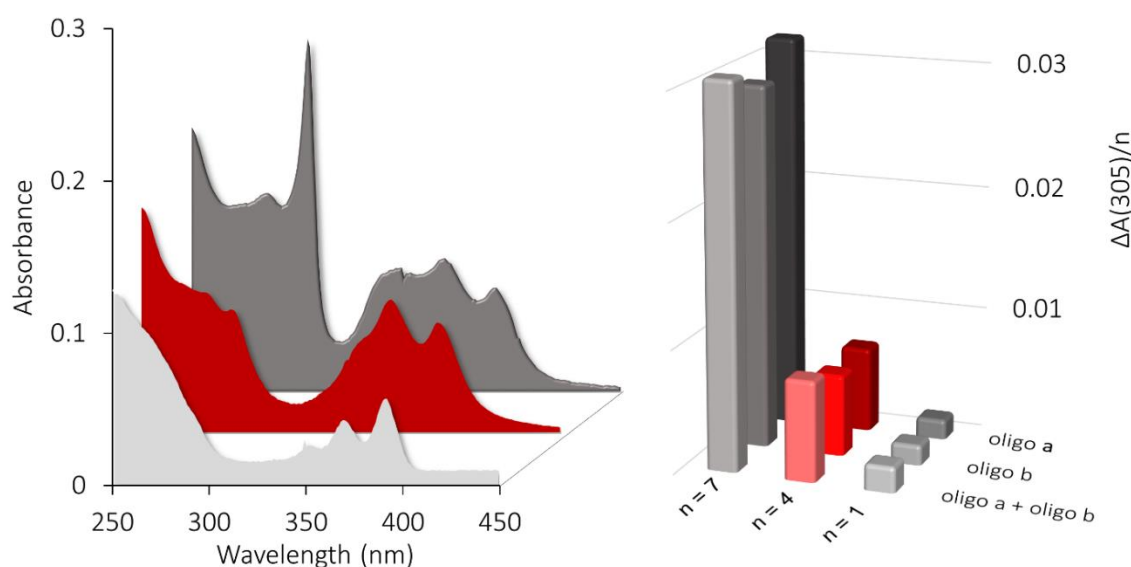


Figure 2-11. Left: UV/vis for the binary mixtures **Py1a10/Py1b10** (dark grey), **Py7a10/Py7b10** (red) and **Py7a10/Py7b10** (light grey) at 20°C. Right: changes in absorbance at 305 nm (J-band) per pyrene unit (n) upon heating the oligomer solutions from 20°C to 90°C. Conditions: 2 μ M total strand concentration, 10 mM phosphate buffer, pH 7, 100 mM NaCl.

To study the ability of the pyrene-DNA amphiphiles with a longer pyrene chain to self-assemble into defined structures, a **Py10b10** conjugate was synthesized. It comprises ten pyrene units and an identical DNA sequence. The self-assembled **Py10b10** exhibits common for the aggregated pyrenes spectroscopic and microscopic characteristics (Figure 2-12). Upon slow cooling, J- and H-bands with maxima at 305 nm and around 340 nm were observed (Figure 2-12 D inset). The CD spectrum measured at 20 °C showed only weak

signals in the regions specific for DNA (below 300 nm) and pyrenes (above 300 nm) (Figure 2-12 E).

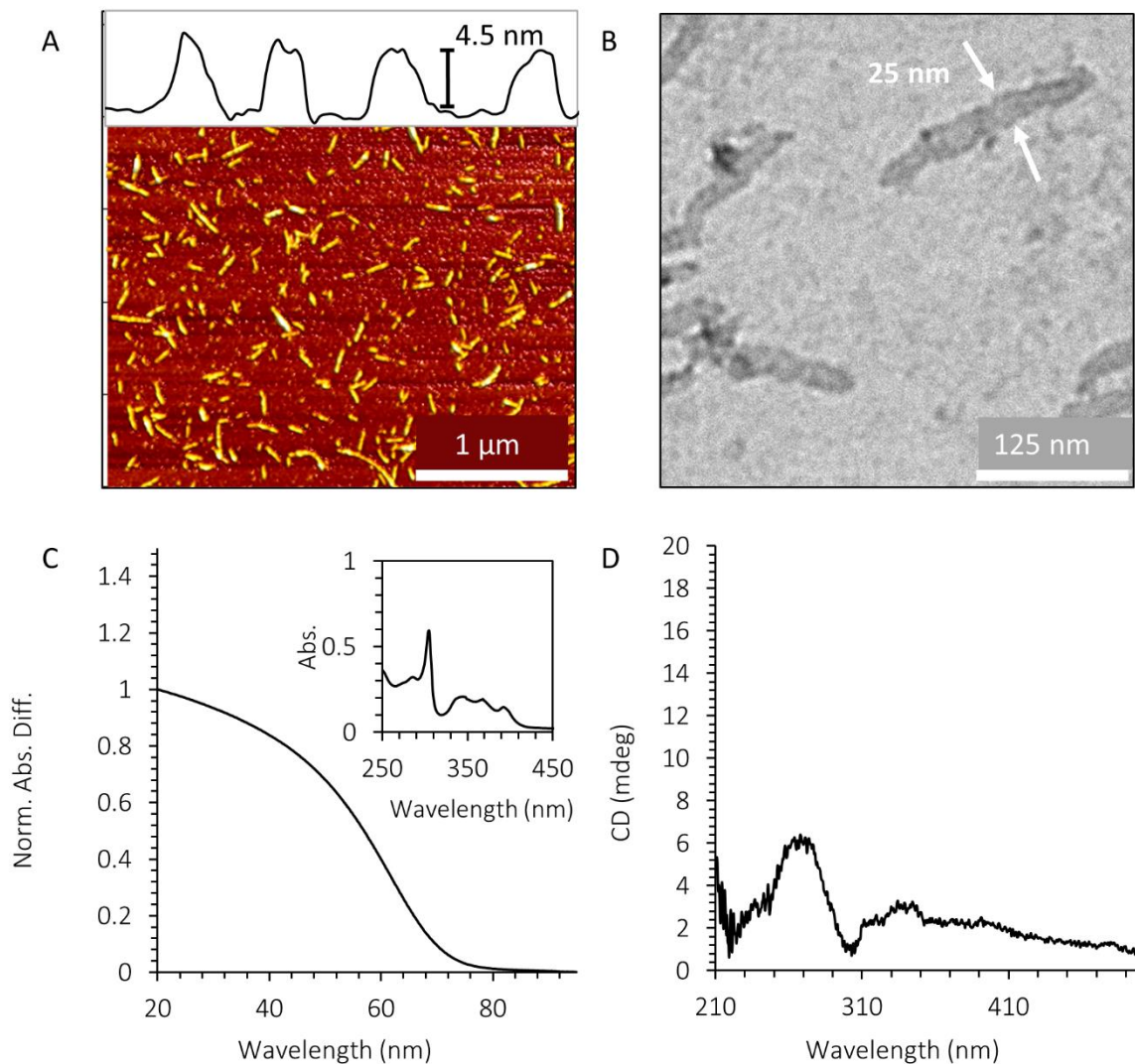


Figure 2-12. AFM (A) and TEM (B) images of the self-assemblies of **Py10b10**. D: Cooling curve for the 2 μM solution of **Py10b10** in 50 mM NaCl, 10 mM PBS, pH=7; inset picture shows absorption spectra of the solution of self-assemblies after preparation. E: CD spectra of the solution of **Py10b10**.

Further microscopic studies revealed the formation of elongated ribbon-like structures with the thickness of 4.5 nm (Figure 2-12 A). The width of 25±2 nm determined by TEM analysis (Figure 2-12 B) is close to the estimated DNA-pyrene-DNA distance (assuming the stacking distance of 0.34 nm). The latter

parameter was estimated to be 11 ± 2 nm; it is strongly dependent on the type of oligonucleotide folding.

Fluorescence spectroscopy provides additional information on the nature of the DNA-grafted supramolecular polymers. The fluorescence spectra of **Py7a10**-and/or **Py7b10**-derived 1D ribbons reveal a combination of pyrene monomer and excimer emission (Figure 2-13). The pyrenes are confined in a rigid network of ladder-type folded oligomers. This reduces the probability of pyrenes to form excimers. Therefore, a relatively large part of the relaxation occurs via monomer emission leading to monomer and excimer signals of comparable intensity for the polymers. In comparison, samples containing oligomers **Py4a10** and/or **Py4b10** do not form equally well-defined aggregates; the pyrenes are conformationally less restricted and exhibit predominantly excimer emission.

The self-assembly of lipid-modified DNA hybrids has been intensively studied. Most morphological experiments reveal the formation of micelles or vesicles.^{121,151–154} The controlled formation of one-dimensional DNA-grafted platforms, however, is rather unusual.^{94,155,156} It is also noteworthy that the 1D-shape of the polymers described here is in sharp contrast to the two-dimensional (2D) polymers formed by pyrene trimers.^{47,140} The confinement of polymeric growth in one direction is explained by the presence of the oligonucleotide attached to one end of the oligopyrenes strand. Supramolecular polymerization is driven by hydrophobic and stacking interactions between the pyrenes. Due to the presence of the negatively charged edges, the growth of the polymers can take place only in a planar way. The presence of the DNA strand represents a further delimitation and directs the addition of subsequent pyrene oligomers in a linear (or quasi-linear) way as illustrated in Scheme 2-4. For reasons of repulsive forces between the negatively charged individual DNA strands it can be reasonably assumed that they are positioned along either side of the ribbon-like pyrene polymer with more or less equal distribution.

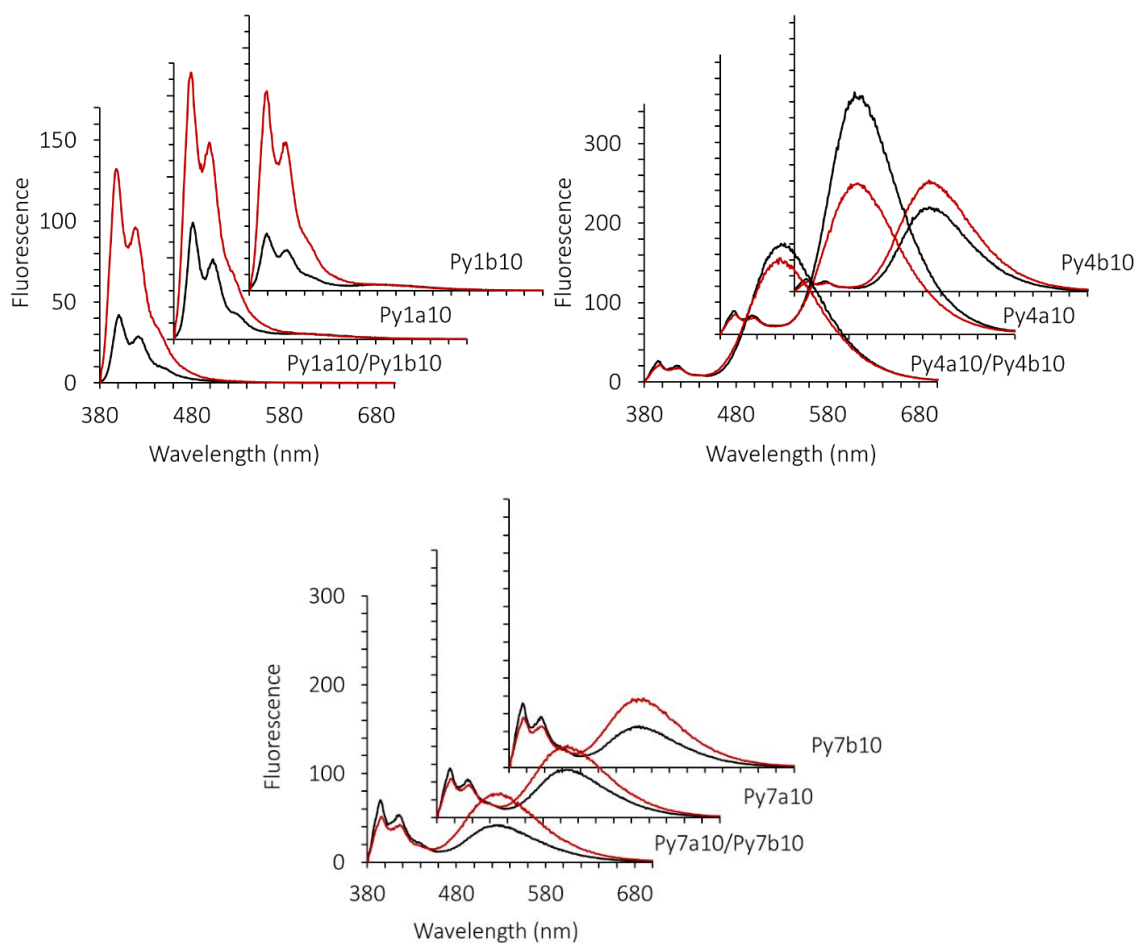


Figure 2-13. Fluorescence spectra for single component self-assemblies and 1:1 binary mixtures (excitation wavelength = 365 nm) at 20 °C (black) and at 95 °C (red). Conditions: 2 μ M total strand concentration, 10 mM phosphate buffer, pH 7, 100 mM NaCl.

2.2.1.2 Dependence of the self-assembly on the length of the DNA chain

In the current section, we demonstrate that the self-assembly of DNA-linked pyrene oligomers (Figure 2-14) can lead to one- or two-dimensional supramolecular polymers in aqueous solution. The morphology of the polymers is controlled by the length of the DNA moiety.

Oligophosphodiester **Py7b1N-Py7b20** were prepared via solid-phase synthesis using phosphoramidite chemistry as described previously (Figure 2-14). The

assemblies are formed from oligomers containing a single nucleotide, whereas two or more conjugated nucleotides lead to 1D ribbons of variable length.

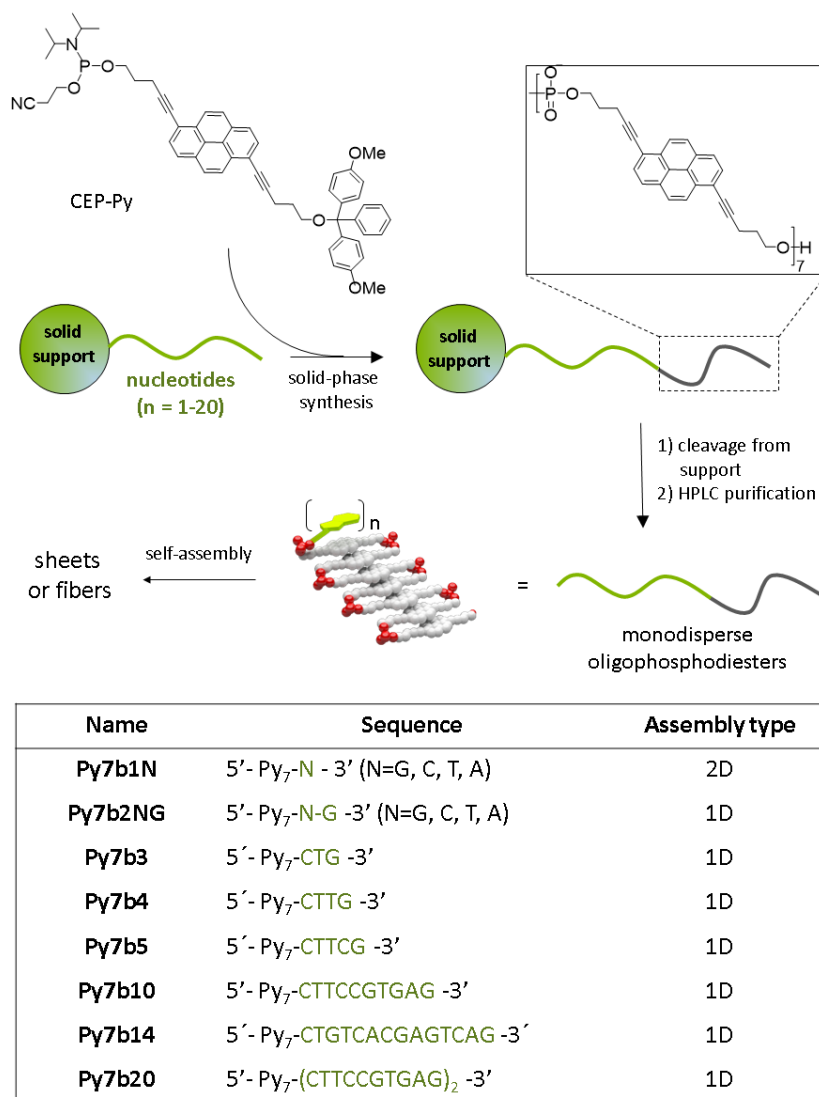


Figure 2-14. Preparation of monodisperse oligophosphodiester (deoxynucleoside in green, phosphates in red, pyrenes in grey) via solid-phase synthesis using CEP-Py. Table: sequences of oligomers and morphology of self-assembly.

All oligomers consist of a heptapyrenotide moiety conjugated to the 5'-end of an oligonucleotide or, in case of **Py7b1N**, a single nucleotide. Supramolecular polymerization occurs during slow cooling of an aqueous solution of the oligomers. Self-assembly is driven by aromatic stacking interactions of pyrenes.

The number of nucleotides, in turn, determines the type of morphology, fibrillary or planar, of the supramolecular polymers.

Two-dimensional supramolecular polymers are formed via annealing of **Py7b1N** from 90 °C to 20 °C in the aqueous buffer using a cooling rate of 0.1 °C/min. The formation of ordered pyrene arrays is confirmed by the appearance of the characteristic J- (305 nm) and H-bands (335 nm) in the UV-vis spectrum (Figure 2-15 A). The bands originate from the exciton interactions between ladder-folded 1,6-substituted pyrenes. Upon cooling, the intensity of the 305 nm band increases, which reflects the cooperative formation of **Py7b1N** supramolecular polymers (Figure 2-15 B). Furthermore, the CD spectrum of **Py7b1G** at 20 °C exhibits a strong exciton-coupled signal (-307 nm/+303 nm) in the region of the J-band (Figure 2-15 C, black).

The bisignate signal disappears upon heating the assemblies above 80 °C (Figure 2-15 D). Self-assembled **Py7b1T** exhibits a similar but weaker CD signal at -307 nm/+303 nm. The CD spectra of **Py7b1A** and **Py7b1C** are almost silent at 20°C. Despite different chiroptical properties, microscopic data unambiguously confirmed the self-assembly of all oligomers **Py7b1N** into 2D supramolecular polymers. AFM experiments show an apparent thickness of ~2 nm for the planar assemblies after deposition onto APTES-modified mica surface (Figure 2-16).

Obviously, a single nucleotide is compatible with a 2D aggregation of pyrenes as illustrated in Figure 2-16. Furthermore, the interaction between the chiral nucleotide and the stacked pyrenes can induce the strong exciton-coupling of pyrene chromophores observed in the CD spectrum. These interactions are highly sensitive to the structure of the conjugated nucleobase, providing a route to modulate the chiroptical response in 2D supramolecular materials.

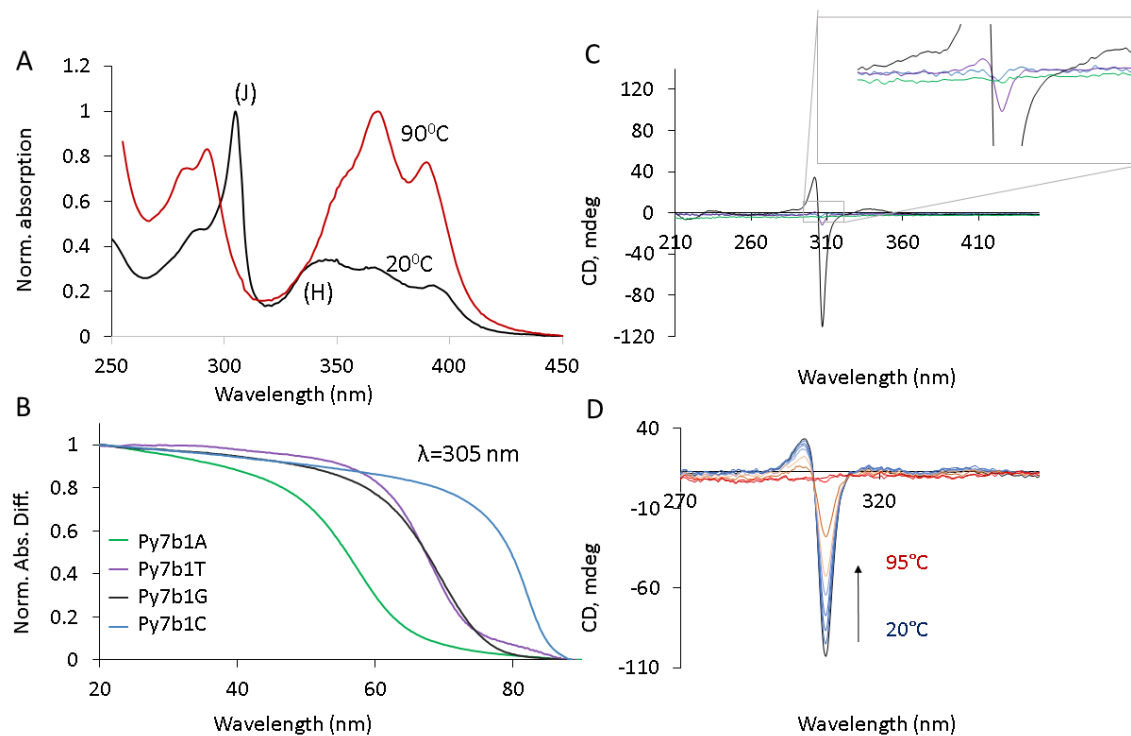


Figure 2-15. A: Representative UV-vis spectra of **Py7b1N** at 20°C and 90°C. B: Temperature-dependent change of absorbance of **Py7b1N** observed at 305 nm (cooling rate: 0.1 °C/min). C: CD spectra of **Py7b1N** at 20 °C (inset: a zoomed region for the CD signals). D: Temperature-dependent CD spectra for 2 μ M **Py7b1G** upon heating from 20 °C (black) to 95 °C (red) in 10 °C steps. Conditions: 2 μ M total strand concentration, 10 mM phosphate buffer, pH 7, 10 mM NaCl

In contrast to **Py7b1N**, chimeric oligomers containing two or more nucleotides (**Py7b2NG-Py7b20**) all form one-dimensional supramolecular polymers in a temperature controlled annealing process. The presence of J- and H-bands at 305 nm and 335 nm in the UV-vis spectra at 20 °C confirm the formation of ordered pyrene arrays by all oligomers. In order to have an elongation phase of supramolecular polymerization around 80 °C, the ionic strength of the solution medium was adjusted for each oligomer individually.

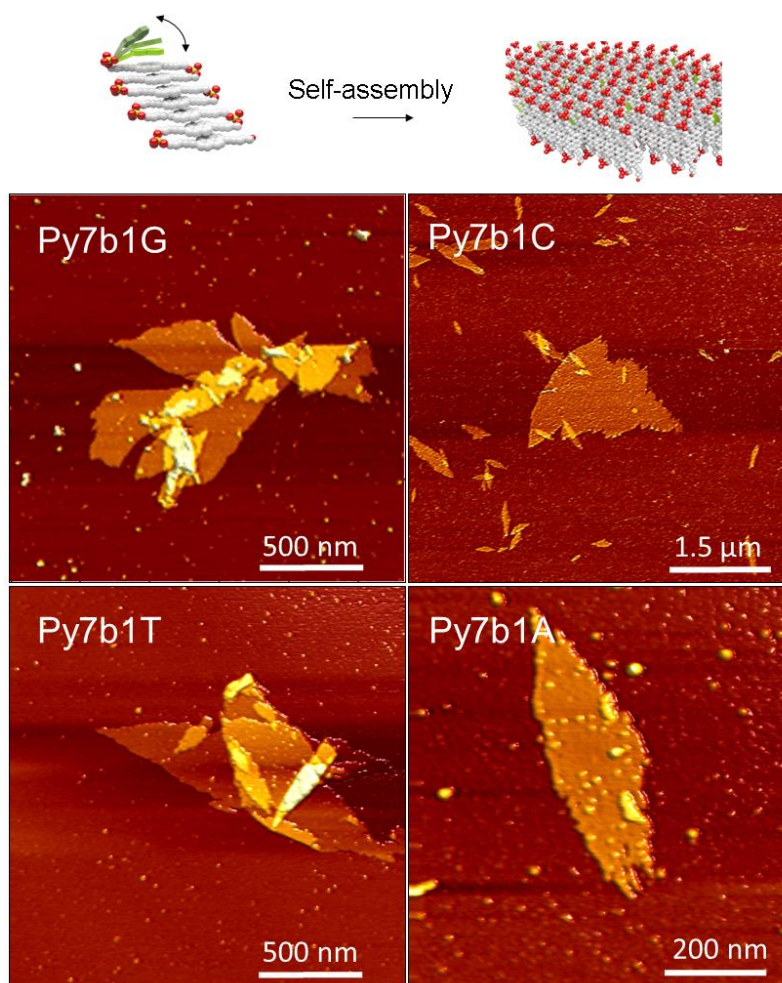


Figure 2-16. Top: Illustration of the self-assembly of **Py7b1N** resulting in the formation of 2D supramolecular polymers. Bottom: AFM images of the different **Py7b1N** oligomers. Conditions: 2 μM total strand concentration, 10 mM phosphate buffer, pH 7, 10 mM NaCl

All temperature-dependent curves depicted in Figure 2-17 A are non-sigmoidal reflecting a cooperative self-assembly process. At 20 °C, CD spectra for the self-assembled **Py7b2NG-Py7b20** contain only weak signals below 300 nm, and the region above 300 nm is almost CD silent (Figure 2-17 B). This is in sharp contrast to the polymers formed by **Py7b1G** and **Py7b1T**. AFM and TEM imaging experiments reveal 1D morphology for the supramolecular polymers of **Py7b2NG-Py7b20**. Significant differences in the length of these linear supramolecular polymers were found. Self-assembly of **Py7b2NG-Py7b5** results in micrometer-long ribbons (Figure 2-18). As determined by AFM

(Figure 2-19), the thickness of the deposited assemblies changes gradually from ~ 1.5 nm for **Py7b2G** to ~ 2.2 nm for **Py7b5**. Oligomer **Py7b10**, however, forms ribbons with a length of a few hundred nanometers only and a slightly larger apparent thickness (~ 2.5 nm). Consistently, the self-assembly of **Py7b14** and **Py7b20** leads to the shortest (tens of nanometers), yet thickest ribbons (~ 3.0 and 3.5 nm, respectively). The increase in thickness throughout the series is in good agreement with the growing length of the DNA segment. The decrease in length of the 1D assemblies, despite the enhanced ionic strength, is rationalized by the repulsion between negatively charged phosphates, which increases with the length of the DNA chains.

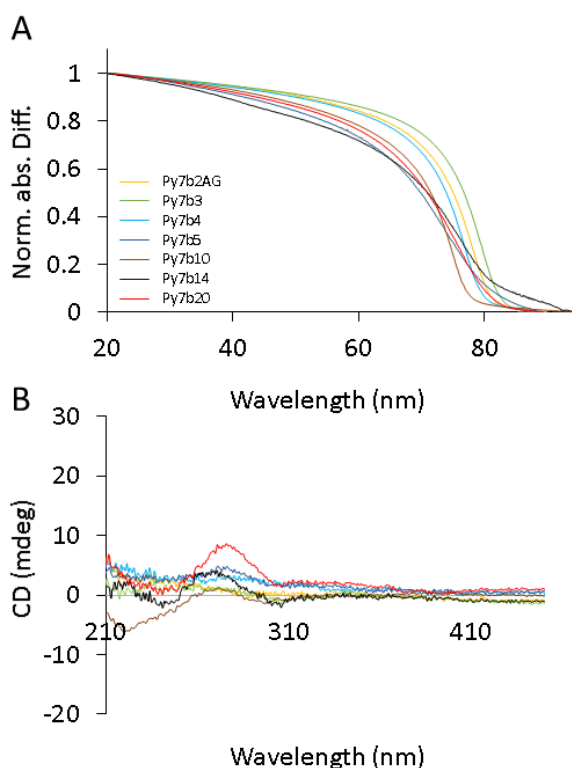


Figure 2-17. A: Temperature-dependent change of absorbance of the oligomers measured at 305 nm using a cooling rate of 0.1 $^{\circ}\text{C}/\text{min}$. B: CD spectra of **Py7b2NG-Py7b20** at 20 $^{\circ}\text{C}$. Conditions: 2 μM total strand concentration, 10 mM phosphate buffer, pH 7, sodium chloride: 100 mM for **Py7b2AG**, 100 mM for **Py7b3**, 150 mM for **Py7b4**, 200 mM for **Py7b5**, 250 mM for **Py7b10**, 250 mM for **Py7b14**, and 350 mM for **Py7b20**.

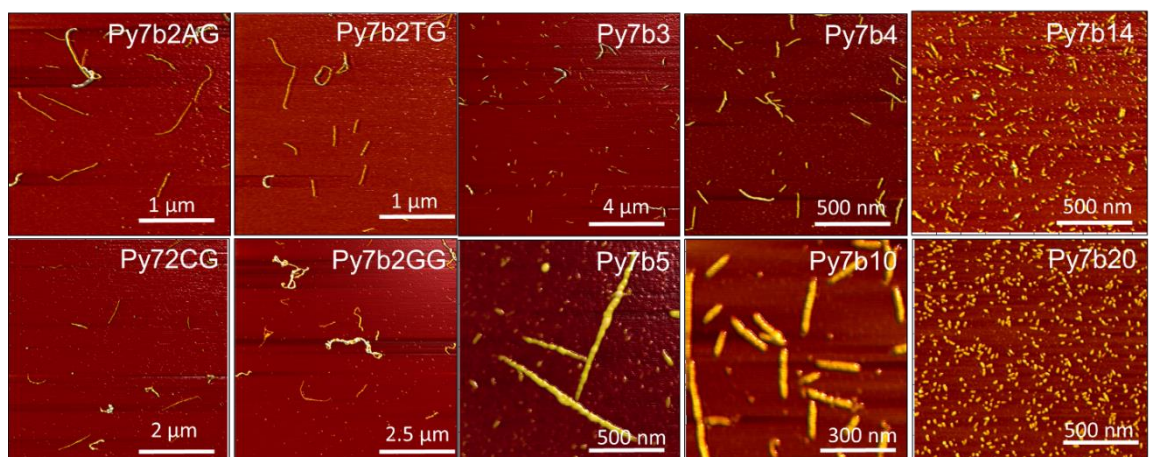
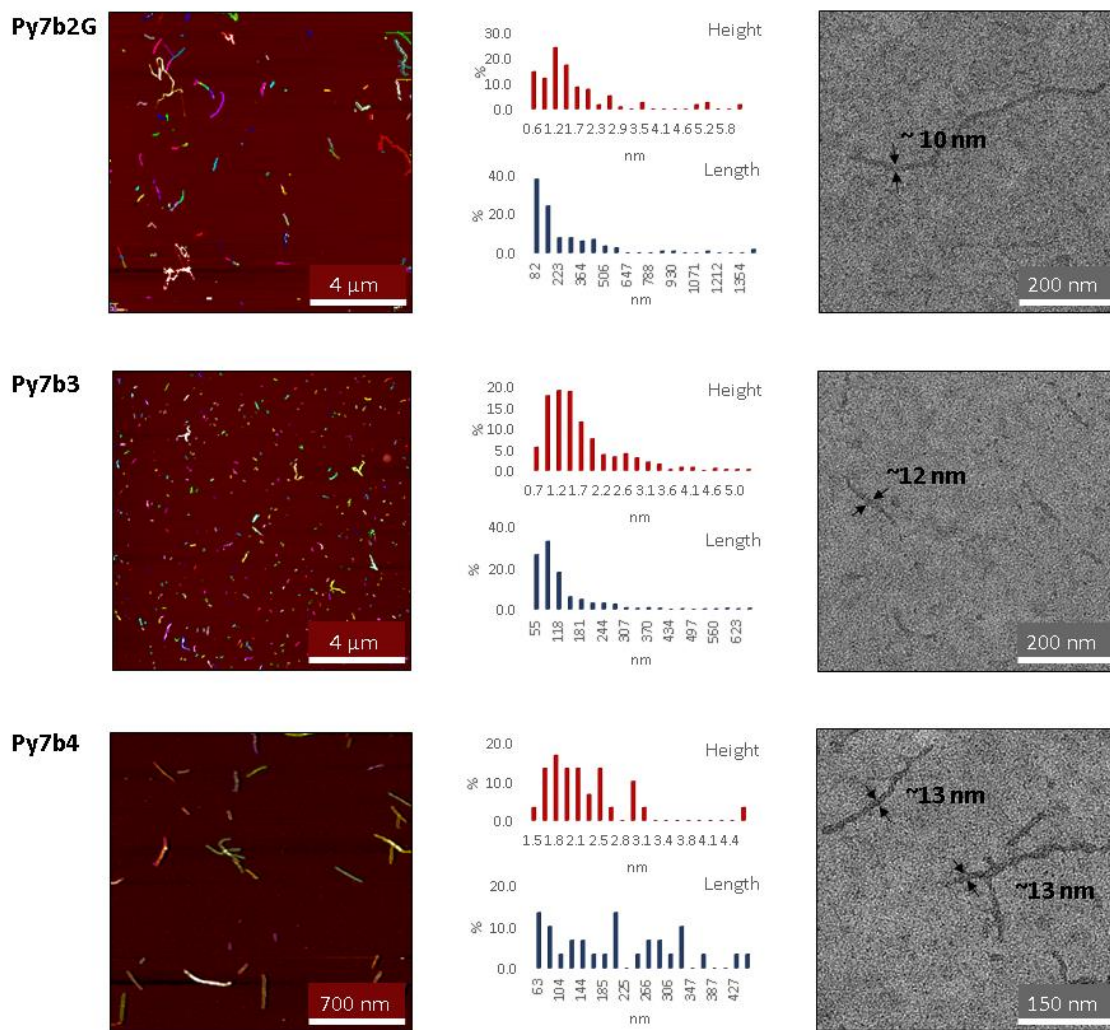


Figure 2-18. AFM images for the supramolecular fibers of Py7b2NG-Py7b20 deposited on amino-modified mica surface.



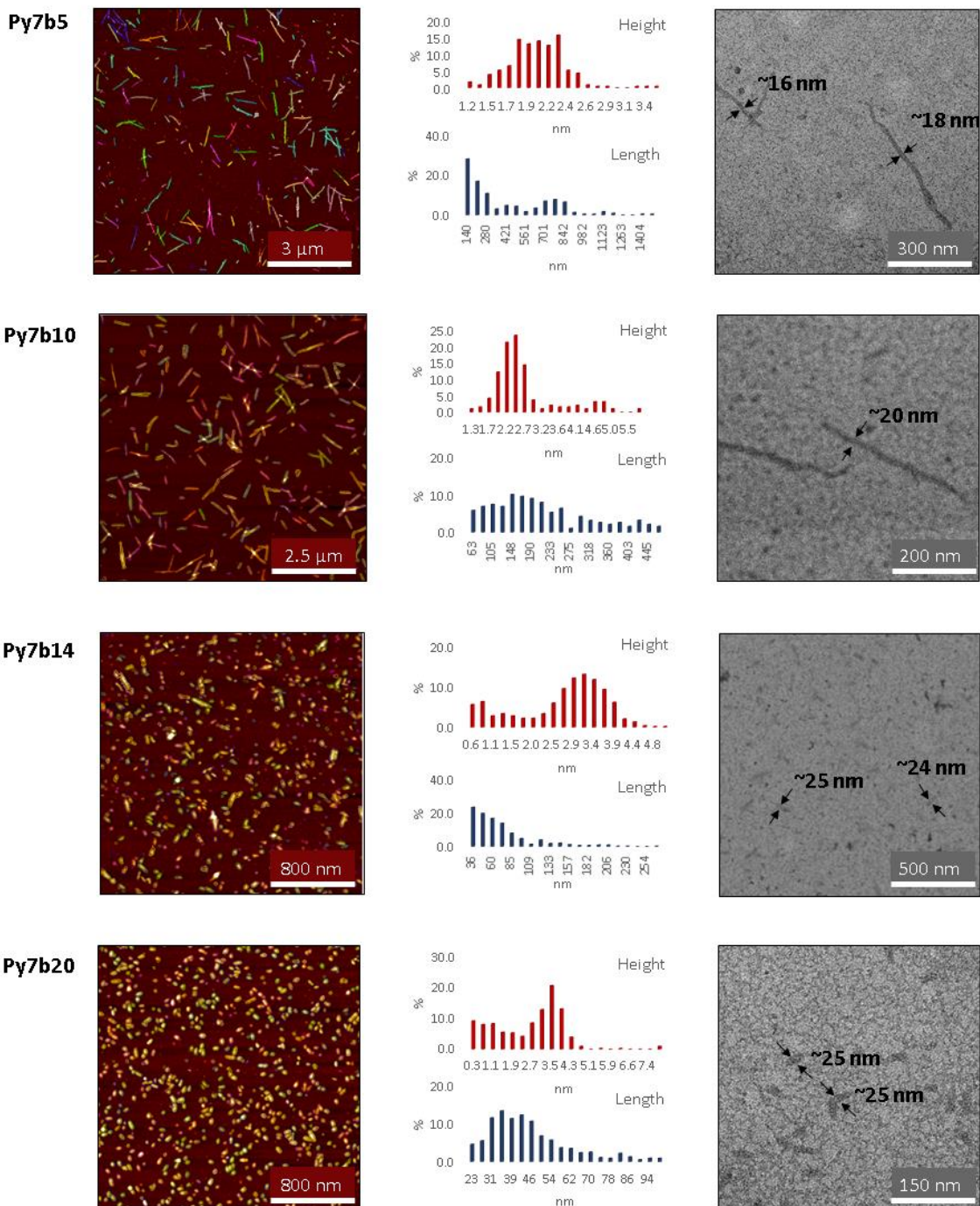
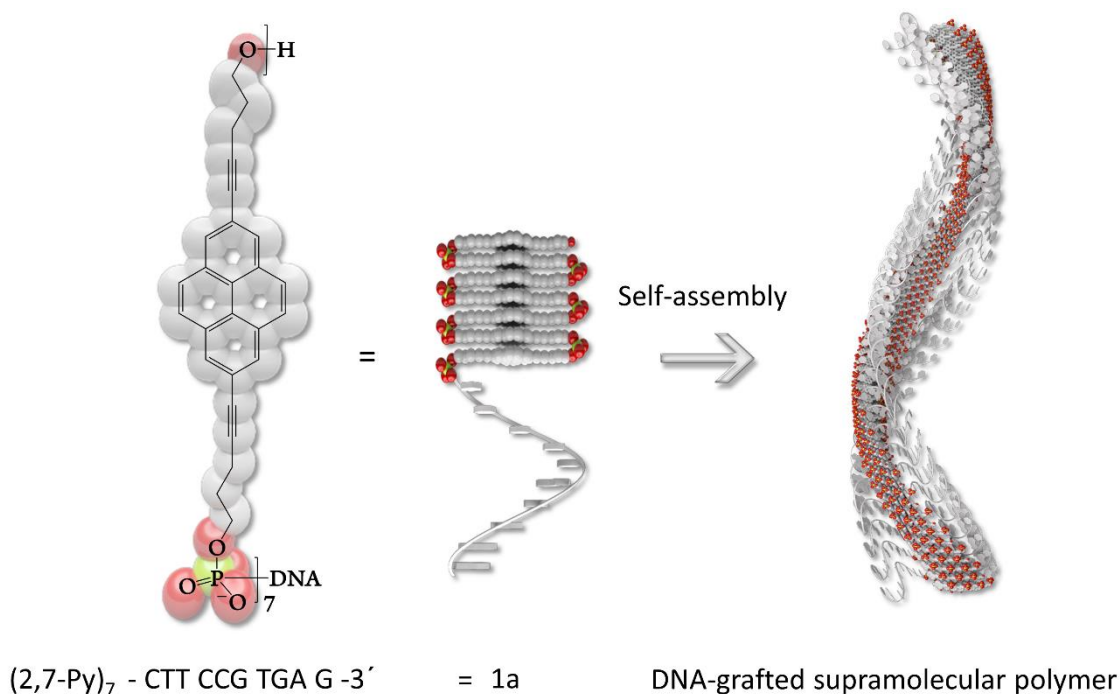


Figure 2-19. AFM images (left), corresponding height and length analysis (middle) and TEM images (right) for the supramolecular polymers.

2.2.2 DNA-pyrene conjugates based on 2,7-modified pentynyl pyrene

In this section, we extend a toolbox of self-assembling motifs leading to DNA-grafted supramolecular assemblies and successfully demonstrate some of their properties. Herein, we introduce a 2,7-dipentynyl substituted pyrene isomer as a convenient unit to form and study chiral DNA-grafted supramolecular polymers. The design of an oligomer **27Py7b10** is depicted in Scheme 2-5. The strand **27Py7b10** consists of seven 2,7-substituted pyrenes conjugated through a phosphodiester bond with a 10nt DNA strand; **27Py7b10** was synthesized using solid-phase synthesis followed by the RP-HPLC purification.

Scheme 2-5. Chemical structure of the 2,7-disubstituted pyrene unit and sequence of pyrene-DNA conjugate **27Py7b10**; illustration of oligomer **27Py7b10** and its assembly into a DNA-grafted supramolecular polymer



The self-assembly of **27Py7b10** was followed by different spectroscopic methods. UV/vis absorption spectra of **27Py7b10** in ethanol correspond to the disassembled, single-chain state (blue line, Figure 2-20 A).¹⁵⁷ In aqueous solution, on the contrary, supramolecular polymerization takes place upon

cooling from 95 °C to 15 °C (0.1 °C/min) and leads to the appearance of a blue-shifted ($\lambda_{\text{max}} = 252$ nm) and a red-shifted band ($\lambda_{\text{max}} = 352$ nm; see Figure 2-20 A, black line). The temperature-dependent UV/vis curve (Figure 2-20 C) shows a cooperative self-assembly process of **27Py7b10** below 90 °C. The fluorescence spectrum of **27Py7b10** at 20 °C displays two maxima at 416 and 443 nm, that are attributed to pyrene monomer emission, and a broad red-shifted band with λ_{max} at 485 nm, which is characteristic for pyrene excimer (Figure 2-20 D). The CD spectrum at 20 °C shows a bisignate signal with negative and positive peaks at 259 and 246 nm, respectively (Figure 2-20 B). The value of zero crossing of the CD signal corresponds to the absorption maximum in the UV-vis spectrum at 252 nm.

The exciton coupled CD spectrum indicates that pyrenes adopt a stable helical conformation with a preferred supramolecular chirality that originates from interactions with the oligonucleotide chains grafted to the polymer.¹⁵⁸ The intensity of the bisignate signal strongly depends on the temperature and grows by cooling from 25 to 15 °C (Figure 2-20 B). Such behavior is expected for chiral supramolecular systems since the conformational flexibility of the assemblies is reduced by lowering the temperature. Importantly, UV/vis spectrum remains essentially unchanged between 25 and 15 °C.

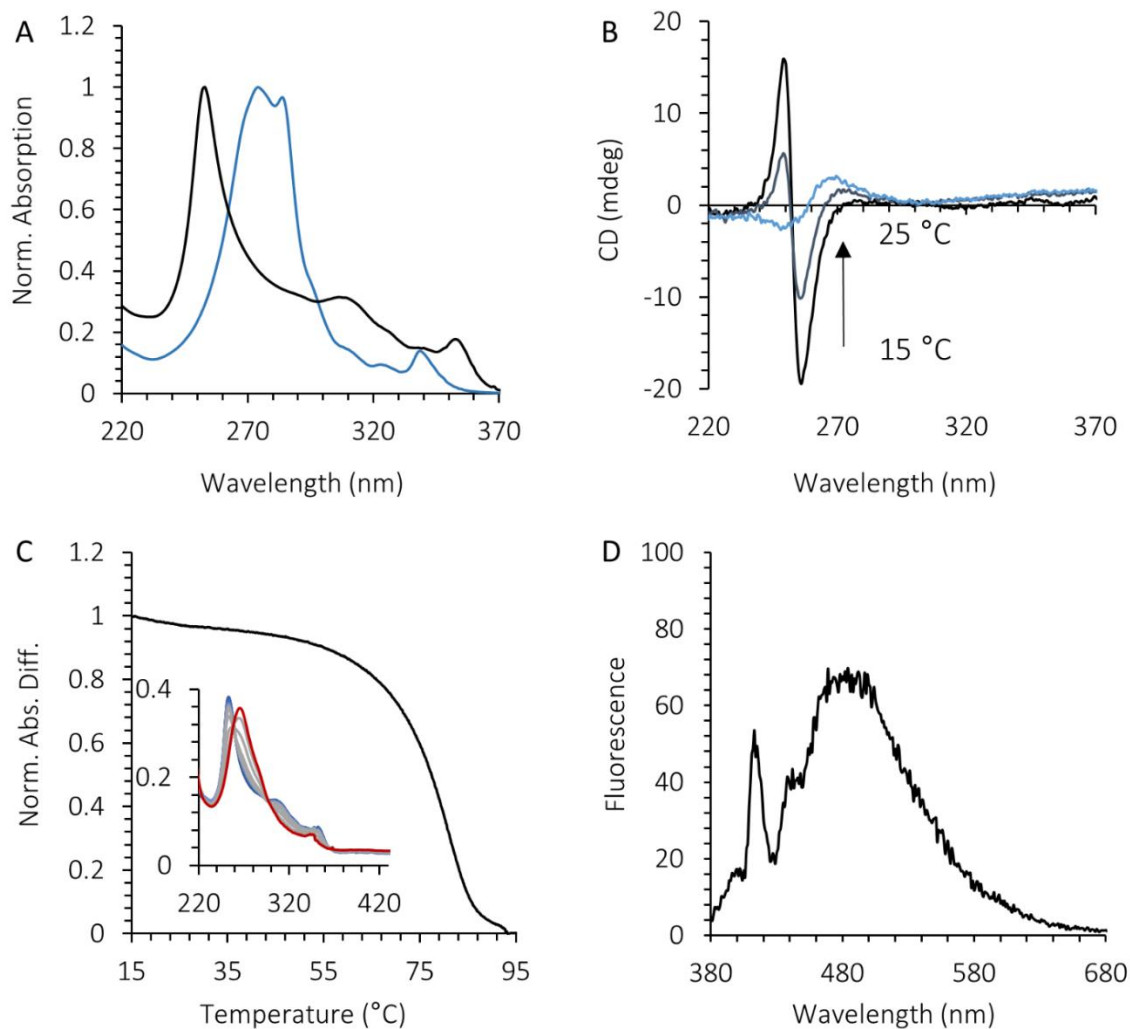


Figure 2-20. A: Absorption spectra of $27\text{Py}7\text{b}10$ in water (black) and ethanol (blue). B: CD spectra of $27\text{Py}7\text{b}10$ in water at 25, 20 and 15 °C. C: Normalized absorption difference of $27\text{Py}7\text{b}10$ against temperature at 252 nm. The inset shows temperature-dependent changes of UV/Vis spectra for $27\text{Py}7\text{b}10$ in water from 90 (red) to 15 °C (blue). D: Fluorescence emission spectrum of the supramolecular polymers $27\text{Py}7\text{b}10$ in aqueous solution at 20 °C ($\lambda_{\text{exc}} = 352$ nm). Conditions: oligomer concentration 2 μM ; aqueous buffer: 10 mM PBS, 150 mM NaCl, pH=7.

Figure 2-21 D displays a TEM image of the supramolecular polymers. $27\text{Py}7\text{b}10$ forms 1D ribbons with a width of 10-15 nm. These results were confirmed by AFM on APTES-modified mica surface (Figure 2-21 A-C). Both microscopic techniques revealed that three types of aggregates are formed during a slow annealing process: 1) ribbons with a length of several

micrometers; 2) ribbons of a few hundred nanometers length; and 3) unresolved aggregates with dimensions below 20 nm. Similar types of pathway complexity have been described for supramolecular polymerization processes.¹⁵⁹ The thickness of aggregates of types 1 and 2 is 2.6 ± 0.1 nm according to AFM analysis.

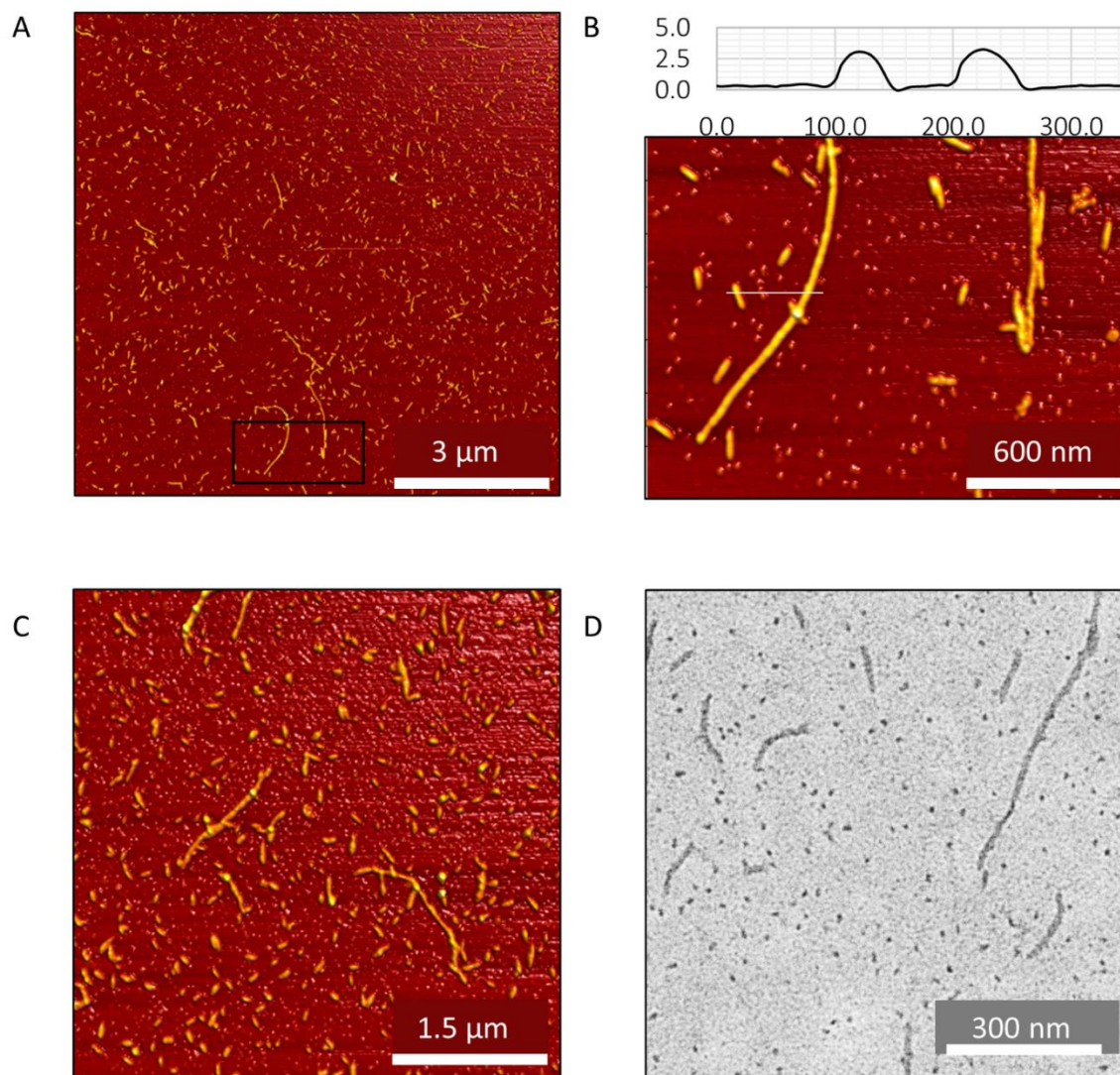


Figure 2-21. AFM images of $27\text{Py}7\text{b}10$ supramolecular polymers on APTES-modified mica surface from aqueous solutions deposited at 20 °C (A) and 4 °C (C). B: zoomed region from image A and cross-section analysis. D: TEM images of DNA-grafted supramolecular polymers of $27\text{Py}7\text{b}10$. Conditions: oligomer concentration 2 μM; aqueous buffer: 10 mM PBS, 150 mM NaCl, pH=7.

2.3 CONCLUSIONS

In summary, we have shown that the self-assembly of chimeric DNA-pyrene oligomers in water into either 1D or 2D supramolecular polymers is governed by the length of the DNA. While the presence of a single terminal nucleotide yields supramolecular nanosheets, longer DNA chains direct the assembly towards the formation of 1D ribbon-like polymers. Oligodeoxynucleotide strands are arranged along the edges of a ribbon-shaped helical aggregate of self-assembled pyrene segments. The length of the polymers can reach up to several hundred nm and depends on the composition of the monomeric unit, ionic strength of the medium and overall concentration of the monomers. Hydrophobic and stacking interactions between intramolecularly folded pyrene chains are the major driving force for the polymerization, which occurs through a nucleation–elongation process. Furthermore, we have demonstrated the design and synthesis of functional DNA-grafted supramolecular polymers from monodisperse di-block oligophosphodiester containing 2,7-linked pyrenes. The DNA strands induce supramolecular chirality to the pyrene arrays, which is manifested by strong exciton coupled CD signals. The findings provide insight into the process of supramolecular polymerization of amphiphilic oligomers in water leading to polymers with different morphology and chiroptical activity. The type of DNA-grafted polymer described here may serve as a model for the development of structurally and functionally diverse supramolecular platforms with applications in materials science and diagnostics. The results demonstrate the value of DNA-grafted supramolecular polymers as versatile, functional platforms by using the dynamic and responsive properties of non-covalent polymers.

2.4 EXPERIMENTAL SECTION

Materials and General Methods.

All chemical reagents and solvents required for the synthesis were purchased from commercial suppliers (Aldrich, Glen Research,

Proligo® Reagents or TCI) and used without further purification. All dilutions were carried out using MilliQ water. For AFM studies, mica plates were purchased from Plano GmbH. For TEM measurements, Carbon Films on 200 Mesh Copper Grids from Agar Scientific were used. 5-(6-(5-(Bis(4-methoxyphenyl)(phenyl)methoxy)pent-1-ynyl)pyren-1-yl)pent-4-ynyl-2-cyanoethyl diisopropylphosphoramidite and 5-(7-(5-(Bis(4-methoxyphenyl)(phenyl)methoxy)pent-1-yn-1-yl)pyren-2-yl)pent-4-yn-1-yl (2-cyanoethyl) diisopropylphosphoramidite required for solid-phase synthesis were prepared as previously reported.^{157,160}

Synthesis of Oligomers.

All oligomers were synthesized in a 1 μ M scale using the standard cyanoethyl phosphoramidite DNA solid phase synthesis protocol on an ABI 394 (Applied Biosystems Instruments) automated synthesizer. dG-CPG 500, dC-CPG 500, dA-CPG 500 and dT-CPG 500 were used as solid supports. Cleavage of the sequences from the support was achieved by treatment with 0.8 ml of 25% NH_3 at 55 $^\circ\text{C}$ in a closed vial with vigorous shaking for 16 hours. The solid support was removed by centrifugation and separation from the supernatant. After the evaporation of the solvent, the samples were dissolved in distilled water (MilliQ) and purified by HPLC. The purity of the sequences was confirmed by mass spectroscopy.

HPLC Purification

HPLC purification was carried out on a Shimadzu HPLC system using Lichrospher 100 RP-18 250 x 4 mm column or Reprosil 100 C8 250 x 4 mm column. The mobile phase is composed of:

A) 0.1 M triethylammonium acetate (TEAA) buffer (pH 7.0) and HPLC grade acetonitrile in 80/20 v/v.

B) HPLC grade Acetonitrile

Gradient: 0–40% B over 22 min, then 40–100% B over 5 min.

All unmodified DNA strands were purified on the C18 column using 0.1 TEAA pH 7.0 and acetonitrile.

Detection was carried out using a Shimadzu SPD-10A UV/Vis Detector, monitoring absorbance at 260 or 360 nm.

Flow rate: 1 ml/min

Temperature: 55 °C

Spectroscopic Measurements.

Absorption spectra were recorded on a Varian Cary-300 Bio-UV/VIS. Fluorescence data were collected on a Varian Cary Eclipse fluorescence spectrofluorimeter at an excitation wavelength of 365 nm (for the strands with 1,6-substituted pyrene) and 352 (for the strand with 2,7-substituted pyrene). For the CD measurements, a JASCO J-715 spectropolarimeter was used. All measurements were performed in quartz cuvettes with an optical path of 1 cm.

Transmission Electron Microscopy (TEM) Measurements.

Experiments were performed on an FEI Model Morgagni 268 device, using an operating voltage of 80 kV. For sample preparation, 5 μ l of the solution was dropped on a copper grid coated with carbon. After 5 minutes, the grid was tapped with filter paper to remove surface water. Then a drop of aqueous uranyl acetate solution (0.8%) was added onto the copper grid. After 1 min, the water was removed by tapping the grid with filter paper.

Atomic Force Microscopy (AFM) Measurements

AFM imaging was acquired with a Nanosurf FlexAFM using Tap190Al-G cantilevers from BudgetSensors (resonance frequency \approx 190 kHz, force constant = 48 N/m). Sample preparation involved depositing of 20 μ l of the aggregates' solution in buffer (10 mM PBS PH 7.0) onto an APTES-modified mica plate. After 5 min incubation, the samples were rinsed with 5 ml of distilled water. All images were recorded using a soft tapping mode.

Preparation of the Aggregates.

Unless otherwise noted, the following conditions for the aggregates preparation were used: 10 mM phosphate buffer solution (PBS), 100 or 250 mM NaCl, overall concentration of the sequences = 2 μ M The mixtures were heated

to 90 °C in a conventional heating block thermostat and after 2 minutes of equilibration were cooled to 20 °C at a controlled rate of 0.1 °C/min.

Thermodynamic analysis

The temperature-dependent degree of aggregation ($\alpha_{agg}(T)$) could be estimated based on the following equation:

$$\alpha_{agg}(T) = \frac{Abs(T) - Abs_M}{Abs_P - Abs_M} \quad (1)$$

In this equation $Abs(T)$ is the absorbance at a given temperature, Abs_M is the absorbance of the molecularly dissolved strands, Abs_P corresponds to the absorption of the polymerized sequences. The absorbance was measured at 305 nm, the maximum of J-band.

For the elongation aggregated species could be estimated by:

$$\alpha_{agg}(T) = \alpha_{sat} \left(1 - \exp \left[\frac{-\Delta H_e(T - T_e)}{RT_e^2} \right] \right) \quad (2)$$

In this equation $\alpha_{sat} = 1$, H_e is the enthalpy of aggregation at T_e , and R is the ideal gas constant.

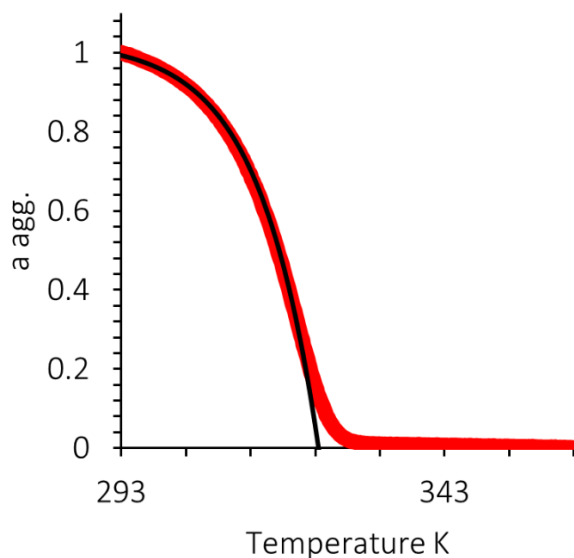


Figure 2-22. The fitting of the experimental data for the cooling curve of 2 μM **Py7a10/Py7b10** in an aqueous medium. Conditions: 2 μM total strand concentration, 10 mM phosphate buffer, 100 mM sodium chloride; temperature gradient: 0.1 °C/min.

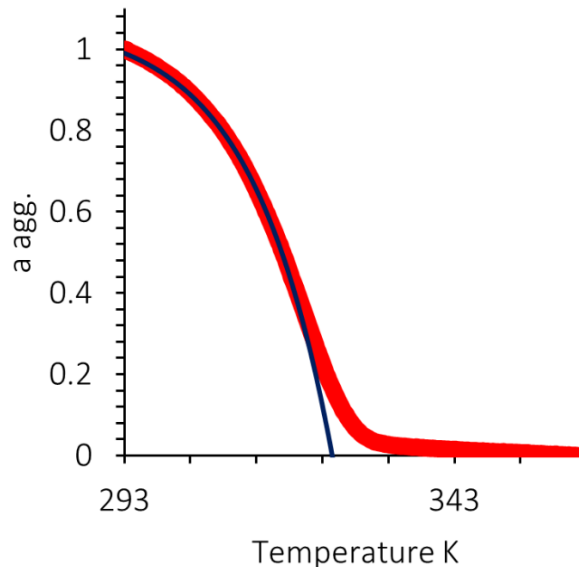


Figure 2-23. The fitting of the experimental data for the cooling curve of 2 μM **Py7a10** in an aqueous medium. Conditions: 2 μM total strand concentration, 10 mM phosphate buffer, 100 mM sodium chloride; temperature gradient: 0.1 $^{\circ}\text{C}/\text{min}$.

In the nucleation regime the fraction of aggregated species can be defined by the following equation:

$$\alpha_{agg}(T) = \sqrt[3]{K_a} \exp \left[\left(\frac{2}{3\sqrt[3]{K_a}} - 1 \right) \frac{\Delta H_e(T - T_e)}{RT_e^2} \right] \quad (3)$$

Here K_a is the dimensionless equilibrium constant of the activation step at the elongation temperature. The average number of molecules in an aggregate at the elongation temperature, $\langle N(T_e) \rangle$ gives an estimate of the size of the aggregation nucleus:

$$\langle N_n(T_e) \rangle = \frac{1}{\sqrt[3]{K_a}} \quad (4)$$

Applying equation (2) to the supramolecular polymers of **Py7a10/Py7b10**, the following values were found: $T_e=323.5$ K, $\Delta H_e= -95000$ J/mol, $K_a= 6.3 \cdot 10^{-}$

3, $\langle N(\text{Te}) \rangle = 6$. Accordingly, for the system of 2 μM **Py7a10**: $T_e = 324.5 \text{ K}$, $\Delta h_e = -72000 \text{ J/mol}$, $K_a = 2.7 \cdot 10^{-3}$, $\langle N(\text{Te}) \rangle = 7$.

Spectroscopic measurements

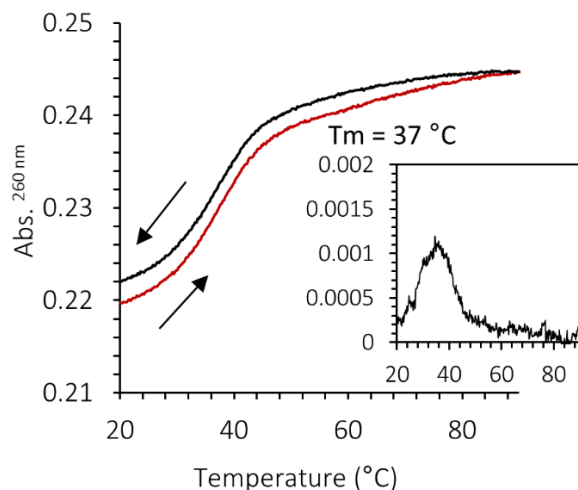


Figure 2-24. Heating (red) and cooling (black) curves recorded for a solution of a 1:1-mixture of **a10/b10**; the direction of arrows indicates a change of temperature. The inset shows the first derivatives of the cooling curve. Conditions: 2 μM total strand concentration, 10 mM phosphate buffer, 100 mM sodium chloride; temperature gradient: 0.1 $^{\circ}\text{C}/\text{min}$.

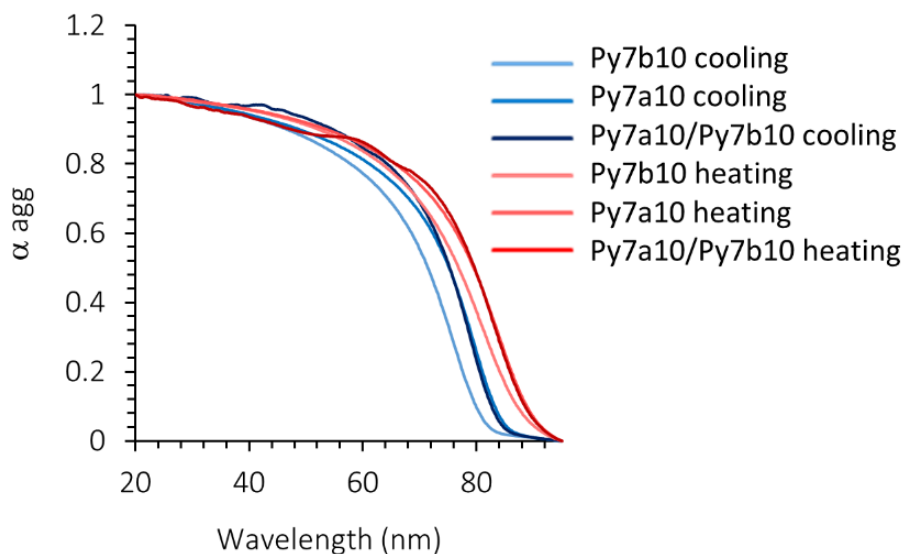


Figure 2-25. Heating and cooling curves recorded for the solutions of **Py7a10**, **Py7b10** and **Py7a10/Py7b10**. Conditions: 2 μM total strand concentration, 10 mM phosphate buffer, 250 mM sodium chloride; temperature gradient: 0.1 $^{\circ}\text{C}/\text{min}$.

CHAPTER 3. PATHWAY DIVERSITY IN THE SELF-ASSEMBLY OF
DNA-GRAFTED SUPRAMOLECULAR POLYMERS

ABSTRACT

The pathway diversity of the self-assembly of amphiphilic DNA-pyrene conjugates is described. The hydrophobic pyrene units drive the self-assembly of the anionic oligomers in an aqueous environment into ribbon-shaped, DNA-grafted supramolecular polymers. Isothermal mixing of two types of sorted ribbons, each of which contains only one kind of two complementary oligonucleotides, results in the formation of tight networks. Thermal disassembly of these kinetically trapped networks and subsequent re-assembly of the liberated components leads to mixed supramolecular polymers, which now contain both types of oligonucleotides. The scrambling of the oligonucleotides prevents the interaction between ribbons and, thus, network formation. The results show that a high local density of DNA strands in linear arrays favors hybridization among sorted polymers, whereas hybridization among mixed arrays is prevented. The lack of DNA hybridization among mixed ribbons is ascribed to the electrostatic repulsion between identical, hence non-complementary, oligonucleotides. The findings highlight the importance of kinetically trapped states on the structural and functional properties of supramolecular polymers containing orthogonal self-assembly motifs.

Part of this work has been published:

Y. Vyborna, M. Vybornyi and R. Häner, *Bioconjugate Chem.*, 2016, **27**, 2755-2761.

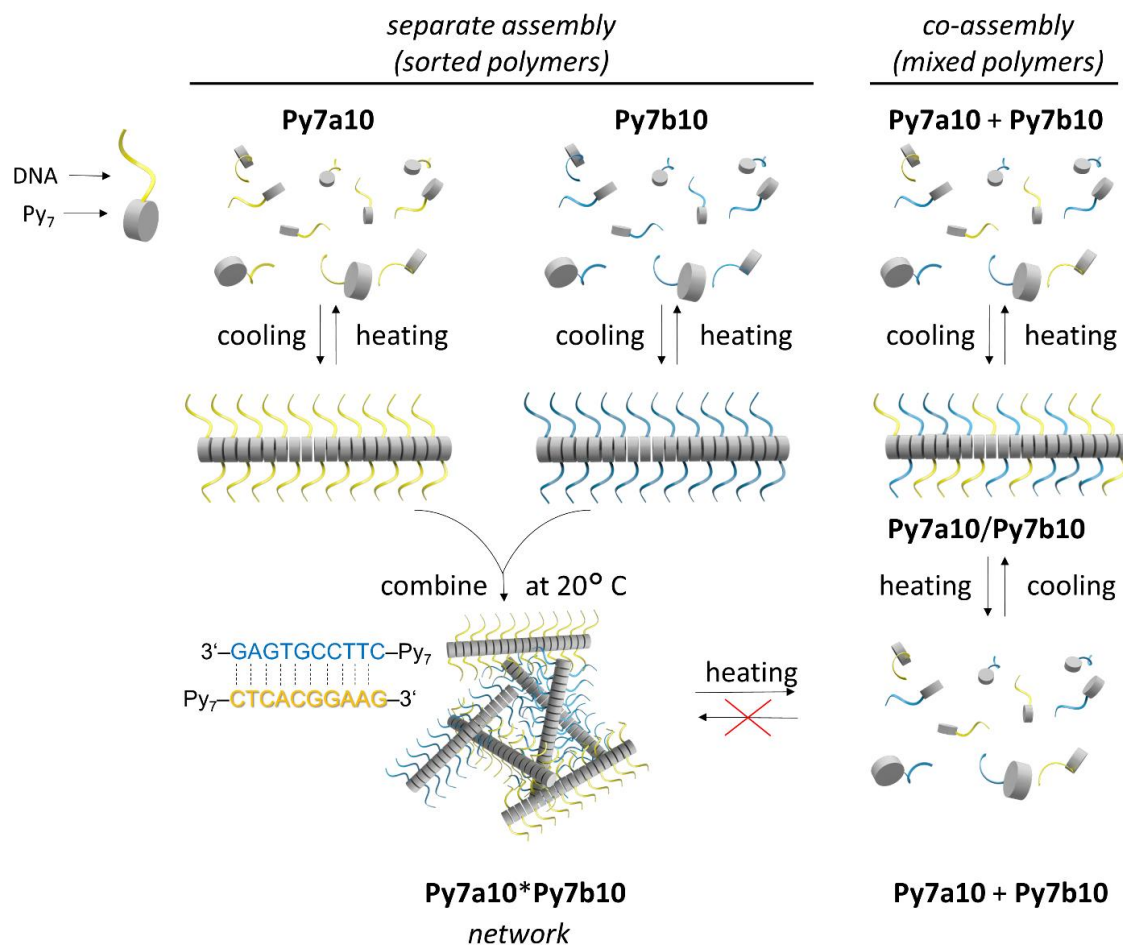
3.1 INTRODUCTION

Supramolecular polymers provide direct access to a vast diversity of functional materials due to their dynamic nature, their responsiveness to external stimuli as well as the tunability and reversibility of the non-covalent interactions governing their assembly.^{106,161} A thorough understanding of the self-assembly pathways is essential for extending the functionalities of these materials.^{10,162–165} Directing the non-covalent interactions allows controlling the properties of the resulting supramolecular constructs.^{166–170} Also, the proper choice of assembly protocols helps in tuning the properties of biomaterials¹⁷¹ or improves the performance of organic semiconductors.¹⁷² Thus, the chemical composition alone is often insufficient to achieve the best performance of complex supramolecular assemblies, among which DNA-based materials take a prominent role.¹⁰⁸ DNA-assembled objects are of interest in the design and development of drug carriers, nanomachines, and other types of sophisticated nanomaterials.^{97,119,173–176} The wide range of potential applications has led to considerable interest in the properties of oligonucleotides conjugated to polymers or lipophilic chains.^{99,111,121,177–182} DNA conjugates often combine multiple self-assembly motifs enabling selective and orthogonal non-covalent interactions.^{100,135,183–187} To date, little is known about materials from DNA conjugates, in which the interactions between the non-DNA parts are central to the hierarchical organization. Therefore, the study of the mechanistic details of self-assembly in such systems is critical. The characterization of individual processes leading to morphologically different products, as well as the identification of escape pathways from kinetically trapped states into the thermodynamically favored structure, are of particular interest. In the previous chapter, we have reported on the synthesis of one-dimensional DNA-grafted supramolecular polymers using short, chimeric DNA-pyrene oligomers.¹⁸⁸ Here, we describe different competitive aggregation pathways of these oligomers and highlight the importance of kinetically trapped states for the controlled self-assembly of DNA hybrid materials.

3.2 RESULTS AND DISCUSSIONS

The system used in this study consists of two chimeric oligomers, **Py7a10** and **Py7b10** (Scheme 2-2). As established before,¹⁸⁸ these oligomers self-assemble in an aqueous medium into one-dimensional (1D) ribbon-like supramolecular polymers via stacking interactions between pyrene units (Scheme 3-1). The ribbons consist of a pyrene core with DNA single strands tethered along the edges.

Scheme 3-1. Schematic illustration of the self-assembly pathways of pyrene-DNA hybrids into one-dimensional DNA-grafted supramolecular polymers and networks.



The supramolecular polymers are prepared by cooling a solution of oligomers **Py7a10** and/or **Py7b10** from 95 °C to 20 °C using a temperature

gradient of 0.1 °C/min. At 95 °C, the oligomers are dissolved. The slow cooling gradient ensures that the self-assembly process takes place at or near the thermodynamic equilibrium. Nucleation starts around 80 °C and is followed by a cooperative elongation process. The objects obtained via co-annealing of **Py7a10** and **Py7b10** to give **Py7a10/Py7b10** are morphologically indistinguishable from the ones obtained in the single-component systems **Py7a10** or **Py7b10** (Figure 3-1).

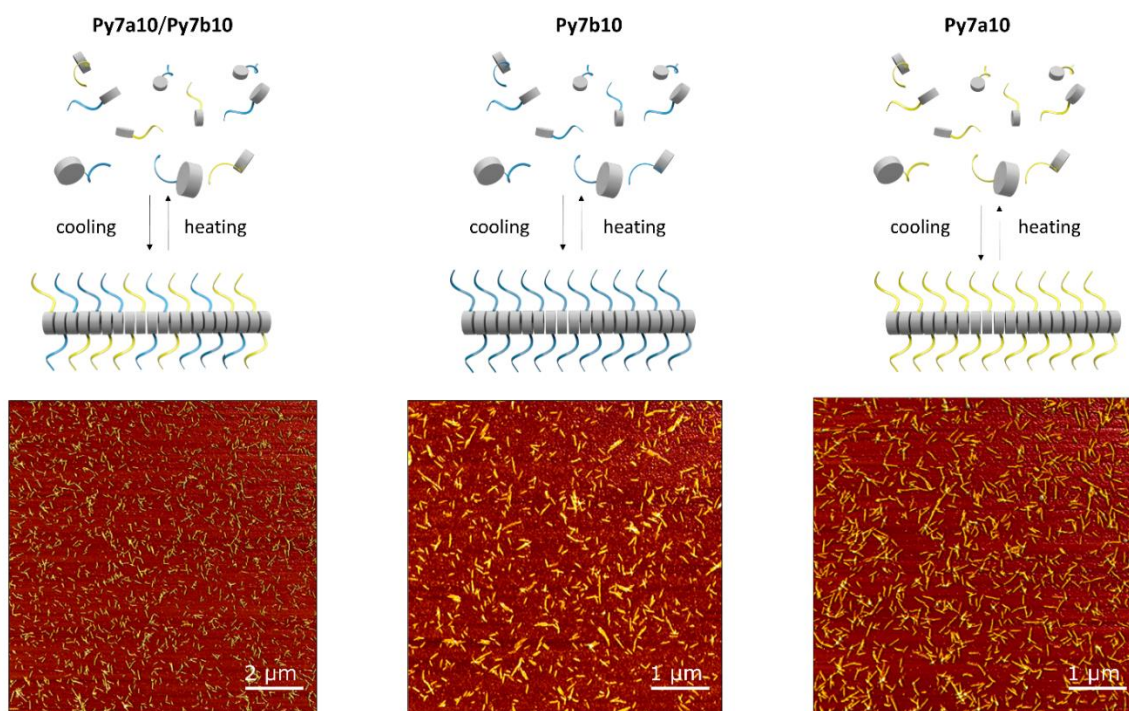


Figure 3-1. AFM images (bottom) and illustrative schemes (top) of the self-assemblies **Py7a10/Py7b10**, **Py7a10** and **Py7b10**. Conditions: 200 mM NaCl, 10 mM phosphate buffer system pH = 7, concentration of each oligomer = 2 μM.

Isothermal mixing of equal quantities of the separately prepared, sorted **Py7a10** and **Py7b10** results in the formation of **Py7a10*Py7b10** networks through base pairing as illustrated in Scheme 3-1. **Py7a10/Py7b10**, on the other hand, does not form this type of networks although these polymers are quantitatively composed of the same components. Figure 3-2 shows typical atomic force microscopy (AFM) images of **Py7a10/Py7b10** copolymers and **Py7a10*Py7b10** networks.

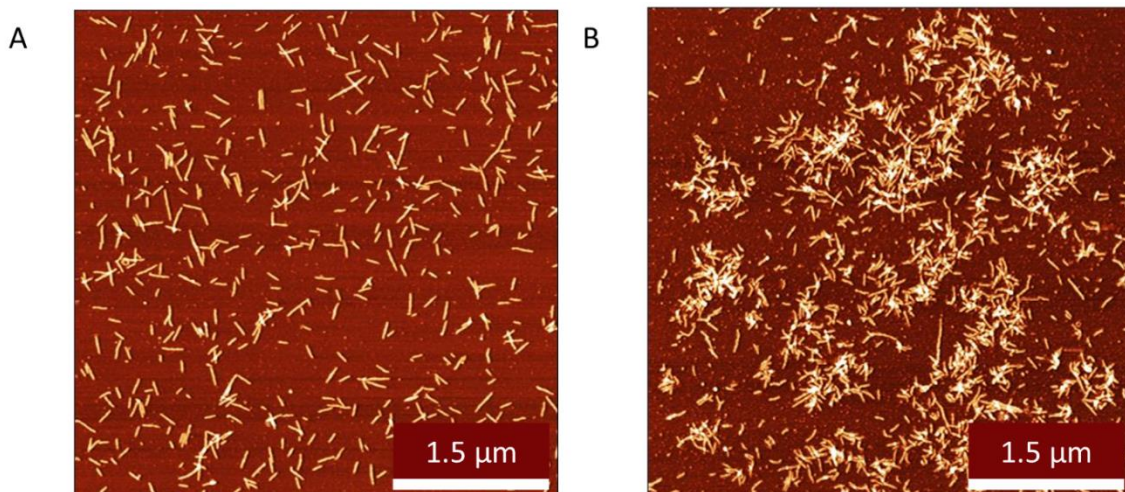


Figure 3-2. Representative AFM images of discrete ribbons **Py7a10/Py7b10** (A) and interconnected polymer networks **Py7a10*Py7b10** (B). Conditions: 200 mM NaCl, 10 mM phosphate buffer system pH=7, concentration of each oligomer = 2 μ M.

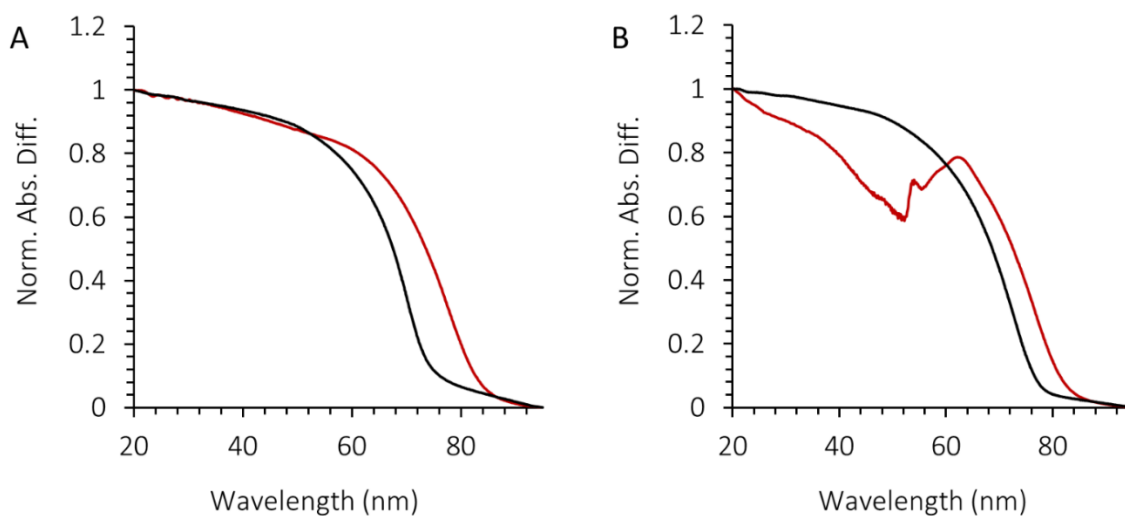


Figure 3-3. Normalized temperature-dependent change of absorption measured at 305 nm for **Py7a10/Py7b10** (A) and **Py7a10*Py7b10** (B). Heating (red) and cooling (black) were performed using a gradient of 0.1 $^{\circ}$ C/min. Conditions: 200 mM NaCl, 10 mM phosphate buffer system pH=7, concentration of each oligomer = 2 μ M.

Figure 3-3 shows the disassembly-reassembly cycles of **Py7a10*Py7b10** (kinetically trapped product) and **Py7a10/Py7b10** (thermodynamically favored product) monitored by temperature dependent intensity changes at 305 nm.

This wavelength corresponds to the maximum of the absorption band for the aggregated pyrenes (J-band) and serves as a reliable indicator of the aggregation state of pyrenes.¹⁴⁸ Upon slowly heating to 95 °C, both **Py7a10*Py7b10** and **Py7a10/Py7b10** disassemble into molecularly dissolved **Py7a10** and **Py7b10** chains as indicated by the complete disappearance of the J-band (Figure 3-4). However, the normalized heating curves (red lines in Figure 3-3 A and B) exhibit a similar shape only in the range from 65 °C to 95 °C. Below 65 °C, the pyrene absorbance of **Py7a10*Py7b10** reveals competing processes which occur in the course of the heating event (Figure 3-3 B).

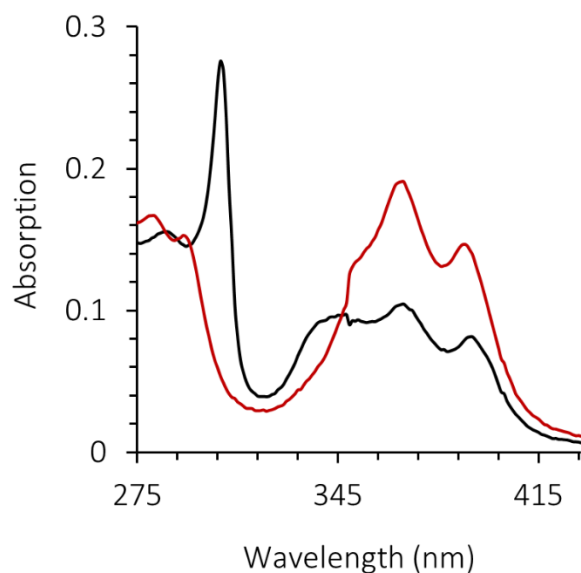


Figure 3-4. UV-vis spectra for **Py7a10*Py7b10** at 20 °C (black) and 90 °C (red). Conditions: 200 mM NaCl, 10 mM phosphate buffer system pH=7, concentration of each oligomer = 2 μ M.

The initial gradual decrease in absorption from 20 to 50 °C is probably due to the sedimentation of large network aggregates.⁷⁵ Between 50 and 65 °C, a stepwise recovery of the signal takes place until the same value is reached as in the heating curve (Figure 3-3 A) of the mixed polymer **Py7a10/Py7b10**. Above 65 °C, the decrease of the absorbance reflects the disassembly of pyrenes solely, which is indicated by the identical shapes of the melting curves of both,

Py7a10*Py7b10 and **Py7a10/Py7b10**. Renewed slow cooling of the obtained molecularly dissolved chains from 95 °C to 20 °C leads in both cases to the formation of the mixed polymer **Py7a10/Py7b10** in a cooperative process.

The disassembly process of the networks was further studied by performing additional heating-cooling experiments and analyzing the morphology of the newly formed aggregates by AFM at 20 °C. The experiments consisted of heating **Py7a10*Py7b10** from 20 °C to a certain temperature T and cooling it back to 20 °C. The observed morphology turned out to be highly dependent on T . For example, heating to $T = 35$ °C and further cooling to 20 °C results in the exclusive formation of large and tightly packed networks (Figure 3-5 A). Apparently, increasing the temperature to 35 °C seems to favor the interactions between individual ribbons. The sedimentation of the large aggregates would explain the decrease in absorption. Heating **Py7a10*Py7b10** to $T = 55$ °C, which is still in a region with a descending pyrene absorption, led to the formation of networks together with short polymers (Figure 3-5 B). This indicates the partial dissolution of the large networks at this temperature liberating individual **Py7a10** and **Py7b10** oligomers, which subsequently reassemble into mixed polymers **Py7a10/Py7b10**. Heating to 75 °C yielded morphologically similar structures as the experiment conducted to $T = 55$ °C (Figure 3-5 C). Finally, at $T = 95$ °C, the networks are entirely disassembled, which is demonstrated by the exclusive formation of **Py7a10/Py7b10** after reassembly; no networks could be detected (Figure 3-5 D). These results imply that the networks are metastable and rearrange into thermodynamically favored 1D supramolecular polymers in a temperature-induced disassembly-assembly process.

Scheme 3-1 summarizes the processes occurring in the two-component system. The separate self-assembly of **Py7a10** and **Py7b10** leads to linear polymers. Mixing these two types of sorted supramolecular polymers at 20 °C results in the formation of metastable networks **Py7a10*Py7b10**, in which individual ribbons are interconnected by DNA hybridization. These aggregates

are converted by subsequent thermal denaturation and reassembly into the thermodynamically favored **Py7a10/Py7b10**, which has mixed DNA strands and, thus, forms only one-dimensional supramolecular polymers but no networks.

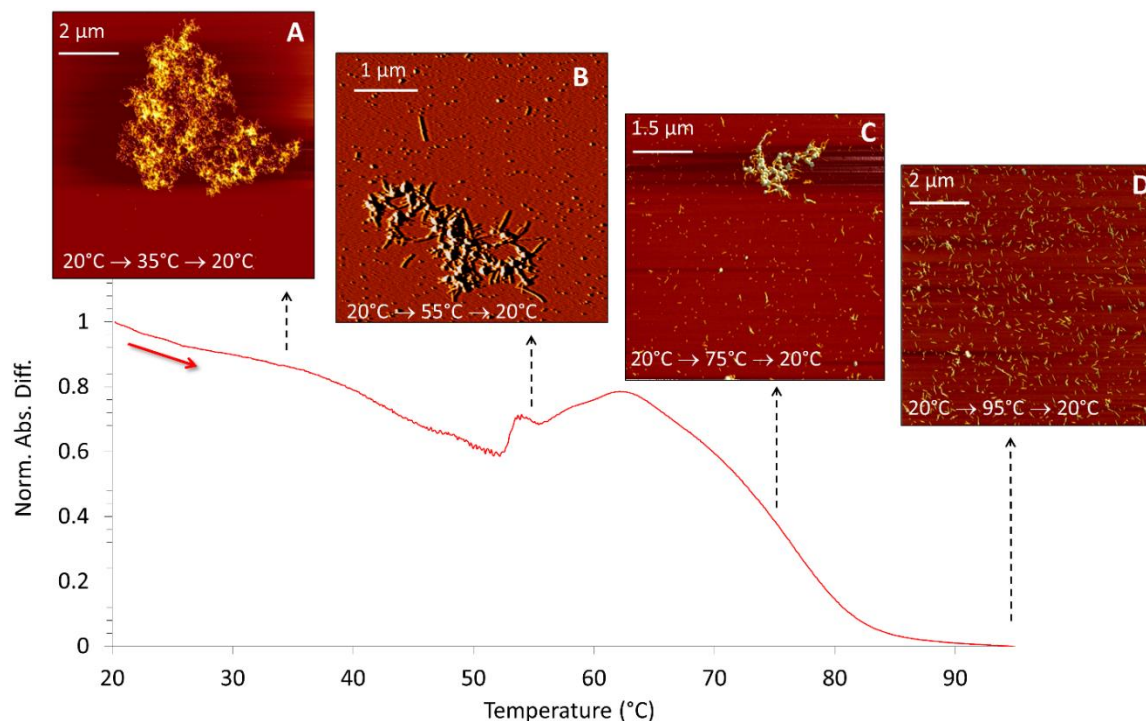


Figure 3-5. Melting curve and AFM images of materials obtained upon applying heating-cooling cycles (for more details see main text) to **Py7a10*Py7b10**. Conditions 200 mM NaCl, 10 mM phosphate buffer system pH=7, concentration of each oligomer = 2 μ M.

The absence of networks is rationalized by the electrostatic repulsion between non-complementary DNA strands.^{66,189} On the other hand, the hybridization of complementary DNAs between sorted ribbons, **Py7a10** and **Py7b10**, leads to the networks observed for **Py7a10*Py7b10**. Multiple sites of interactions between individual ribbons render the aggregation process highly cooperative. The results show that individual oligomers **Py7a10** and **Py7b10** remain kinetically trapped in **Py7a10*Py7b10** and only thermal activation allows their transformation into the energetically more favored product.

We tested the property of **Py7a10*Py7b10** and **Py7a10*Py7b10** to entrap hydrophobic molecules using Nile Red as a fluorescent reporter. Nile red is an uncharged hydrophobic molecule. Its fluorescence is strongly influenced by the polarity of the environment. It is almost nonfluorescent in water solution but the emission efficiency increases in a hydrophobic environment.

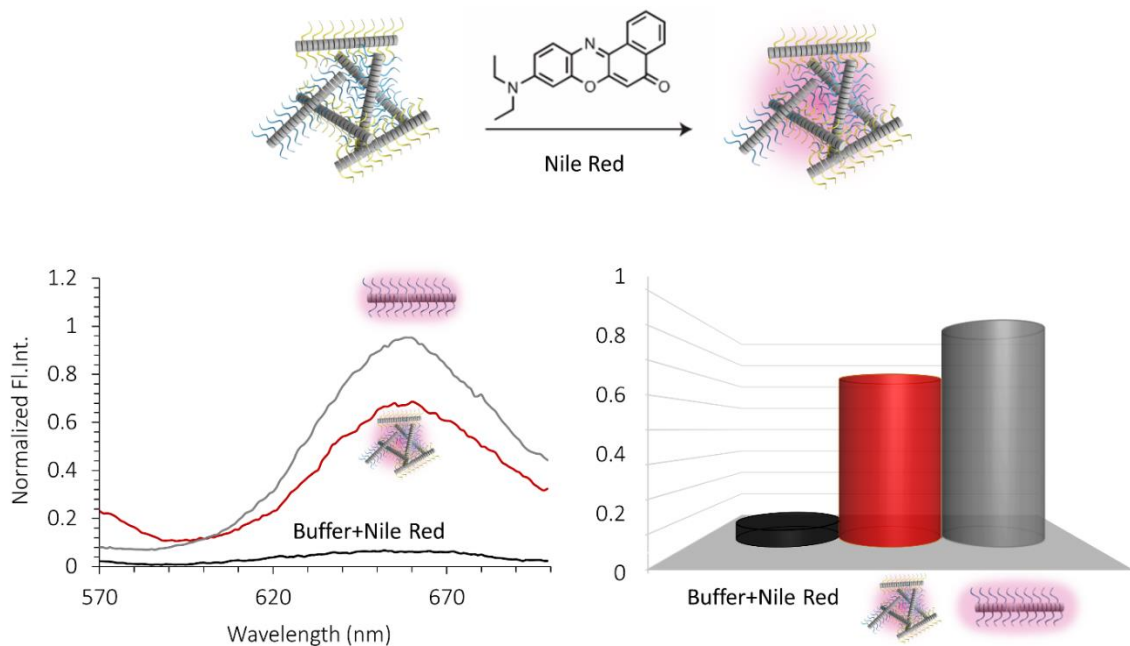


Figure 3-6. Top: schematic representation of an encapsulation of the Nile Red into the networks. Bottom left: normalized fluorescence emission spectra of the Nile Red in buffer (black), in the presence of networks (red) and the presence of individual nanoribbons (gray). Bottom right: plot on the normalized fluorescence intensities at 660 nm.

Also, its absorption maximum is at 553 nm and does not interfere absorption of the pyrene. To compare the efficiency of encapsulation, 50 μl of $3.14 \cdot 10^{-5}$ M of Nile Red in CH_2Cl_2 was added to three vials, and CH_2Cl_2 was evaporated. To the first and second vial, the **Py7a10*Py7b10** networks and **Py7a10** solutions respectively were then added, followed by 10 mM pH 7 phosphate buffer. To the third vial, only phosphate buffer was added. The vials were stirred at room temperature overnight. Fluorescence emission was recorded at the excitation wavelength of 550 nm. The emission spectra show

that both linear supramolecular polymers and networks accommodate the dye in their hydrophobic environments (Figure 3-6).

3.3 CONCLUSIONS

The pathway complexity of the self-assembly in systems containing pyrene-DNA conjugates **Py7a10** and **Py7b10** has been elucidated. Supramolecular polymerization of a mixture of equal amounts of **Py7a10** and **Py7b10** leads to the formation of **Py7a10/Py7b10**. These mixed polymers contain both types of complementary DNA strands arranged along their edges and network formation is completely prevented. Alternatively, combining the separately preassembled, sorted polymers formed from **Py7a10** and **Py7b10** leads to the formation of metastable networks via crosslinking of individual ribbons by DNA hybridization. The networks are stable at room temperature due to a slow rate of oligomer exchange between the polymers. However, temperature induced disassembly of the networks and subsequent reannealing of the released oligomers **Py7a10** and **Py7b10** results in the formation of the thermodynamically preferred mixed polymer **Py7a10/Py7b10**, which does not form networks. The lack of DNA hybridization among ribbons of **Py7a10/Py7b10** is ascribed to the electrostatic repulsion between identical, hence non-complementary, oligonucleotides that are present in a high density at the edges of the polymeric ribbons. The findings illustrate the importance of kinetically trapped states on the structural and functional properties of supramolecular polymers.

3.4 EXPERIMENTAL SECTION

Unless otherwise noted, all chemicals and general methods were used as described in section 2.4.

Preparation of the Samples

For a typical experiment, supramolecular polymers **Py7a10**, **Py7b10** and **Py7a10/Py7b10** were prepared according to the following procedure: 10 mM

phosphate buffer solution (PBS), 200 mM NaCl and 2 μ M sequences were mixed. The mixtures were heated to 95 °C in a conventional heating block thermostat and after 2 minutes of equilibration were cooled to 20 °C at a controlled rate of 0.1 °C/min. To prepare assemblies **Py7a10*Py7b10**, pre-annealed assemblies **Py7a10** were mixed with **Py7b10** and incubated at room temperature for 2 hours.

CHAPTER 4. FROM RIBBONS TO NETWORKS: HIERARCHICAL
ORGANIZATION OF DNA-GRAFTED SUPRAMOLECULAR
POLYMERS

ABSTRACT

DNA-grafted supramolecular polymers (SPs) allow the programmed organization of DNA in a highly regular, one-dimensional array. Oligonucleotides are arranged along the edges of pyrene-based helical polymers. The addition of complementary oligonucleotides triggers the assembly of individual nanoribbons resulting in the formation of extended supramolecular networks. Network formation is enabled by cooperative coaxial stacking interactions of terminal GC base pairs. The process is accompanied by structural changes in the pyrene polymer core that can be followed spectroscopically. Network formation is reversible and disassembly into individual ribbons is realized either via thermal denaturation or by the addition of a DNA separator strand.

Part of this work has been published:

Y. Vyborna, M. Vybornyi and R. Häner, *J. Am. Chem. Soc.* 2015, **137**, 14051-14054.

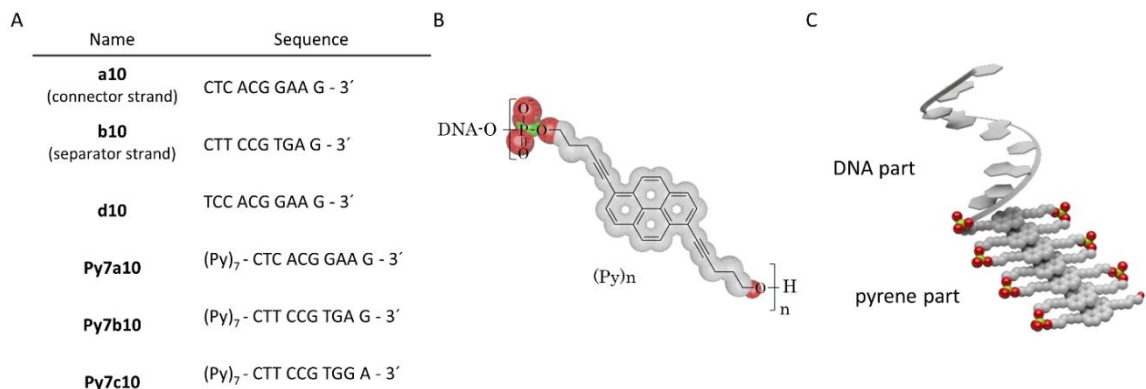
4.1 INTRODUCTION

The creation of functional nanoscale structures represents a major goal of today's nanotechnology. DNA-based materials are of primary interest for the construction of functional platforms.^{108,190–192} A proper choice of the nucleotide sequence provides control over aromatic stacking and hydrogen bonding interactions,^{42,44,193} thus enabling the assembly of systems with a high degree of complexity.^{183,194–196} Approaches towards the preparation of functional DNA materials include the designed DNA self-assembly,^{197–200} the grafting of oligonucleotides onto metal nanoparticles (NPs)²⁰¹ and other surfaces,^{202–204} as well as polymers.^{84,130,205–209} The latter class, DNA-grafted polymers, were pioneered by Nguyen and Mirkin and gained increasing attention over the last years.^{77,140,143,210–213} In previous chapters, we have introduced DNA-grafted supramolecular polymers (SPs). These self-assembled structures appear as one-dimensional (1D) ribbons, consisting of an oligopyrenotide core¹⁴⁵ with arrays of single-stranded oligonucleotides appended onto its edges. The non-covalent nature of SPs brings the additional feature of reversibility of the polymerization process.^{107,214–217} Furthermore, it enables the formation of polymers with a high DNA grafting density.²¹⁸ Herein we describe the hierarchical organization of DNA-grafted SPs. It is shown that individual ribbons assemble into extended networks through a highly cooperative mesh of DNA blunt-end stacking interactions.

4.2 RESULTS AND DISCUSSIONS

Chimeric oligomers **Py7a10**, **Py7b10** and **Py7c10** (Scheme 4-1) are all composed of a heptapyrenotide part and an appended oligonucleotide. They were prepared via solid-phase synthesis, purified by RP-HPLC and characterized by MS (Appendix). The two complementary oligonucleotides **a10** (connector strand) and **b10** (separator strand) have the same nucleobase sequence as the respective corresponding chimeric oligomers **Py7a10** and **Py7b10**; **d10** is complementary to the oligonucleotide part of **Py7c10**.

Scheme 4-1: A: Sequences of chimeric oligomers and oligonucleotides; B: chemical structure of phosphodiester-linked pyrene part; C: graphic representation of chimeric oligomers.



As previously described, DNA-grafted SPs are typically performed by slow annealing. Thus, a 2 μM solution of DNA-pyrene oligomers in aqueous buffer (10 mM sodium phosphate, pH=7.0 and 250 mM sodium chloride) is cooled from 95 $^{\circ}\text{C}$ to 20 $^{\circ}\text{C}$ using a gradient of 0.1 $^{\circ}\text{C}/\text{min}$. Stacking interactions between pyrenes drive the self-assembly of polymeric ribbons. The polymerization process leads to the development of two distinct absorption bands in the UV/vis spectrum at 335 (H-band; $S_0 \rightarrow S_1$ transition) and 305 nm (J-band; $S_0 \rightarrow S_2$ transition; see Figure 4-1 A).^{149,160}

The assembly/disassembly process is most conveniently followed by changes of the 305 nm band (Figure 4-1 B-D and Figure 4-2 A, B). Figure 4-1 B shows the assembly of ribbons from **Py7b10** upon cooling. The polymerization occurs via a single transition that starts at ~ 85 $^{\circ}\text{C}$. The process is reversible, albeit some hysteresis is observed. Surprisingly, if the same procedure is performed in the presence of the complementary oligonucleotide **a10**, a second transition appears below 30 $^{\circ}\text{C}$ (Figure 4-1 C). The change in the intensity of the J-band reflects a conformational reorganization of the supramolecular pyrene backbone. The sharpness of this transition, characterized by the full-width at half-maximum (fwhm)²¹⁹ of 1.5 $^{\circ}\text{C}$ (melting) and 2.5 $^{\circ}\text{C}$ (annealing), suggests a high degree of cooperativity. Also, this process is reversible and

shows hysteresis. In contrast, annealing/melting curves for a system containing **Py7b10** and the non-complementary oligonucleotide **b10** exhibit only a single transition below 85 °C, which coincides with the formation of **Py7b10** nanoribbons (Figure 4-1 D).

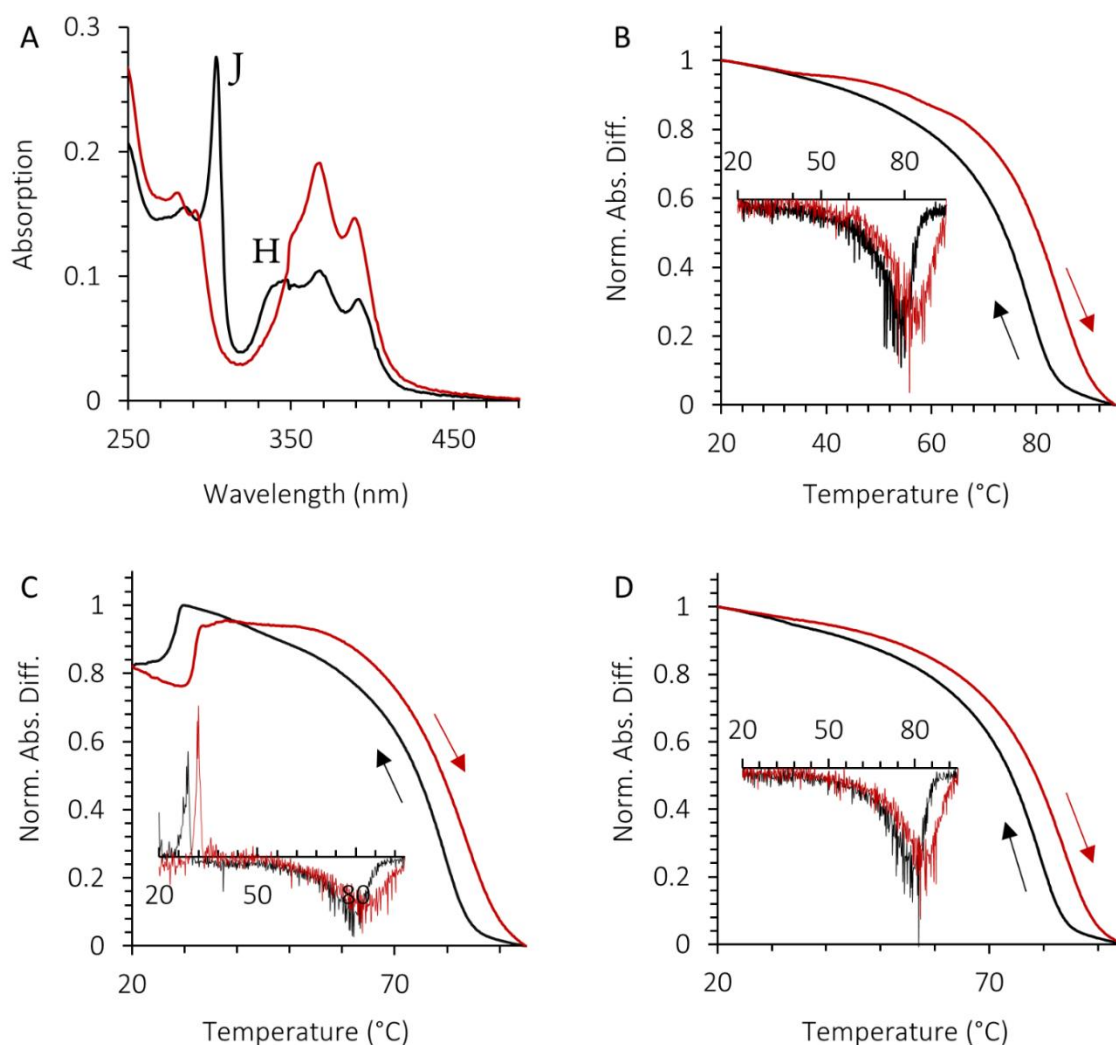


Figure 4-1. A) UV/vis of **Py7b10** at 20 °C (black) and 95 °C (red). Temperature-dependent change of absorbance at 305 nm of **Py7b10** (B), **Py7b10*****a10** (C) and **Py7b10**+**b10** (D). Arrows indicate cooling and heating. Cooling (black) and heating (red) were performed using a 0.1°C/min ramp. Conditions: 2 μ M **Py7b10** and 6 μ M of **a10** (C) or **b10** (D); 10 mM phosphate buffer, pH=7.0, 250 mM sodium chloride. The insets in (B)-(D) show the first derivatives of the corresponding curves.

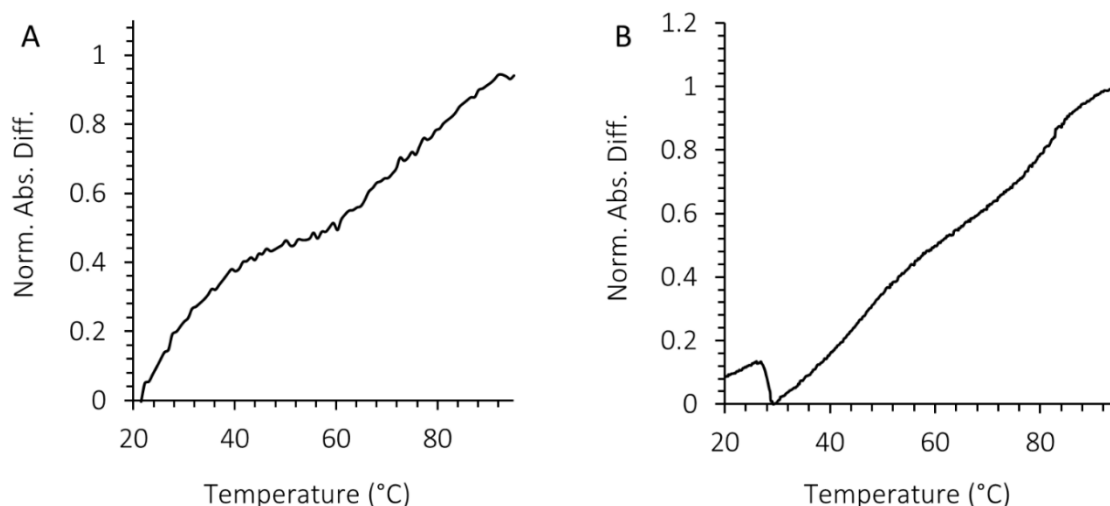


Figure 4-2. Annealing absorption curves at 260 nm of **Py7b10** (A), **Py7b10*a10** (B). Conditions: 2 μM **Py7b10** and 6 μM of **a10**; 10 mM phosphate buffer, pH=7.0, 250 mM sodium chloride.

Circular dichroism (CD) spectroscopy provides further insight into the nature of the transition observed around 30 °C. The CD spectrum for the **Py7b10*a10** system resembles the one of the B-DNA below 300 nm, it exhibits a strong exciton-coupled signal (Figure 4-3 A, red curve) in the 300-320 nm region at 20°C. The bisignate signal (+307/-303 nm) corresponds to the J-band of assembled pyrenes.²²⁰ After heating to 35 °C the signal disappears (Figure 4-4), which clearly shows that it is linked to the transition taking place in this temperature range. This suggests that the stacking arrangement of the pyrenes, and hence, their electronic interaction is altered during the observed process. In contrast, the samples prepared either from **Py7b10** alone or **Py7b10+b10** are CD silent in the same region (Figure 4-4 A, black and gray curves). Thus, the low-temperature transition only occurs when **a10** (connector strand) is hybridized to the DNA part of **Py7b10**.

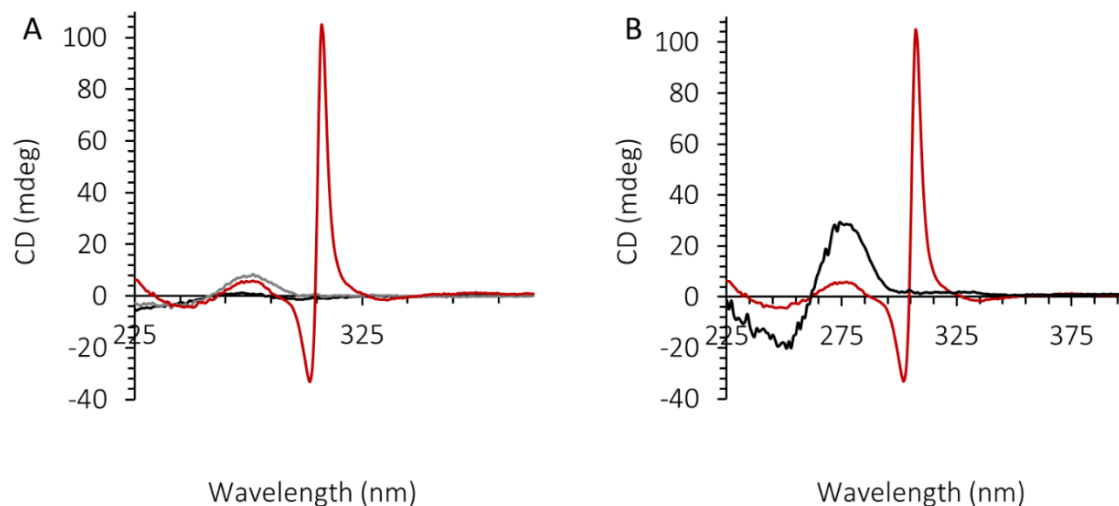


Figure 4-3. CD spectra at 20 °C; A) **Py7b10** (black), **Py7b10+b10** (gray), **Py7b10*a10** (red) prepared by slow annealing; Conditions: 2 μM **Py7b10** and 6 μM of **a10** © or **b10** (D); 10 mM phosphate buffer, pH=7.0, 250 mM sodium chloride; B) **Py7b10*a10** before (red) and after (black) addition of **b10** (conditions: as before, except **b10** was used at 12 μM conc.).

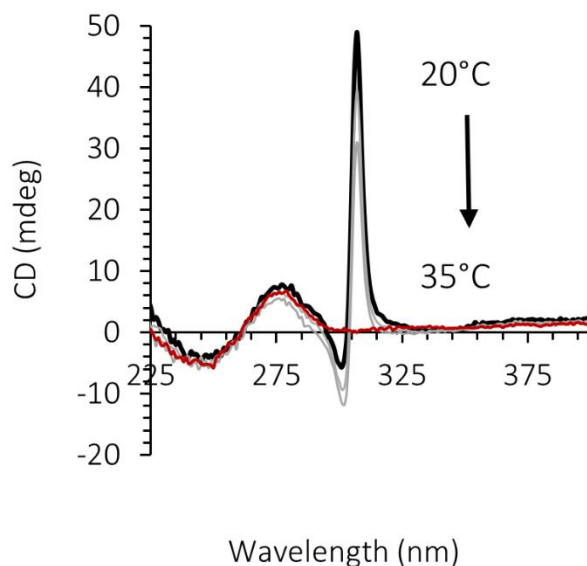


Figure 4-4. Temperature-dependent CD spectra of **Py7b10*a10** (2 μM + 6 μM) system: 20 °C (black), 25 °C (grey), 30 °C (grey), 35 °C (red). Conditions: 2 μM **Py7b10** and 6 μM of **a10**; 10 mM phosphate buffer, pH=7.0, 250 mM sodium chloride.

Atomic force microscopy (AFM) was used to correlate the spectroscopic data with the morphological appearance of aggregates. Supramolecular polymers were deposited and visualized on an amino-modified mica surface. As shown previously, self-assembly of **Py7b10** leads to the formation of ribbons that exhibit a length of several hundred nanometers and are randomly distributed on the surface (Figure 4-5 A). The **Py7b10+b10** mixture leads to identical results (Figure 4-5 B). In the complementary **Py7b10*a10** system, however, polymers exist as high-density networks (Figure 4-5 C), reminiscent of haystacks in a field, rather than as individual ribbons. The formation of networks is confirmed by transmission electron microscopy (TEM; Figure 4-6).

The two transitions appearing in the annealing curves of **Py7b10** in the presence of a complementary oligonucleotide **a10** reflect the hierarchical structural organization of chimeric oligomers. Based on the combined spectroscopic and morphologic data, we propose a model for the network formation as illustrated in Scheme 4-2.

The first transition is due to the formation of nanoribbons via supramolecular polymerization of **Py7b10**. The second cooperative transition occurs only in the presence of the complementary oligonucleotide **a10**. DNA hybridization between **a10** and the single-stranded oligonucleotides grafted onto the pyrene nanoribbons results in the formation of duplexes. These duplexes are arranged along the edges of the ribbons (Scheme 4-2) and contain GC base pairs at their termini. Cooperative interactions between individual ribbons through coaxial stacking of these blunt-ended GC base pairs lead to network formation. We assume that each ribbon, through short patches of a few GC base pairs, is connected to neighboring ribbons; long-range collinear stacking of ribbons is unlikely.

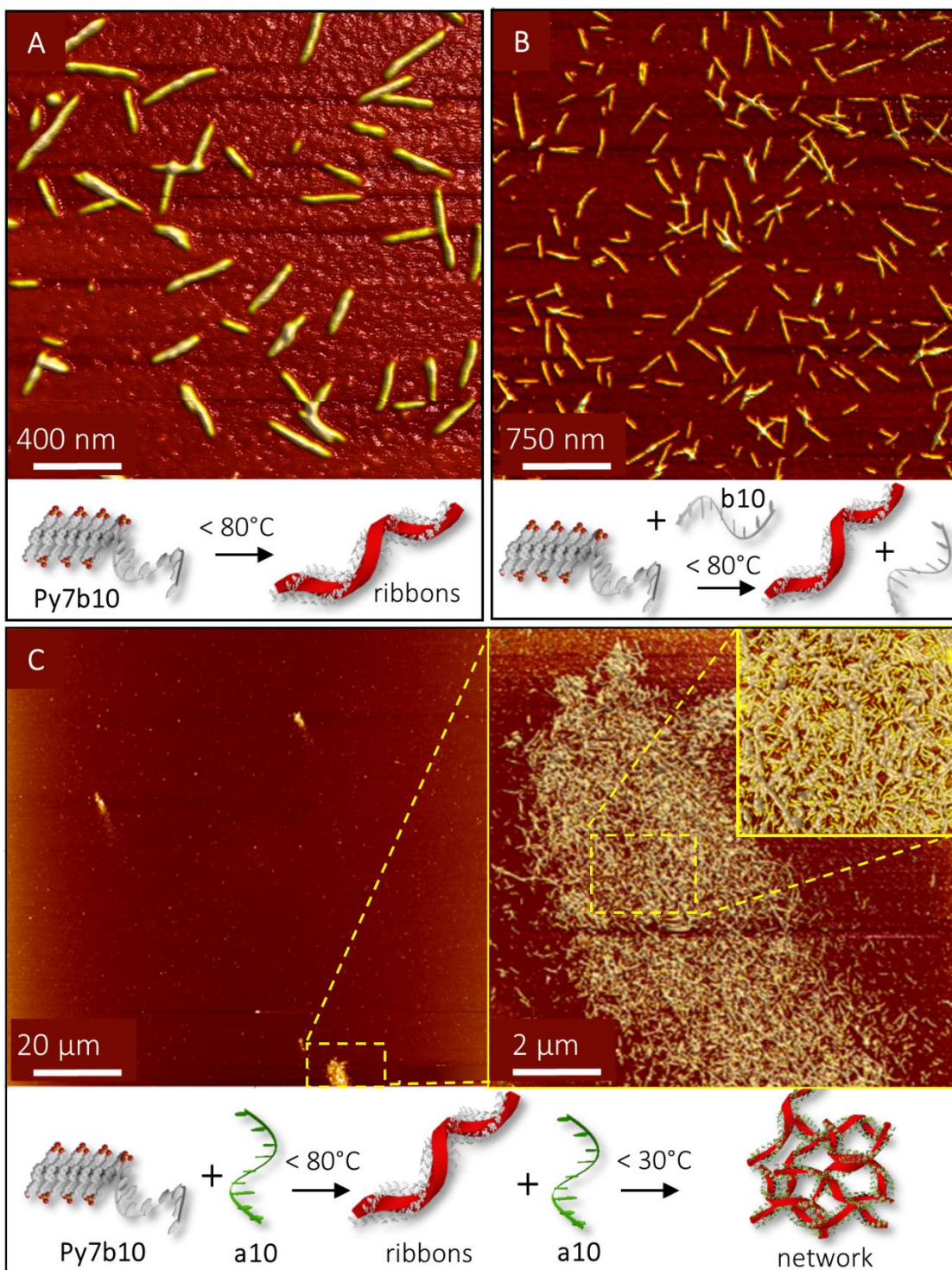


Figure 4-5. AFM images and illustration of supramolecular assemblies formed from **Py7b10** (A), **Py7b10 + b10** (B) and **Py7b10*a10** (C). Conditions: 2 μM **Py7b10** and 6 μM of **a10** or **b10**; 10 mM phosphate buffer, pH=7.0, 250 mM sodium chloride.

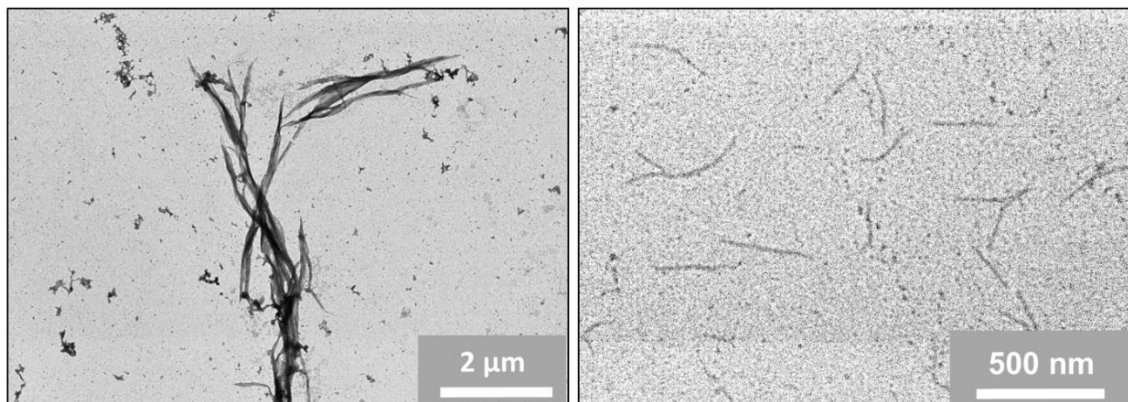
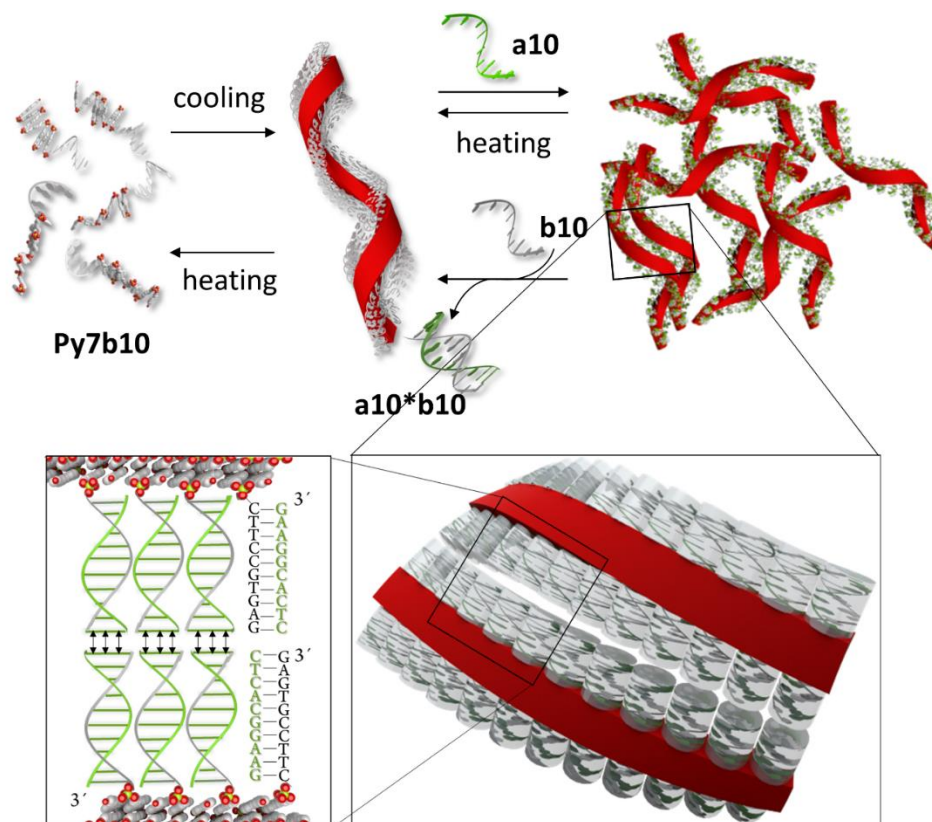


Figure 4-6. TEM images of networks **Py7b10*a10** (left) and individual ribbons **Py7b10** (right). Conditions: 2 μM **Py7b10** and 6 μM of **a10** or **b10**; 10 mM phosphate buffer, pH=7.0, 250 mM sodium chloride.

Scheme 4-2. Illustration of hierarchical self-assembly process. Nanoribbons are formed through the assembly of chimeric oligomers (**Py7b10**) in a first step. Subsequent hybridization of oligonucleotide **a10** to the DNA part of the nanoribbons leads to the formation of duplexes containing GC base pairs at their ends. Networks are then formed via cooperative blunt-end stacking interactions.



4.2.1 Effect of AT base pairs on the self-assembly via blunt-ended interactions

The importance of blunt-end stacking interactions for the controlled assembly of DNA nanostructures and devices is well documented.^{42,200,221–224} Coaxial stacking²²⁵ of GC base pairs is significantly stronger than of AT base pairs.²²⁶ This is also observed in the present case. In oligomer **d10**, the two 3'-terminal bases are switched in comparison to **a10** (Scheme 4-1). The annealing curve of oligomer **Py7c10** in the presence of **d10** shows only a single transition occurring at 80 ± 5 °C (Figure 4-7) and no CD signal at the region of the pyrene absorption (Figure 4-8).

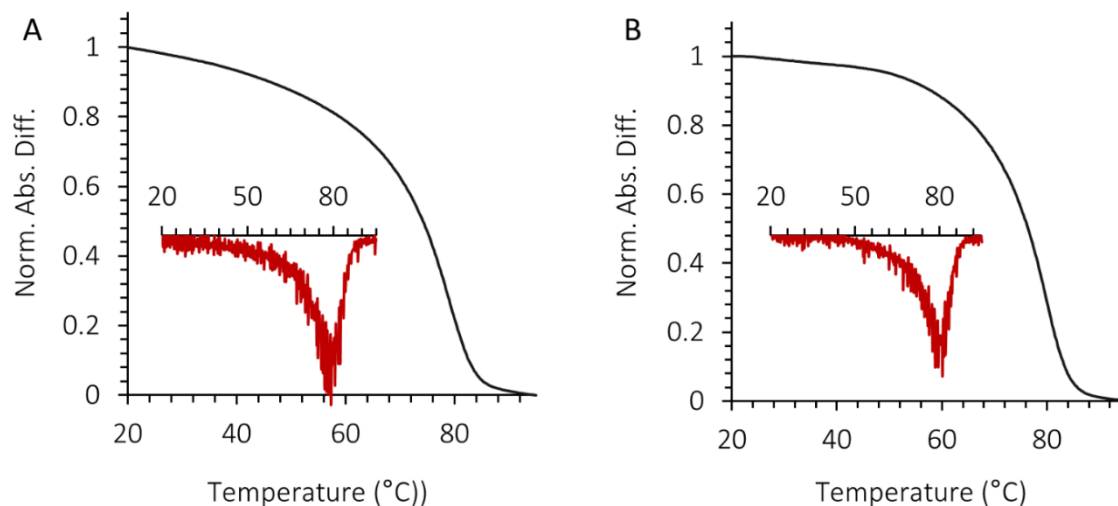


Figure 4-7. Annealing absorption curves at 305 nm with corresponding first derivatives for **Py7c10** (A), **Py7c10*d10** (B); CD spectra (C) of the assemblies of **Py7c10** (black), **Py7c10*d10** (red). Conditions: 2 μ M **Py7c10** and 6 μ M of **d10**; 10 mM phosphate buffer, pH=7.0, 250 mM sodium chloride.

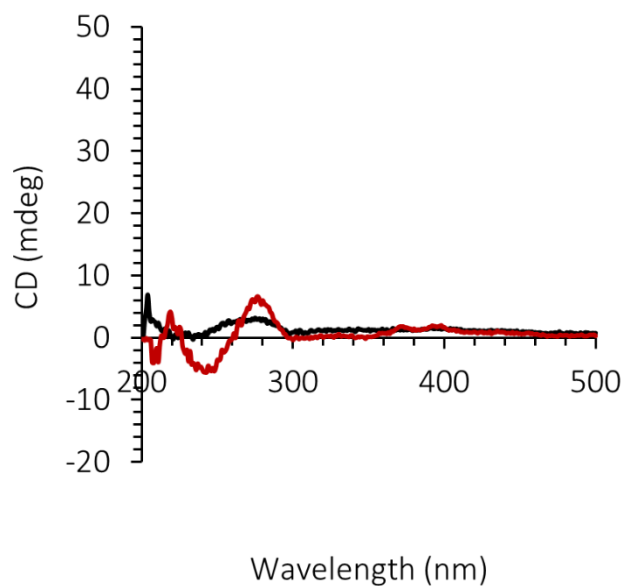


Figure 4-8. CD spectra of the assemblies of **Py7c10** (black), **Py7c10*d10** (red). Conditions: 2 μM **Py7c10** and 6 μM of **d10**; 10 mM phosphate buffer, pH=7.0, 250 mM sodium chloride.

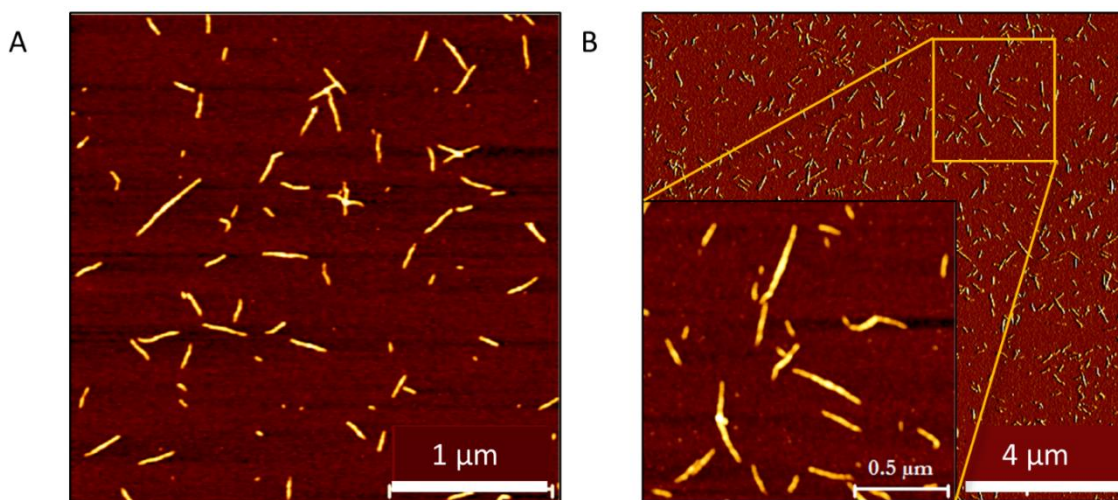


Figure 4-9. AFM images of supramolecular assemblies formed from **Py7c10** (A), **Py7c10 *d10** (B). Conditions: 2 μM **Py7c10** and 6 μM of **d10**; 10 mM phosphate buffer, pH=7.0, 250 mM sodium chloride.

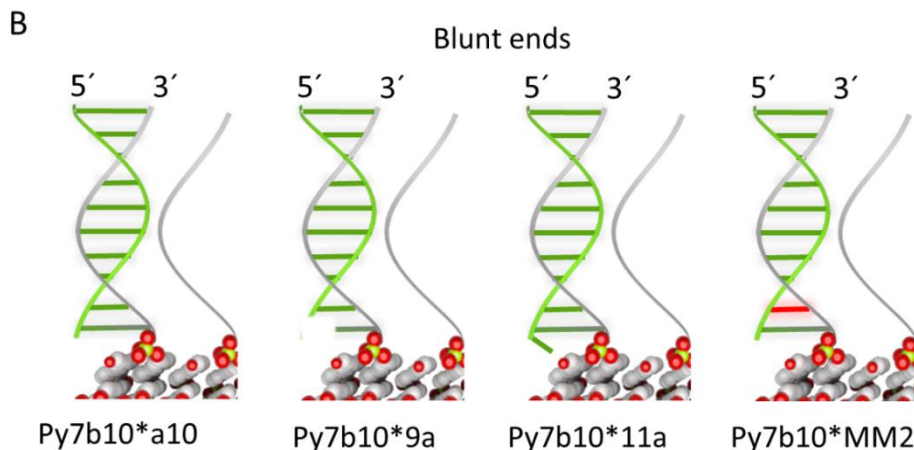
Thus, the blunt-ended AT base pairs, which are formed by hybridization of **d10** with **Py7c10**, do not support network formation due to decreased stability of their blunt-end stacking interactions.

4.2.2 Effect of nucleobase mismatches on the formation of the networks

The influence of base composition on network formation was further elicited by a series of control oligonucleotides differing in length and nucleotide sequence (Scheme 4-3).

Scheme 4-3. A) DNA sequences of the strands in Set 1 and Set 2. Hierarchical assembly: all transitions occurring higher 20°C are assigned as “yes” with a corresponding value (a maximum of the first derivative). The modifications of the **a10** strand are highlighted in red. B) Illustrations of the double strands on a polymerized **Py7b10** platform leading to the networks. Blunt ends are present in all cases.

A	Name	Base sequence	Hierarchical assembly
Set 1	a30	5' - (CTC ACG GAA G) ₃	No
	a20	5' - (CTC ACG GAA G) ₂	No
	a10	5' - CTC ACG GAA G	Yes/30°C
	a8	5'- C ACG GAA G	No
	a9	5'- TC ACG GAA G	No
	8a	5' - CTC ACG GA	No
	9a	5' - CTC ACG GAA	Yes/25°C
	11a	5' - CTC ACG GAA <u>GC</u>	Yes/27°C
	12a	5' - CTC ACG GAA <u>GCT</u>	No
	a11	5' - <u>G</u> CTC ACG GAA	No
	a12	5' - <u>AG</u> CTC ACG GAA	No
	Set 2	MM2	5' - CTC ACG GAT <u>I</u> G
MM3		5' - CTC ACG G <u>I</u> A G	No
MM5		5' - CTC ACC <u>C</u> GAA G	No
MM8		5' - CT <u>G</u> ACG GAA G	No
MM9		5' - <u>C</u> A C ACG GAA G	No



The data show that mismatches, overhanging nucleobases or shorter duplexes have the expected negative impact on the formation and the stability of networks. To get a better understanding of the network formation depending on mismatches, we designed two sets of connector sequences (Scheme 4-3). Set 1 contains 11 strands and aims to evaluate the importance of a connector oligonucleotide length. Set 2 consists of five probes, which contain mismatches at different positions. In Set 1, co-annealing of **Py7b10** and **a10** leads to the highest stability of the networks (Figure 4-10 A) and the most intense CD signal (Figure 4-10 B).

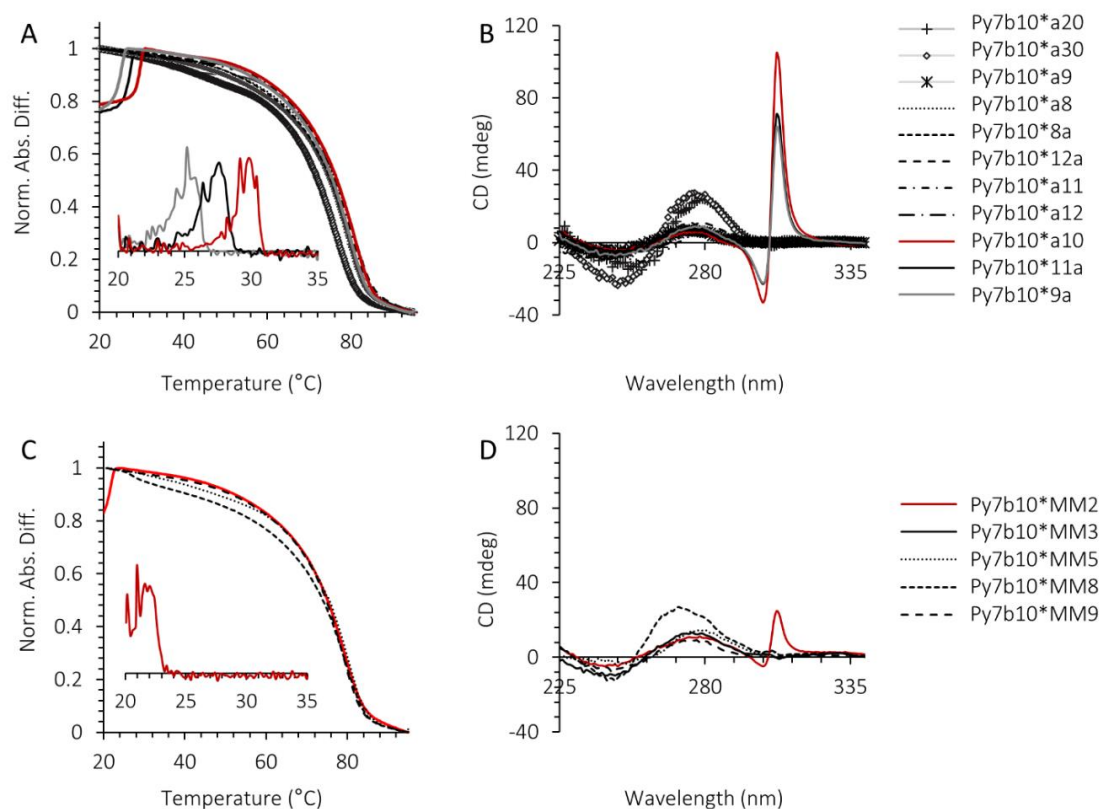


Figure 4-10. A: Annealing (0.1 °C/min) absorption curves with corresponding first derivatives (20-35°C region) for **Py7b10*a10** (red), **Py7b10*11a** (solid black), **Py7b10*9a** (gray), and other **Py7b10/Set 1** strands. B: CD spectra of the samples prepared in (A) at 20°C. C) Cooling (0.1°C/min) absorption curves with corresponding first derivatives (20-35°C) for **Py7b10*MM2** (red) and other **Py7b10/Set 2** strands. D: CD spectra of the samples prepared in (C) at 20°C. Conditions: 2 μ M **Py7c10** and 6 μ M of the strands from Set 1 and Set 2; 10 mM phosphate buffer, pH=7.0, 250 mM sodium chloride.

In Set 2, a single mismatch was introduced at different positions. A transition was detected only for **MM2**. The decreased stability is also reflected by a weak CD signal (Figure 4-10 C, D).

Among shorter connector strands, the second transition is observed only for **9a**. This strand lacks a single base at the 3'-end. For the longer overhanging strands, the transition was found only for **11a**. This sequence contains an additional base at the 3'-end.

Thus, the 5'-position of connector strands plays a more important role in the network formation, and the influence of the bases at 3'-end, located closer to a polymer core, is reduced. The energetic penalty on the hierarchical process applied by structural changes closer to the 5'-end of a sequence is larger with respect to the 3'-end.

Again, the mismatch is positioned close to the 3'-end, which is the closest to a polymer chain. This result shows that a single mismatch results in a less efficient hybridization and hampers the network formation compared to the fully matched strand **a10**. Therefore, hybridization of all ten nucleobases of **a10** is essential for efficient blunt-end stacking and the formation of networks.

4.2.3 Effect of **Py7b10/a10** ratio on the hierarchical organization.

The variation of a **Py7b10/a10** ratio (concentration of **Py7b10** is kept constant) allows monitoring the stability of the network formation. The temperature of the second transition is strongly dependent on a **a10** concentration. An addition of only 15 mol. % of **a10** is sufficient to induce this transition higher 20°C (Figure 4-11, solid gray lines). Additionally, correlative CD data show that the intensity of the Cotton effect becomes stronger upon increasing the concentration of **a10** (Figure 4-12).

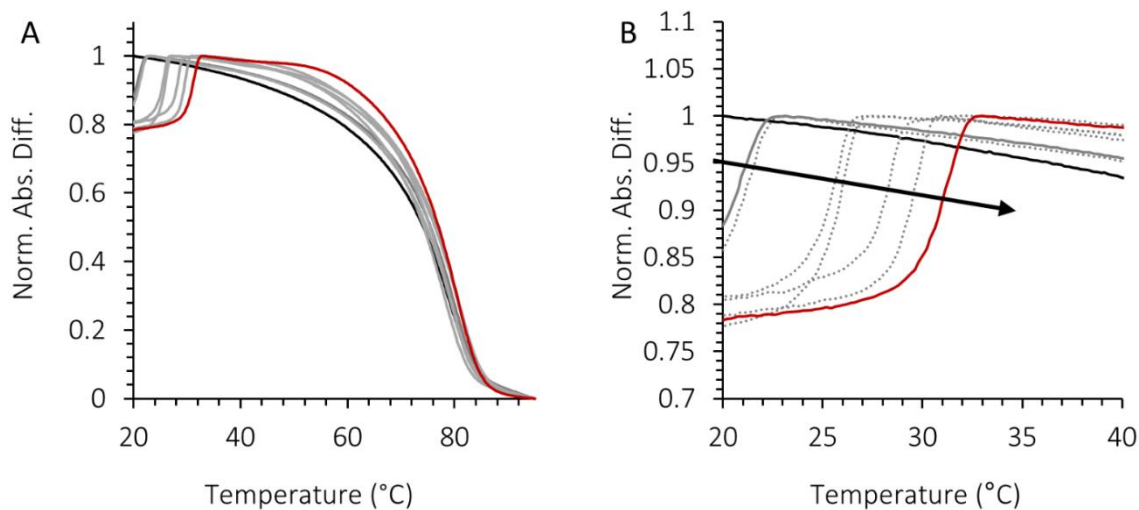


Figure 4-11. A: Annealing curves, normalized at 305 nm of **Py7b10*a10** system with various content of **a10**. B: Enlarged area of (A). The arrow indicates an increase of **a10** concentration from 10% (black), 15% (solid gray) to 1000% (red). Conditions: 2 μM **Py7b10**; 10 mM phosphate buffer, pH=7.0, 250 mM sodium chloride.

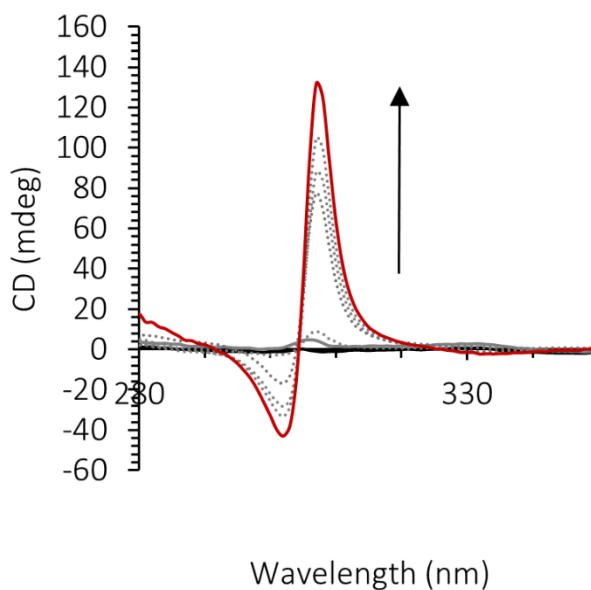


Figure 4-12. CD spectra of **Py7b10*a10** 20°C. The arrow indicates an increase of **a10** concentration from 10% (black), 15% (solid gray) to 1000% (red). Conditions: 2 μM **Py7b10**; 10 mM phosphate buffer, pH=7.0, 250 mM sodium chloride.

4.2.4 Reversibility of networks upon addition of **b10** (separator strand).

The supramolecular nature of the interactions of nanoribbons allows reversing the network formation under the isothermal condition, as shown by competition experiments. Thus, the addition of the separator strand (**b10**, the 2-fold excess over **a10**) to the **Py7b10*a10** network at 20°C results in the disassembly of the aggregates (illustrated in Scheme 4-2). Formation of the duplex **a10*b10** ($T_m=47^\circ\text{C}$, Figure 4-13) leads to the removal of the connector strand **1b** from the network.

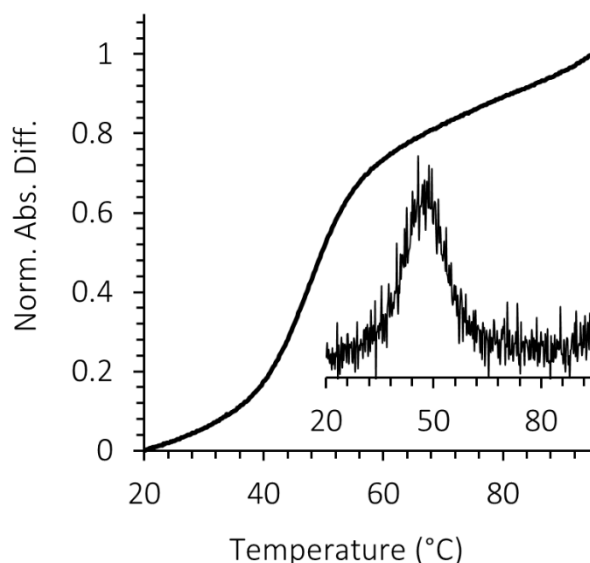


Figure 4-13. Annealing curve (0.1°C/min) for system containing 2 μM **a10** + 6 μM **b10**. The difference of intensity was normalized at 260 nm. Conditions: 10 mM phosphate buffer, pH=7.0, 250 mM sodium chloride.

A complete disappearance of the network is accomplished within 2 hours (Figure 4-14 C). AFM imaging shows only individual ribbons after addition of **1a** (Figure 4-15). The disassembly process is also confirmed by the disappearance of the CD signal at 305 nm (Figure 4-3). We assume that such a strong CD signal, which is characteristic for the networks, originates from the decreased flexibility of the pyrenes in the polymer core caused by the confined environment. Such conformation leads to slightly different

orientation of transition dipole moments in long pyrene stacks compared to relatively flexible individual ribbons.²²⁷

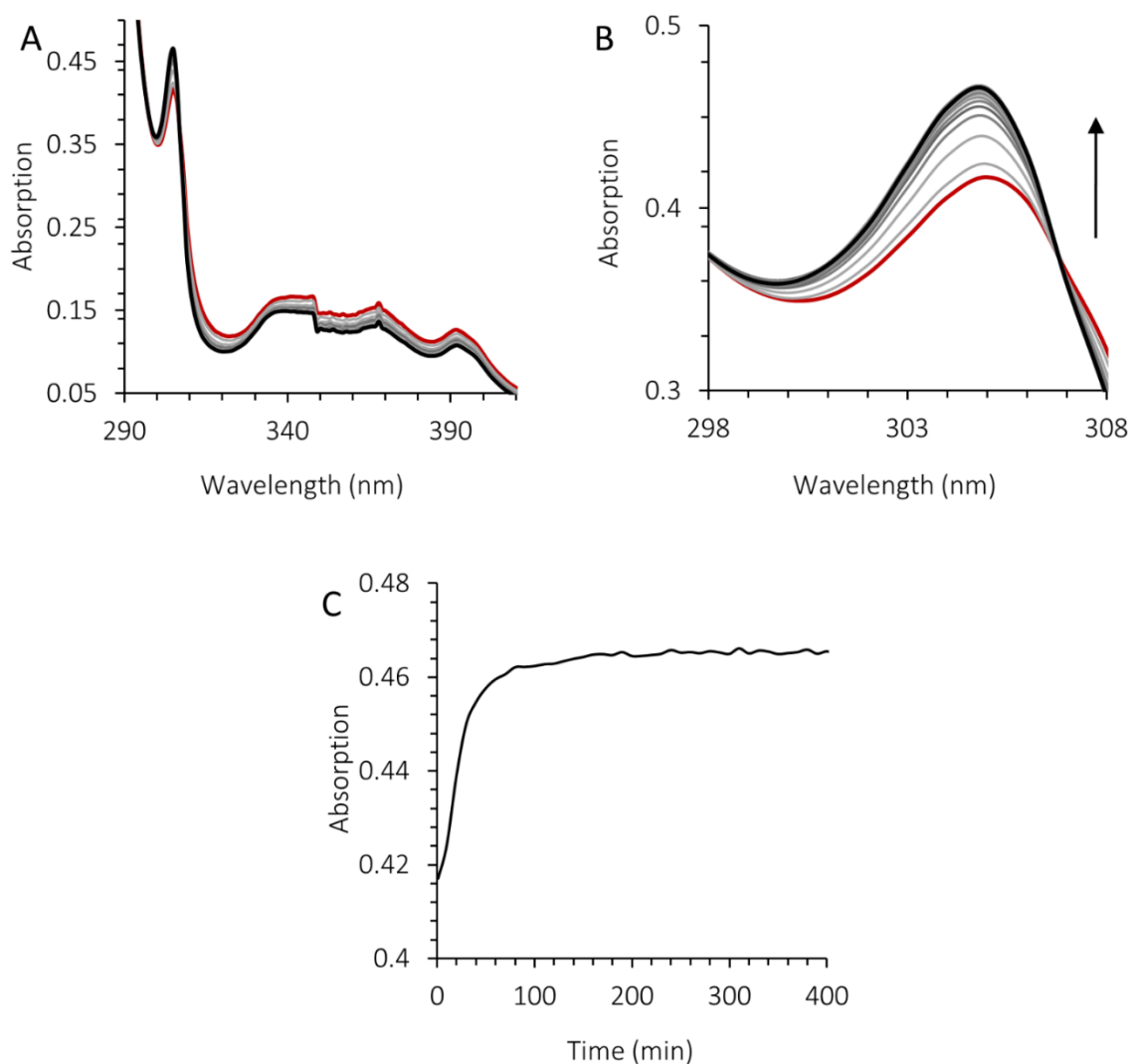


Figure 4-14. Network disassembly experiments. A: Time-dependent absorption spectra at 20°C upon addition of **b10** (separator strand, 12 μM) to networks prepared by annealing 2 μM **Py7b10** + 6 μM **a10**. B: Enlarged area of (A). The arrow indicates changes with time. C: Time-dependent absorption at 305 nm after the addition of **b10** (12 μM) to networks **Py7b10*****a10**. Conditions: 10 mM phosphate buffer, pH=7.0, 250 mM sodium chloride.

Furthermore, the hierarchical assembly is not limited to the **Py7b10*****a10** pair. The spectroscopic response was also observed for the combination **Py7a10*****b10** (Figure 4-16), which also contains GC blunt ends.

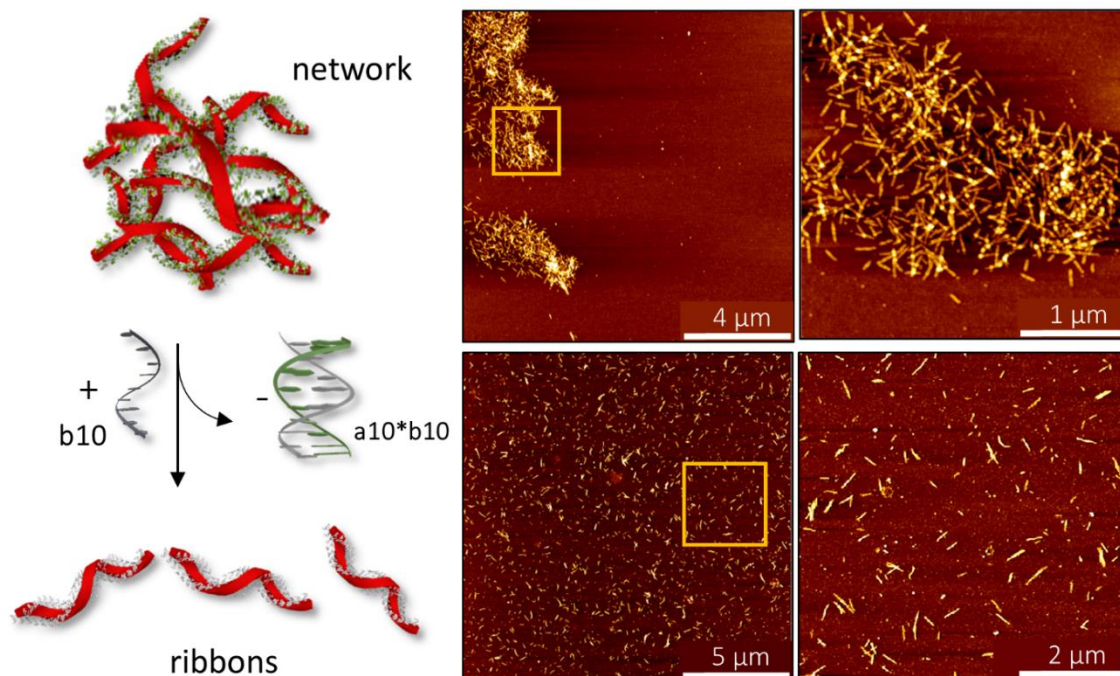


Figure 4-15. AFM images (right) and illustrative schemes (left) describing disassembly of the networks upon addition of 1a (separator strand); red: assembled pyrenes forming the core of the ribbons; light gray: oligonucleotide chains appended on edges of the ribbons; green: complementary oligonucleotide.

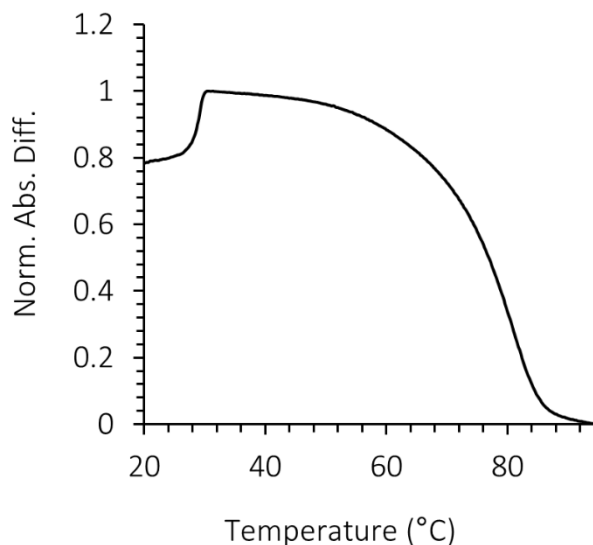


Figure 4-16. Annealing absorption curves at 305 nm with corresponding first derivatives for **Py7a10*****b10**. Conditions: 2 μM **Py7a10** and 6 μM of **b10**; 10 mM phosphate buffer, pH=7.0, 250 mM sodium chloride.

4.2.5 Network formation from ribbons composed of $27\text{Py}7\text{b}10$

The DNA duplexes formed by annealing of **a10** to $27\text{Py}7\text{b}10$ were expected to enable blunt-end stacking interactions along the edges of the supramolecular polymers. In a typical experiment, a mixture of $27\text{Py}7\text{b}10$ and **a10** was slowly co-annealed from 95 °C to 15 °C. In addition to the transition due to the supramolecular polymerization process, the temperature-dependent absorption at 252 nm shows a second transition below 20 °C (Figure 4-17).

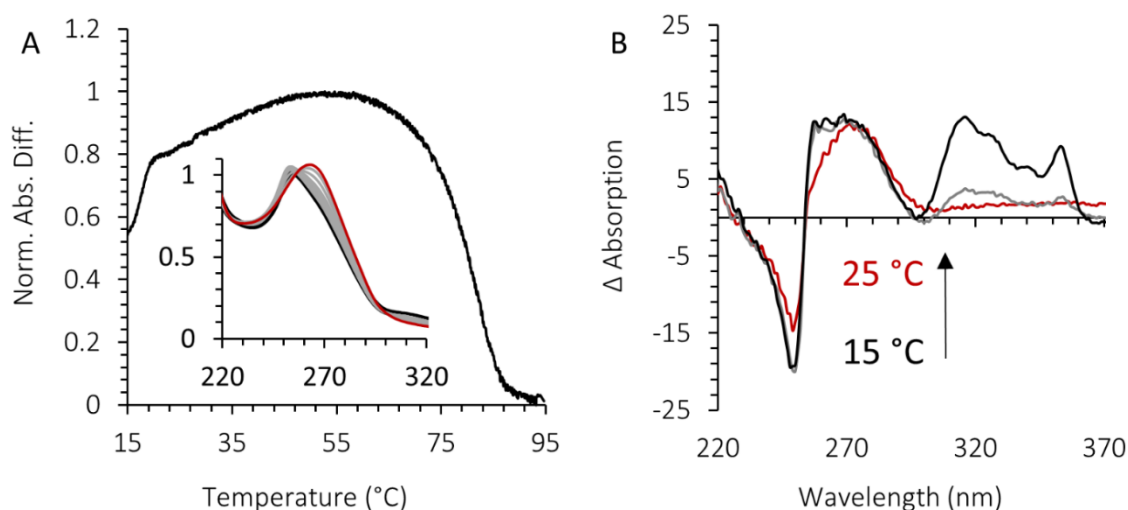


Figure 4-17. A: Normalized cooling curve for $27\text{Py}7\text{b}10*\text{a}10$ ($2\mu\text{M}/6\mu\text{M}$) mixture monitored at 252 nm. The inset shows temperature-dependent UV/Vis absorption for $27\text{Py}7\text{b}10*\text{a}10$. B: CD spectra of $27\text{Py}7\text{b}10*\text{a}10$ in aqueous solution at different temperatures (15 °C, 20 °C, 25 °C). Arrow indicates increasing temperature. Conditions: 10 mM PBS, 150 mM NaCl, pH=7.

This transition corresponds to the process of polymer aggregation via blunt-end stacking interactions and induces conformational changes in pyrene arrays. Similarly to the previous systems, AFM images reveal micrometer-sized networks formed by the mixture $27\text{Py}7\text{b}10*\text{a}10$ (Figure 4-18). However, the CD spectrum of $27\text{Py}7\text{b}10*\text{a}10$ differs and consists of two regions. In the range of 225-300 nm, a strong exciton coupled signal (+275/-250 nm) is overlapped with the bands of the DNA duplex (Figure 4-17 B). In the range of 300-400 nm, which reflects the absorption spectrum of aggregated 2,7-substituted pyrenes, the CD spectrum is dominated by several induced bands.

All spectroscopic fingerprints of the networks disappear upon heating above their stability temperature (~ 20 °C). The successful implementation of the 2,7 – substituted pyrenes into the hierarchical assembly via blunt-end interactions shows the modularity of our design strategy.

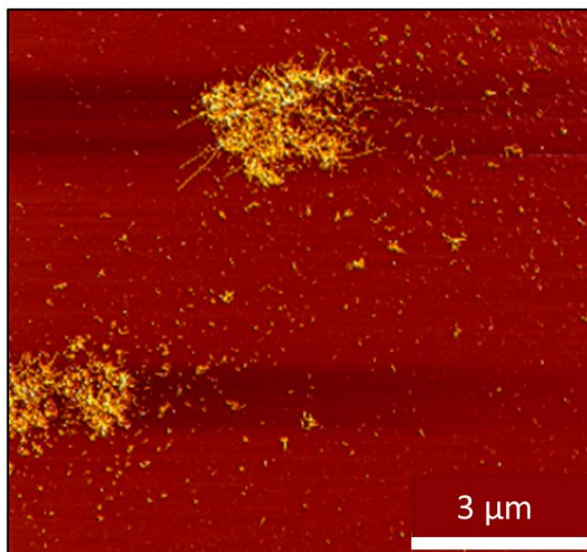


Figure 4-18. AFM image of networks formed from supramolecular polymers **27Py7b10*a10**. Conditions: 10 mM PBS, 150 mM NaCl, pH=7.

4.2.6 Self-assembly pathway in a three-component system which involves blunt-end stacking

The three-component system involves **Py7a10**, **Py7b10** oligonucleotide **a10**, which is complementary to **Py7b10**. AFM imaging shows that the addition of **a10** to preformed **Py7a10*Py7b10** networks at 20 °C does not affect the appearance of the networks (Figure 4-19 B, C).

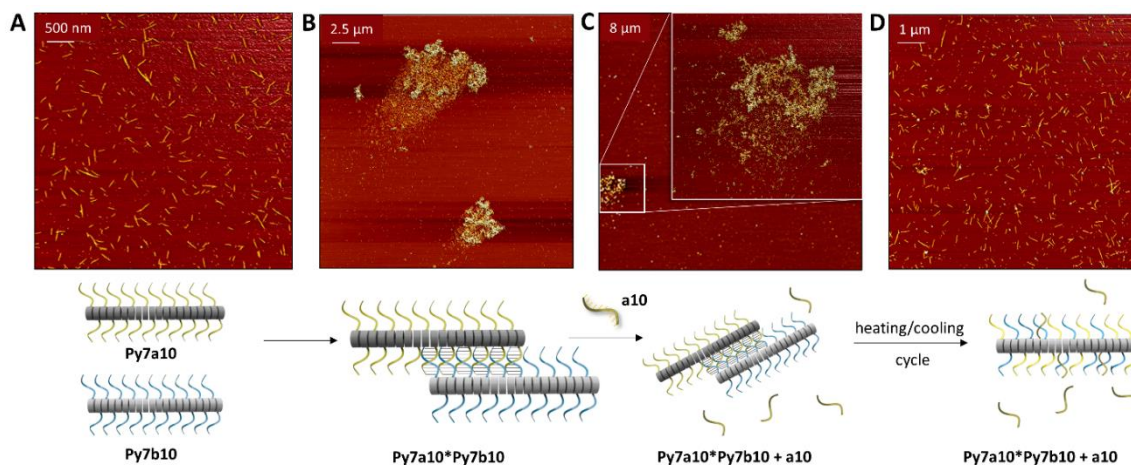


Figure 4-19. AFM images of materials obtained at different stages in a three-component mixture using **Py7a10*Py7b10** networks. Conditions: 200 mM NaCl, 10 mM phosphate buffer system pH = 7, concentration of **Py7a10** and **Py7b10** = 2 μ M; **a10** = 6 μ M.

Disassembly of these aggregates **Py7a10*Py7b10 + a10** by heating to 95 $^{\circ}$ C leads to the molecularly dissolved chains (Figure 4-21 A). Renewed cooling from 95 $^{\circ}$ C to 20 $^{\circ}$ C exhibits a single transition by a nucleation-elongation mechanism and exclusively leads to linear supramolecular polymers (Figure 4-19 D). Next, **Py7b10** and **a10** were mixed to form networks of **Py7b10*a10** as confirmed by AFM (Figure 4-20 B) and CD analysis (Figure 4-22).

After addition of **Py7a10** to this system, AFM images show the presence of both, **Py7b10*a10** networks and linear **Py7a10** (Figure 4-20 C). These results indicate that hybridization of DNA chains of **Py7b10** with **a10** precludes duplex formation between complementary strands of **Py7a10** and **Py7b10**. This underlines the slow dynamics of hybrid oligomer exchange. Performing an additional heating/cooling cycle (Figure 4-21 B) leads again to the formation of the thermodynamically favored, mixed supramolecular polymers (Figure 4-20 D).

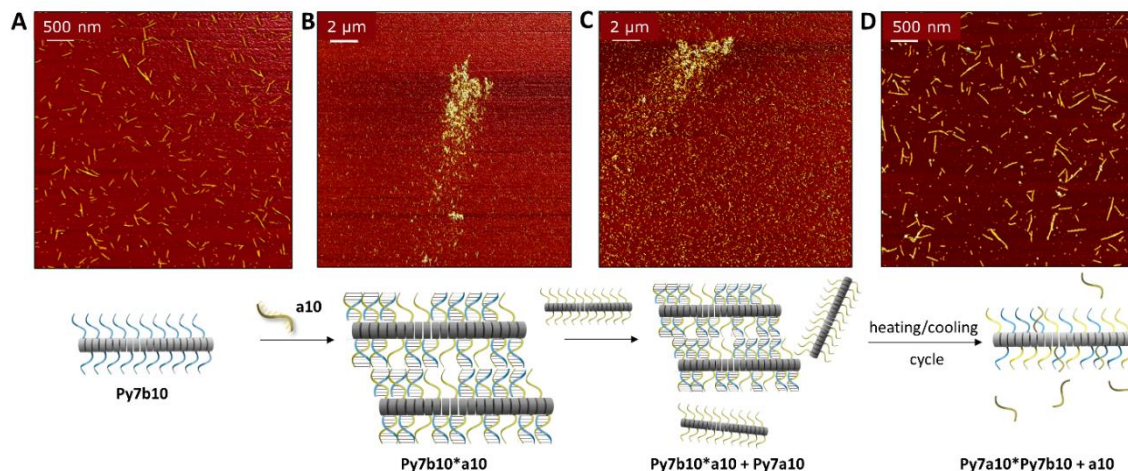


Figure 4-20. AFM images of materials obtained at different stages in a three-component mixture using **Py7b10*a10** networks. Conditions: 200 mM NaCl, 10 mM phosphate buffer system pH = 7, concentration of **Py7a10** and **Py7b10** = 2 μ M; **a10** = 6 μ M.

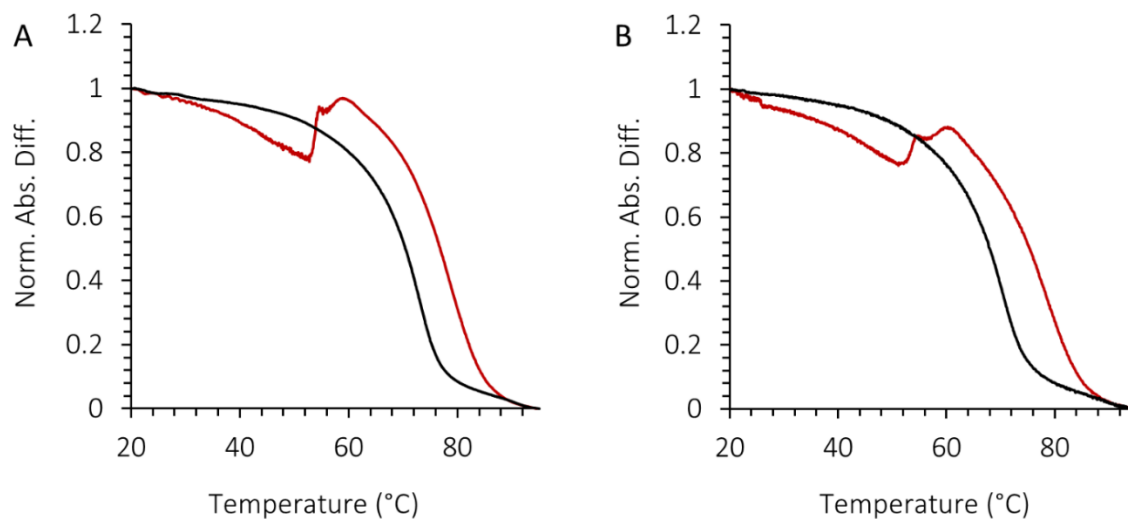


Figure 4-21. Normalized temperature-dependent absorption measured at 305 nm for **Py7a10*Py7b10 + a10** (A) and **Py7b10*a10 + Py7a10**(B). Conditions: 200 mM NaCl, 10 mM phosphate buffer system pH = 7, concentration of **Py7a10** and **Py7b10** = 2 μ M; **a10** = 6 μ M.

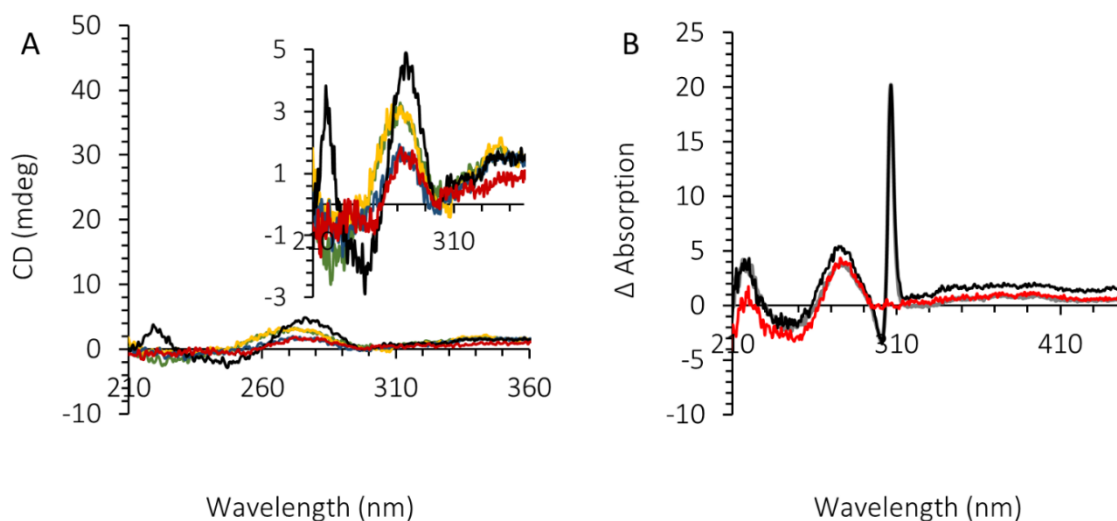


Figure 4-22. (A) CD spectra for **Py7a10** (yellow), **Py7b10** (green), **Py7a10/Py7b10** (red), **Py7a10*Py7b10** (blue) and **Py7a10*Py7b10 + a10** (black) at 20°C. The inset shows enlarged signals of (B). CD spectra for **Py7b10*a10** (black) and **Py7b10*a10 + Py7a10** at 20°C before (gray) and after heating-cooling cycle (red). Conditions: 200 mM NaCl, 10 mM phosphate buffer system pH = 7, concentration of **Py7a10** and **Py7b10** = 2 μ M; **a10** = 6 μ M.

4.3 CONCLUSIONS

In conclusion, we have demonstrated that chimeric pyrene-DNA oligomers assemble into extended networks via hierarchical assembly pathways. The first step, self-assembly of oligomers into helical nanoribbons, is driven by aromatic stacking interactions among pyrene units. The supramolecular polymerization is independent of the nucleotide sequence of the DNA part. The second step, aggregation of individual nanoribbons into extended networks, only takes place in the presence of a complementary oligonucleotide. Hybridization leads to the formation of duplexes along the helical nanoribbon core. Blunt-end stacking interactions of GC base pairs trigger the formation of a network in a highly cooperative process. The networks can be disassembled by destroying the coaxial stacking interactions either by heating or through the addition of a separator strand. Supramolecular polymeric networks of this type may be relevant for the development of DNA-based smart materials, such as stimuli-responsive carriers of active ingredients.

4.4 EXPERIMENTAL SECTION

Unless otherwise noted, all chemicals and general methods were used as described in section 2.4.

Unmodified oligonucleotides from Set 1 were synthesized using phosphoramidite approach and purified on the C18 column using 0.1 M TEAA at pH=7.0 and acetonitrile according to the procedure described previously. Strands from Set 2 and strands with overhangs from Set 1 were purchased from Microsynth AG and used without further purification.

CHAPTER 5. POTENTIAL APPLICATIONS OF DNA-GRAFTED
SUPRAMOLECULAR POLYMERS

ABSTRACT

The synthesis, characterization, and functionalization of chiral DNA-grafted supramolecular polymers are reported. One-dimensional supramolecular polymers are assembled from monodisperse, sequence-specific oligophosphodiester consisting of natural nucleosides (A, G, C, T) and pyrene chromophores linked by phosphodiester bonds. These chiral DNA-grafted supramolecular polymers were successfully used for energy transfer and as templates for cargo binding (AuNP). The formation and properties of supramolecular polymers were followed by atomic force microscopy (AFM), transmission electron microscopy (TEM) and fluorescence.

Part of this work has been published:

Y. Vyborna, M. Vybornyi, A. V. Rudnev and R. Häner, *Angew. Chemie Int. Ed.*, 2015, **54**, 7934–7938.

Y. Vyborna, M. Vybornyi and R. Häner, *Chem. Commun.* 2017, **53**, 5179-5181.

5.1 INTRODUCTION

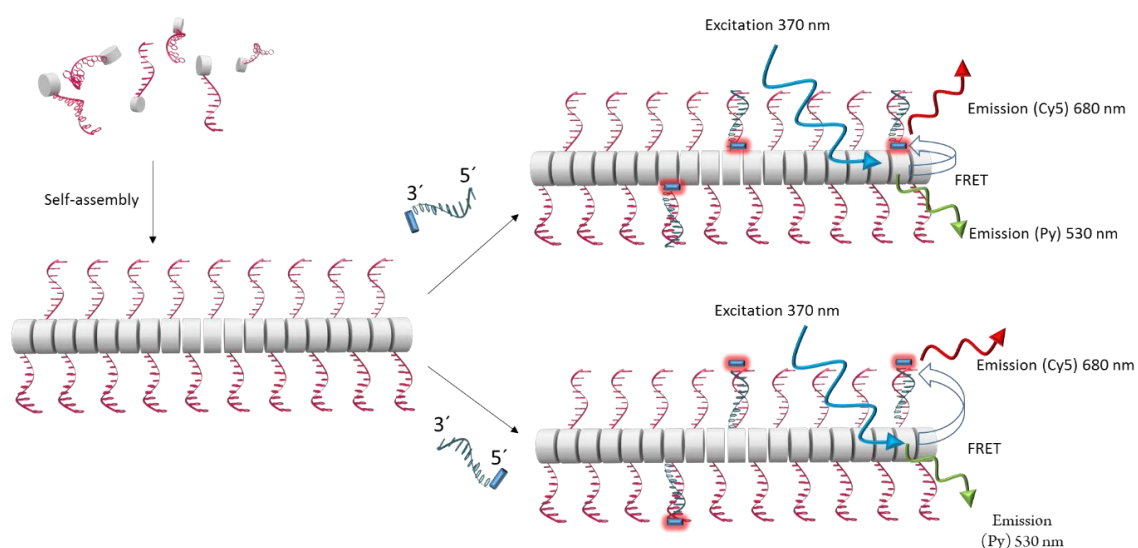
Supramolecular polymers have proved their potential for the preparation of functional systems with tailor-made biomimetic properties.^{3,14,22,228,229} Since their assembly is based on non-covalent interactions, supramolecular polymers exhibit pronounced stimuli-responsiveness, and their adaptability to environmental factors may exceed that of covalent polymers. These qualities are essential for applications in various fields,^{13,214} including biosensing,²¹⁴ drug delivery²³⁰ and protein scaffolding.²³¹ The rapid expansion of the field recently also led to the emergence of DNA-grafted supramolecular polymers as smart, programmable assemblies.^{84,218,232,233} These materials are accessible via self-assembly of DNA strands conjugated to hydrophobic oligomers or polymers.^{109,179,234,235} DNA-grafted supramolecular polymers combine the intrinsic functionalities of a non-covalent polymer core with the recognition properties of the nucleic acids.^{153,236} The self-assembly of the two parts proceeds orthogonally, thus affording a route for versatile functionalization of the pre-assembled polymer via DNA hybridization.¹³⁶ For example, oligonucleotide domains can be used as handles to attach and release different types of cargoes in a sequence-specific way^{108,237} or form other stimuli-responsive functional assemblies, e.g., hydrogels.²³⁸ While numerous practical applications of DNA-grafted polymers have been reported,^{94,99,143,239,240} their supramolecular counterparts suffer from limited knowledge of how to build DNA arrays of different dimensionality on supramolecular scaffolds. We have recently shown that DNA-grafted supramolecular polymers are formed as a result of hydrophobic interactions in aqueous solution between pyrene units.²¹⁸ The approach largely relies on the programmable properties of monodisperse, sequence-specific oligophosphates.^{101,145,241,242} In this chapter, we present some of the potential applications of the DNA-grafted supramolecular polymers – energy transfer platforms and cargo carriers.

5.2 RESULTS AND DISCUSSIONS

5.2.1 FRET Analysis

In the current model system, we demonstrate the hybridization ability of tethered DNA and the usage of a fluorescent supramolecular platform for the energy transfer applications. Aiming this goal, we added a labeled DNA strand containing an acceptor dye Cy5 (at 3' or 5' terminal positions) to the DNA-grafted supramolecular polymers (Scheme 5-1).

Scheme 5-1. Illustration of the concept of FRET experiment.



Excimer emission of pyrenes is efficiently transferred to the cyanine dye. The FRET efficiency is inversely proportional to the distance between donor and acceptor.²⁴³ Energy transfer occurs in a distance-dependent way. An increase in the FRET efficiency from 33% to 46% with the decreasing distance

between Cy5 and pyrene was observed (Figure 5-1). This result confirms that the DNA strands are accessible for hybridization and retain their functionality.

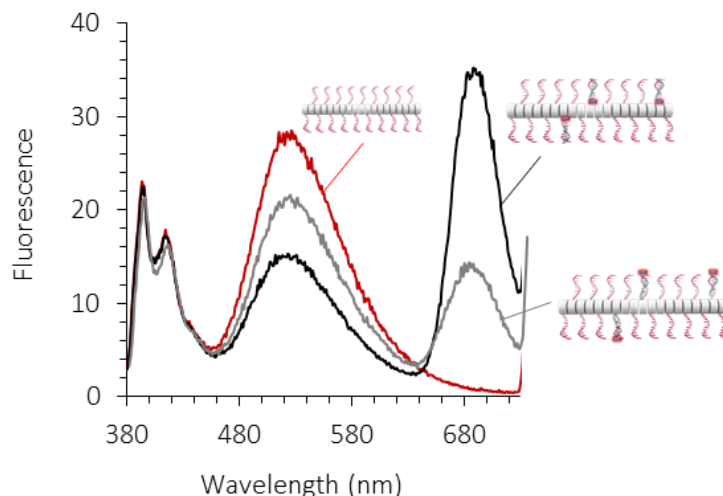


Figure 5-1. FRET analysis of the hybridization of the tethered DNA of the single-component self-assembly: for the 3' modified DNA (closer to the pyrene) the efficiency was as high as 46% and decreased to 33% for the 5' modified DNA (donor-acceptor is expected to be separated by 10 base pairs).

5.2.2 Arrangement of gold nanoparticles

DNA is widely used for the precise arrangement of nanoscale objects, such as inorganic NPs^{61,244,245} and proteins.²³¹ The potential of DNA-grafted polymers as a cargo system is demonstrated by the selective arrangement of gold nanoparticles (AuNPs) along the supramolecular ribbons. AuNPs with an average diameter of 5 nm were prepared by the citrate reduction method²⁴⁷ and conjugated to thiol-modified oligonucleotides (Experimental Section). AuNPs were densely packed with oligonucleotides. This allows to leverage repulsive charge interactions and attractive hybridization interactions and, at the same time, also minimizes cross-linking events by potential annealing to multiple binding sites.²⁴⁶ Hybridization of the supramolecular polymers with the complementary AuNP-oligonucleotides led to the selective attachment of the AuNPs along the edges of the nanoribbons. As illustrated by the TEM

images (Figure 5-2), AuNPs are aligned along both edges of the supramolecular polymers, confirming that the polymer appended single-stranded oligonucleotides are amenable to sequence-specific hybridization.

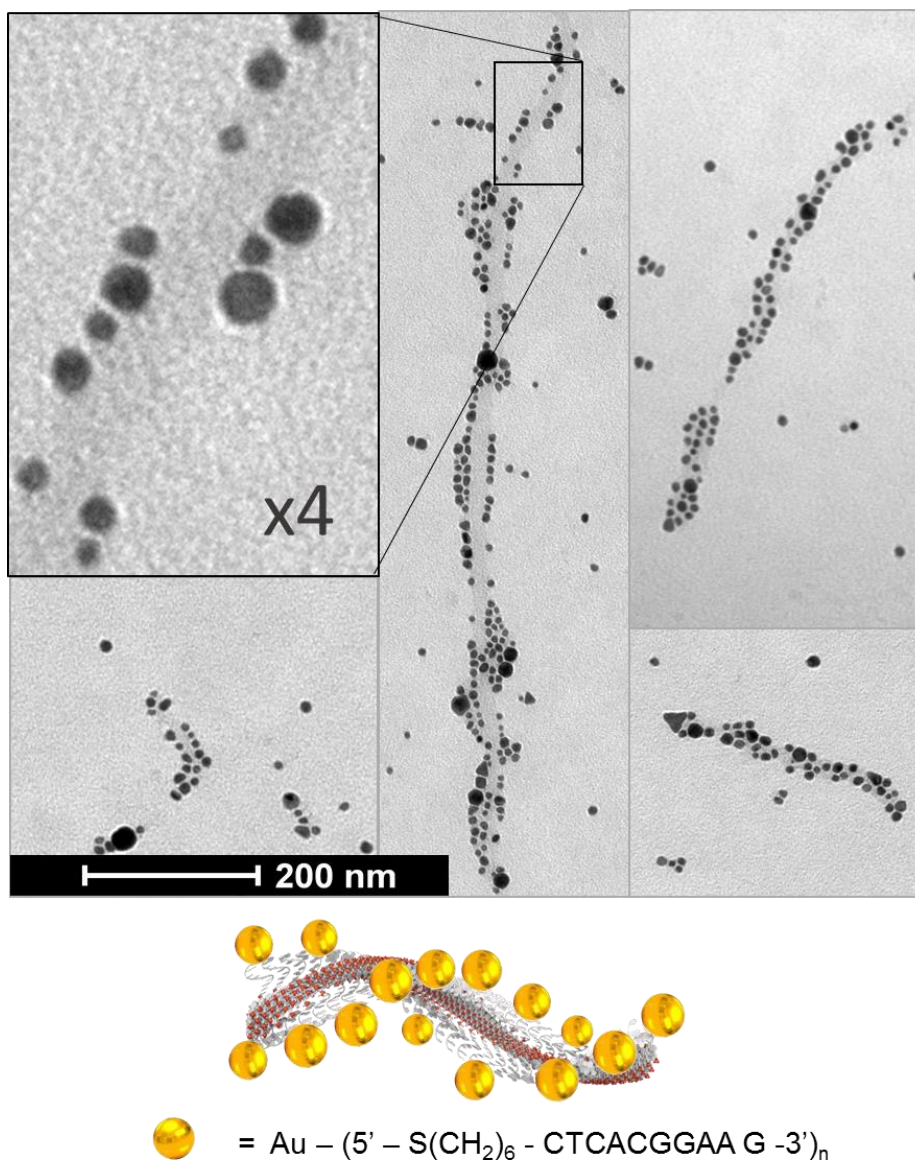


Figure 5-2. TEM images AuNPs attached to DNA-grafted supramolecular polymers of **27Py7b10**. An illustration of the immobilization of AuNPs on the DNA-grafted supramolecular nanoribbon is shown at the bottom.

5.3 CONCLUSIONS

We have demonstrated that DNA-grafted supramolecular polymers could be utilized as platforms for the arrangement of functional moieties through hybridization between complementary strands. While pyrene core can serve as a donor, Cy5 (acceptor) was attached along the nanoribbons. Taking advantage of the unique self-recognition properties of the DNA, it is possible to attach target functionalities precisely.

Moreover, the single-stranded DNA chains are efficiently loaded with DNA-modified AuNPs, which serve as a model cargo. Finally, we have shown herein that DNA-grafted supramolecular polymers act as a reliable, functional platform which combines dynamic and responsive nature of non-covalent polymers with an exceptional selectivity of DNA chains hybridization. Further studies in the field can lead to the development of new delivery and sensing systems.

5.4 EXPERIMENTAL SECTION

Unless otherwise noted, all chemicals and general methods were used as described in section 2.4.

Materials and General Methods.

Cyanine-modified DNA strands were purchased from Microsynth AG and used without further purification.

Synthesis of AuNPs

AuNPs with a diameter of ~ 5 nm were synthesized by the citrate reduction method in the presence of a tannic acid as a co-reductant.²⁴⁷ First, 100 ml of a solution of 0.3 mM HauCl_4 was brought to a boil and mixed with 2 ml of 1% citric acid and 7 ml of 1% tannic acid. After the color of the solution changed to burgundy, the solution was refluxed for another 3 min and cooled to room temperature. The AuNPs solution was filtered through a syringe filter with a pore size of 0.2 μm . Next, the citrate coated nanoparticles were stabilized by exchanging the citrate shell for a more stable phosphine ligand. Thus, 11 mg

of BSPP (bis(p-sulfonatophenyl)- phenylphosphine dipotassium salt) was added to 10 ml of the AuNPs solution and was shaken overnight at low speed. For the precipitation of AuNPs, solid NaCl was added slowly until a color changed from red to gray-blue. The solution was then centrifuged for 15 min at 4400 rpm; the supernatant was removed, and the AuNPs were resuspended in 500 μl of an aqueous 0.5 mM BSPP solution. The centrifugation and resuspension were repeated twice. Finally, the concentration was determined photometrically at 520 nm assuming a molar extinction coefficient for the 5 nm AuNP of $1 \cdot 10^7 \text{ M}^{-1} \cdot \text{cm}^{-1}$.

CHAPTER 6. GENERAL CONCLUSIONS

The main goal of the current work was the design and fabrication of the chromophore-templated arrays of DNA with the long-term goal of functionalization of the created structures through hybridization between complementary DNA strands. In the studies, the synthesis procedure of the DNA-pyrene conjugates was established and the self-assembly properties of these amphiphiles were investigated thoroughly.

In Chapter 2, the supramolecular polymerization of chimeric oligomers composed of pyrenes and oligodeoxynucleotides was studied. The polymers self-assemble via aromatic stacking interactions of pyrenes. The length of DNA and pyrene chains, as well as the type of pyrene isomer, controls the appearance of the polymers and their spectroscopic characteristics.

In Chapter 3, we have studied the mechanistic details of the assembly of chimeric DNA-pyrene oligomers. The structural and functional properties of the polymers largely depend on the assembly pathway. DNA interactions between individually prepared (sorted) polymers lead to the formation of polymeric supramolecular networks via hybridization of complementary oligonucleotides. These networks are metastable and can be transformed into the thermodynamically favored species. The latter is characterized by the absence of networks due to scrambling of the oligonucleotides over the polymers

Chapter 4 describes the hierarchical self-assembly of chimeric DNA-pyrene oligomers into supramolecular networks. Interactions between individual ribbons were identified as blunt-ended stacking between GC base pairs. The separate processes were monitored by intensity changes of a characteristic pyrene absorption band originating from the polymer formation. Furthermore, we demonstrate that the supramolecular networks exhibit pronounced CD activity. Network formation is reversible and disassembly into individual

ribbons is realized either via thermal denaturation or by addition of a DNA separator strand.

In Chapter 5, we demonstrate the loading of supramolecular polymers with a model cargo. Thus, gold nanoparticles have been attached along the edges of the ribbons via DNA hybridization. Additionally, we propose a model system, in which we demonstrate the hybridization ability of the tethered DNA and the usage of a fluorescent supramolecular platform for the energy transfer applications. Aiming this goal, we added a labeled DNA strand containing an acceptor dye Cy5 (at 3' or 5' terminal positions) to the DNA-grafted supramolecular polymers. Excimer emission of pyrenes is efficiently transferred to the cyanine dye.

The findings provide insight into the process of supramolecular polymerization of amphiphilic oligomers in water leading to polymers with different morphology and chiroptical activity. Supramolecular polymers of this type may be relevant for the development of DNA-based smart materials, such as stimuli-responsive carriers of active ingredients.

BIBLIOGRAPHY

BIBLIOGRAPHY

- (1) Lehn, J. M. Supramolecular Chemistry - Scope and Perspectives: Molecules - Supermolecules - Molecular Devices. *J. Incl. Phenom.* **1988**, *6*, 351–396.
- (2) Hou, X.; Ke, C.; Zhou, Y.; Xie, Z.; Alngadh, A.; Keane, D. T.; Nassar, M. S.; Botros, Y. Y.; Mirkin, C. A.; Stoddart, J. F. Concurrent Covalent and Supramolecular Polymerization. *Chem. - A Eur. J.* **2016**, *22*, 12301–12306.
- (3) Yang, L.; Tan, X.; Wang, Z.; Zhang, X. Supramolecular Polymers: Historical Development, Preparation, Characterization, and Functions. *Chem. Rev.* **2015**, *115*, 7196–7239.
- (4) Priimagi, A.; Cavallo, G.; Metrangolo, P.; Resnati, G. The Halogen Bond in the Design of Functional Supramolecular Materials: Recent Advances. *Acc. Chem. Res.* **2013**, *46*, 2686–2695.
- (5) Sherrington, D. C.; Taskinen, K. A. Self-Assembly in Synthetic Macromolecular Systems via Multiple Hydrogen Bonding Interactions. *Chem. Soc. Rev.* **2001**, *30*, 83–93.
- (6) Hoeben, F. J. M.; Jonkheijm, P.; Meijer, E. W.; Schenning, A. P. H. J. About Supramolecular Assemblies of Pi-Conjugated Systems. *Chem. Rev.* **2005**, *105*, 1491–1546.
- (7) McConnell, A. J.; Wood, C. S.; Neelakandan, P. P.; Nitschke, J. R. Stimuli-Responsive Metal-Ligand Assemblies. *Chem. Rev.* **2015**, *115*, 7729–7793.
- (8) Yu, G.; Jie, K.; Huang, F. Supramolecular Amphiphiles Based on Host-Guest Molecular Recognition Motifs. *Chem. Rev.* **2015**, *115*, 7240–7303.
- (9) Greef, T. De; Smulders, M. M. M. J.; Wolffs, M.; Schenning, A. P. H. J.; Sijbesma, R. P.; Meijer, E. W. Supramolecular Polymerization. *Chem. Rev.* **2009**, *109*, 5687–5754.

-
- (10) Mattia, E.; Otto, S. Supramolecular Systems Chemistry. *Nat. Nanotechnol.* **2015**, *10*, 111–119.
- (11) Fukui, T.; Kawai, S.; Fujinuma, S.; Matsushita, Y.; Yasuda, T.; Sakurai, T.; Seki, S.; Takeuchi, M.; Sugiyasu, K. Control over Differentiation of a Metastable Supramolecular Assembly in One and Two Dimensions. *Nat. Chem.* **2016**, 4–10.
- (12) Boekhoven, J.; Hendriksen, W. E.; Koper, G. J. M.; Eelkema, R.; van Esch, J. H. Transient Assembly of Active Materials Fueled by a Chemical Reaction. *Science* **2015**, *349*, 1075–1079.
- (13) Dong, R.; Zhou, Y.; Huang, X.; Zhu, X.; Lu, Y.; Shen, J. Functional Supramolecular Polymers for Biomedical Applications. *Adv. Mater.* **2015**, 498–526.
- (14) Stupp, S. I.; Palmer, L. C. Supramolecular Chemistry and Self-Assembly in Organic Materials Design. *Chem. Mater.* **2013**, *26*, 507–518.
- (15) Herbst, F.; Döhler, D.; Michael, P.; Binder, W. H. Self-Healing Polymers via Supramolecular Forces. *Macromol. Rapid Commun.* **2013**, *34*, 203–220.
- (16) Yan, X.; Wang, F.; Zheng, B.; Huang, F. Stimuli-Responsive Supramolecular Polymeric Materials. *Chem. Soc. Rev.* **2012**, *41*, 6042.
- (17) Wu, Y.; Wang, L.; Zhao, X.; Hou, S.; Guo, B.; Ma, P. X. Self-Healing Supramolecular Bioelastomers with Shape Memory Property as a Multifunctional Platform for Biomedical Applications via Modular Assembly. *Biomaterials* **2016**, *104*, 18–31.
- (18) Shigemitsu, H.; Hamachi, I. Design Strategies of Stimuli-Responsive Supramolecular Hydrogels Relying on Structural Analyses and Cell-Mimicking Approaches. *Acc. Chem. Res.* **2017**, *50*, 740–750.
- (19) Anslyn, E. V. Supramolecular Analytical Chemistry. *J. Org. Chem.* **2007**, *72*, 687–699.
- (20) Bähring, S.; Martín-Gomis, L.; Olsen, G.; Nielsen, K. A.; Kim, D. S.; Duedal, T.; Sastre-Santos, Á.; Jeppesen, J. O.; Sessler, J. L. Design and

-
- Sensing Properties of a Self-Assembled Supramolecular Oligomer. *Chem. - A Eur. J.* **2016**, *22*, 1958–1967.
- (21) Bakker, M. H.; Lee, C. C.; Meijer, E. W.; Dankers, P. Y. W.; Albertazzi, L. Multicomponent Supramolecular Polymers as a Modular Platform for Intracellular Delivery. *ACS Nano* **2016**, *10*, 1845–1852.
- (22) Krieg, E.; Bastings, M. M. C.; Besenius, P.; Rybtchinski, B. Supramolecular Polymers in Aqueous Media. *Chem. Rev.* **2016**, *116*, 2414–2477.
- (23) Görl, D.; Zhang, X.; Würthner, F. Molecular Assemblies of Perylene Bisimide Dyes in Water. *Angew. Chemie Int. Ed.* **2012**, *51*, 6328–6348.
- (24) Caruthers, M. H. Gene Synthesis Machines: DNA Chemistry and Its Uses. *Science* **1985**, *230*, 281–285.
- (25) Teo, Y. N.; Kool, E. T. DNA-Multichromophore Systems. *Chem. Rev.* **2012**, *112*, 4221–4245.
- (26) Vybornyi, M.; Nussbaumer, A. L.; Langenegger, S. M.; Häner, R. Assembling Multiporphyrin Stacks inside the DNA Double Helix. *Bioconjug. Chem.* **2014**, *25*, 1785–1793.
- (27) Edwardson, T. G. W.; Carneiro, K. M. M.; Serpell, C. J.; Sleiman, H. F. An Efficient and Modular Route to Sequence-Defined Polymers Appended to DNA. *Angew. Chem., Int. Ed.* **2014**, *53*, 4567–4571.
- (28) Badi, N.; Lutz, J.-F. Sequence Control in Polymer Synthesis. *Chem. Soc. Rev.* **2009**, *38*, 3383–3390.
- (29) Alemdaroglu, F. E.; Alemdaroglu, N. C.; Langguth, P.; Herrmann, a. DNA Block Copolymer Micelles – A Combinatorial Tool for Cancer Nanotechnology. *Adv. Mater.* **2008**, *20*, 899–902.
- (30) Alemdaroglu, F. E.; Ding, K.; Berger, R.; Herrmann, A. DNA-Templated Synthesis in Three Dimensions: Introducing a Micellar Scaffold for Organic Reactions. *Angew. Chem., Int. Ed.* **2006**, *45*, 4206–4210.
- (31) Li, Z.; Zhang, Y.; Fullhart, P.; Mirkin, C. A. Reversible and Chemically Programmable Micelle Assembly with DNA Block-Copolymer

-
- Amphiphiles. *Nano Lett.* **2004**, *4*, 1055–1058.
- (32) Seeman, N. Nucleic Acid Nanostructures and Topology. *Angew. Chem., Int. Ed.* **1998**, *37*, 3220–3238.
- (33) McLaughlin, C. K.; Hamblin, G. D.; Sleiman, H. F. Supramolecular DNA Assembly. *Chem. Soc. Rev.* **2011**, *40*, 5647–5656.
- (34) Wang, Z. G.; Ding, B. DNA-Based Self-Assembly for Functional Nanomaterials. *Adv. Mater.* **2013**, *25*, 3905–3914.
- (35) Wang, F.; Liu, X.; Willner, I.; Nanotechnology, D. N. A.; Wang, F.; Liu, X.; Willner, I. DNA Switches: From Principles to Applications. *Angew. Chem., Int. Ed.* **2015**, *54*, 1098–1129.
- (36) Slinker, J. D.; Muren, N. B.; Renfrew, S. E.; Barton, J. K. DNA Charge Transport over 34 Nm. *Nat. Chem.* **2011**, *3*, 228–233.
- (37) Brodin, J. D.; Auyeung, E.; Mirkin, C. a. DNA-Mediated Engineering of Multicomponent Enzyme Crystals. *Proc. Natl. Acad. Sci.* **2015**, *112*, 4564–4569.
- (38) Jester, S.-S.; Famulok, M. Mechanically Interlocked DNA Nanostructures for Functional Devices. *Acc. Chem. Res.* **2014**, *47*, 1700–1709.
- (39) Veneziano, R.; Ratanalert, S.; Zhang, K.; Zhang, F.; Yan, H.; Chiu, W.; Bathe, M. Designer Nanoscale DNA Assemblies Programmed from the Top down. *Science* **2016**, *352*, 1534–1534.
- (40) Rothmund, P. W. K. The Importance of Being Modular. *Nature* **2012**, *485*, 7–8.
- (41) Ke, Y.; Ong, L. L.; Shih, W. M.; Yin, P. Three-Dimensional Structures Self-Assembled from DNA Bricks. *Science* **2012**, *338*, 1177–1183.
- (42) Woo, S.; Rothmund, P. W. K. Programmable Molecular Recognition Based on the Geometry of DNA Nanostructures. *Nat. Chem.* **2011**, *3*, 620–627.
- (43) Kilchherr, F.; Wachauf, C.; Pelz, B.; Rief, M.; Zacharias, M.; Dietz, H. Single-Molecule Dissection of Stacking Forces in DNA. *Science* **2016**, *353*,

-
- 5508–5508.
- (44) Gerling, T.; Wagenbauer, K. F.; Neuner, A. M.; Dietz, H. Dynamic DNA Devices and Assemblies Formed by Shape-Complementary, Non-Base Pairing 3D Components. *Science* **2015**, *347*, 1446–1452.
- (45) Malinovskii, V. L.; Wenger, D.; Häner, R. Nucleic Acid-Guided Assembly of Aromatic Chromophores. *Chem. Soc. Rev* **2010**, *39*, 410–422.
- (46) Aldaye, F. a; Palmer, A. L.; Sleiman, H. F. Assembling Materials with DNA as the Guide. *Science* **2008**, *321*, 1795–1799.
- (47) Surin, M. From Nucleobase to DNA Templates for Precision Supramolecular Assemblies and Synthetic Polymers. *Polym. Chem.* **2016**, *7*, 4137–4150.
- (48) Albinsson, B.; Hannestad, J. K.; Börjesson, K. Functionalized DNA Nanostructures for Light Harvesting and Charge Separation. *Coord. Chem. Rev.* **2012**, *256*, 2399–2413.
- (49) Ruiz-Carretero, A.; Janssen, P. G. a; Kaeser, A.; Schenning, A. P. H. J. DNA-Templated Assembly of Dyes and Extended π -Conjugated Systems. *Chem. Commun.* **2011**, *47*, 4340.
- (50) Ensslen, P.; Wagenknecht, H. A. One-Dimensional Multichromophor Arrays Based on DNA: From Self-Assembly to Light-Harvesting. *Acc. Chem. Res.* **2015**, *48*, 2724–2733.
- (51) Malinovskii, V. L.; Samain, F.; Häner, R. Helical Arrangement of Interstrand Stacked Pyrenes in a DNA Framework. *Angew. Chem., Int. Ed.* **2007**, *46*, 4464–4467.
- (52) Bouquin, N.; Malinovskii, V. L.; Häner, R. Highly Efficient Quenching of Excimer Fluorescence by Perylene Diimide in DNA. *Chem. Commun.* **2008**, 1974.
- (53) Werder, S.; Malinovskii, V. L.; Häner, R. Triazolylpyrenes: Synthesis, Fluorescence Properties, and Incorporation into DNA. *Org. Lett.* **2008**, *10*, 2011–2014.
- (54) Hemmig, E. A.; Creatore, C.; Wünsch, B.; Hecker, L.; Mair, P.; Parker,

-
- M. A.; Emmott, S.; Tinnefeld, P.; Keyser, U. F.; Chin, A. W. Programming Light-Harvesting Efficiency Using DNA Origami. *Nano Lett.* **2016**, *16*, 2369–2374.
- (55) Ensslen, P.; Brandl, F.; Sezi, S.; Varghese, R.; Kutta, R. J.; Dick, B.; Wagenknecht, H. A. DNA-Based Oligochromophores as Light-Harvesting Systems. *Chem. - A Eur. J.* **2015**, *21*, 9349–9354.
- (56) Uno, S. N.; Dohno, C.; Bittermann, H.; Malinovskii, V. L.; Häner, R.; Nakatani, K. A Light-Driven Supramolecular Optical Switch. *Angew. Chem., Int. Ed.* **2009**, *48*, 7362–7365.
- (57) Kwon, H.; Jiang, W.; Kool, E. T. Pattern-Based Detection of Anion Pollutants in Water with DNA Polyfluorophores. *Chem. Sci.* **2015**, *6*, 2575–2583.
- (58) Zheng, J.; Constantinou, P. E.; Micheel, C.; Alivisatos, A. P.; Kiehl, R. A.; Seeman, N. C. Two-Dimensional Nanoparticle Arrays Show the Organizational Power of Robust DNA Motifs. *Nano Lett.* **2006**, *6*, 1502–1504.
- (59) Kumar, A.; Hwang, J.-H.; Kumar, S.; Nam, J.-M. Tuning and Assembling Metal Nanostructures with DNA. *Chem. Commun.* **2013**, *49*, 2597.
- (60) Tian, Y.; Wang, T.; Liu, W.; Xin, H. L.; Li, H.; Ke, Y.; Shih, W. M.; Gang, O. Prescribed Nanoparticle Cluster Architectures and Low-Dimensional Arrays Built Using Octahedral DNA Origami Frames. *Nat. Nanotechnol.* **2015**, *10*, 637–644.
- (61) Wang, P.; Gaitanaros, S.; Lee, S.; Bathe, M.; Shih, W. M.; Ke, Y. Programming Self-Assembly of DNA Origami Honeycomb Two-Dimensional Lattices and Plasmonic Metamaterials. *J. Am. Chem. Soc.* **2016**, *138*, 7733–7740.
- (62) Zhang, Z.; Yang, Y.; Pincet, F.; C. Llaguno, M.; Lin, C. Placing and Shaping Liposomes with Reconfigurable DNA Nanocages. *Nat Chem* **2017**, *9*, 653–659.
- (63) Geerts, N.; Eiser, E.; Watson, J. D.; Crick, F. H. C.; Caruthers, M. H.;

-
- Saiki, R. K.; Gelfand, D. H.; Stoffel, S.; Scharf, S. J.; Higutchi, R.; *et al.* DNA-Functionalized Colloids: Physical Properties and Applications. *Soft Matter* **2010**, *6*, 4647.
- (64) Kwak, M.; Herrmann, A. Nucleic Acid Amphiphiles: Synthesis and Self-Assembled Nanostructures. *Chem. Soc. Rev.* **2011**, *40*, 5745–5755.
- (65) Lytton-Jean, A. K. R.; Gibbs-Davis, J. M.; Long, H.; Schatz, G. C.; Mirkin, C. a.; Nguyen, S. T. Highly Cooperative Behavior of Peptide Nucleic Acid-Linked DNA-Modified Gold-Nanoparticle and Comb-Polymer Aggregates. *Adv. Mater.* **2009**, *21*, 706–709.
- (66) Qiao, W.; Chiang, H.-C.; Xie, H.; Levicky, R. Surface vs. Solution Hybridization: Effects of Salt, Temperature, and Probe Type. *Chem. Commun.* **2015**, *51*, 17245–17248.
- (67) Díaz, J. A.; Gibbs-Davis, J. M. Sharpening the Thermal Release of Dna from Nanoparticles: Towards a Sequential Release Strategy. *Small* **2013**, *9*, 2862–2871.
- (68) Lei, Q.; Ren, C.; Su, X.; Ma, Y. Crowding-Induced Cooperativity in DNA Surface Hybridization. *Sci. Rep.* **2015**, *5*, 9217.
- (69) Auyeung, E.; Li, T. I. N. G.; Senesi, A. J.; Schmucker, A. L.; Pals, B. C.; de la Cruz, M. O.; Mirkin, C. a. DNA-Mediated Nanoparticle Crystallization into Wulff Polyhedra. *Nature* **2014**, *505*, 73–77.
- (70) Samanta, A.; Medintz, I. L. Nanoparticles and DNA - a Powerful and Growing Functional Combination in Bionanotechnology. *Nanoscale* **2016**, 9037–9095.
- (71) Kundu, A.; Nandi, S.; Nandi, A. K. Nucleic Acid Based Polymer and Nanoparticle Conjugates: Synthesis, Properties and Applications. *Prog. Mater. Sci.* **2017**, *88*, 136–185.
- (72) Raeesi, V.; Chou, L. Y. T.; Chan, W. C. W. Tuning the Drug Loading and Release of DNA-Assembled Gold-Nanorod Superstructures. *Adv. Mater.* **2016**, 8511–8518.
- (73) Liu, J.; Postupalenko, V.; Lörcher, S.; Wu, D.; Chami, M.; Meier, W.;

-
- Palivan, C. G. DNA-Mediated Self-Organization of Polymeric Nanocompartments Leads to Interconnected Artificial Organelles. *Nano Lett.* **2016**, *16*, 7128–7136.
- (74) Jakobsen, U.; Simonsen, A. C.; Vogel, S. DNA-Controlled Assembly of Soft Nanoparticles. *J. Am. Chem. Soc.* **2008**, *130*, 10462–10463.
- (75) Parolini, L.; Kotar, J.; Di Michele, L.; Mognetti, B. M. Controlling Self-Assembly Kinetics of DNA-Functionalized Liposomes Using Toehold Exchange Mechanism. *ACS Nano* **2016**, *10*, 2392–2398.
- (76) Löffler, P. M. G.; Ries, O.; Rabe, A.; Okholm, A. H.; Thomsen, R. P.; Kjems, J.; Vogel, S. A DNA-Programmed Liposome Fusion Cascade. *Angew. Chem., Int. Ed.* **2017**, *56*, 13228–13231.
- (77) Kwak, M.; Herrmann, A. Nucleic Acid/organic Polymer Hybrid Materials: Synthesis, Superstructures, and Applications. *Angew. Chem., Int. Ed.* **2010**, *49*, 8574–8587.
- (78) Madsen, M.; Christensen, R. S.; Krissanaprasit, A.; Bakke, M. R.; Riber, C. F.; Nielsen, K. S.; Zelikin, A. N.; Gothelf, K. V. Preparation, Single-Molecule Manipulation, and Energy Transfer Investigation of a Polyfluorene- Graft -DNA Polymer. *Chem. - A Eur. J.* **2017**, *23*, 10511–10515.
- (79) Krissanaprasit, A.; Madsen, M.; Knudsen, J. B.; Gudnason, D.; Surareungchai, W.; Birkedal, V.; Gothelf, K. V. Programmed Switching of Single Polymer Conformation on DNA Origami. *ACS Nano* **2016**, *10*, 2243–2250.
- (80) Shao, Y.; Jia, H.; Cao, T.; Liu, D. Supramolecular Hydrogels Based on DNA Self-Assembly. *Acc. Chem. Res.* **2017**, *50*, 659–668.
- (81) Kahn, J. S.; Hu, Y.; Willner, I. Stimuli-Responsive DNA-Based Hydrogels: From Basic Principles to Applications. *Acc. Chem. Res.* **2017**, *50*, 680–690.
- (82) Wang, D.; Hu, Y.; Liu, P.; Luo, D. Bioresponsive DNA Hydrogels: Beyond the Conventional Stimuli Responsiveness. *Acc. Chem. Res.* **2017**, *50*,

-
- 733–739.
- (83) Liao, W.-C.; Lilienthal, S.; Kahn, J. S.; Riutin, M.; Sohn, Y. S.; Nechushtai, R.; Willner, I. pH- and Ligand-Induced Release of Loads from DNA–acrylamide Hydrogel Microcapsules. *Chem. Sci.* **2017**, *8*, 3362–3373.
- (84) Tan, X.; Li, B. B.; Lu, X.; Jia, F.; Santori, C.; Menon, P.; Li, H.; Zhang, B.; Zhao, J. J.; Zhang, K. Light-Triggered, Self-Immolative Nucleic Acid-Drug Nanostructures. *J. Am. Chem. Soc.* **2015**, *137*, 6112–6115.
- (85) Noteborn, W. E. M.; Saez Talens, V.; Kieltyka, R. E. Reversible Loading of Nanoscale Elements on a Multicomponent Supramolecular Polymer System by Using DNA Strand Displacement. *ChemBioChem* **2017**, *18*, 1995–1999.
- (86) Wu, F.; Jin, J.; Wang, L.; Sun, P.; Yuan, H.; Yang, Z.; Chen, G.; Fan, Q. H.; Liu, D. Functionalization of DNA-Dendron Supramolecular Fibers and Application in Regulation of Escherichia Coli Association. *ACS Appl. Mater. Interfaces* **2015**, *7*, 7351–7356.
- (87) Al Ouahabi, A.; Kotera, M.; Charles, L.; Lutz, J.-F. Synthesis of Monodisperse Sequence-Coded Polymers with Chain Lengths above DP100. *ACS Macro Lett.* **2015**, *4*, 1077–1080.
- (88) König, N. F.; Al Ouahabi, A.; Poyer, S.; Charles, L.; Lutz, J.-F. A Simple Post-Polymerization Modification Method for Controlling Side-Chain Information in Digital Polymers. *Angew. Chem., Int. Ed.* **2017**, *56*, 7297–7301.
- (89) Steinbach, T.; Ritz, S.; Wurm, F. R. Water-Soluble Poly(phosphonate)s via Living Ring-Opening Polymerization. *ACS Macro Lett.* **2014**, *3*, 244–248.
- (90) Pranantyo, D.; Xu, L. Q.; Kang, E.-T.; Mya, M. K.; Chan-Park, M. B. Conjugation of Polyphosphoester and Antimicrobial Peptide for Enhanced Bactericidal Activity and Biocompatibility. *Biomacromolecules* **2016**, *17*, 4037–4044.

-
- (91) Shen, Y.; Zhang, S.; Zhang, F.; Loftis, A.; Pavía-Sanders, A.; Zou, J.; Fan, J.; Taylor, J. S. A.; Wooley, K. L. Polyphosphoester-Based Cationic Nanoparticles Serendipitously Release Integral Biologically-Active Components to Serve as Novel Degradable Inducible Nitric Oxide Synthase Inhibitors. *Adv. Mater.* **2013**, *25*, 5609–5614.
- (92) Graillot, A.; Field, B.; Monge, S.; Canniccioni, B.; Graillot, A.; Robin, J.; Charles, I.; Montpellier, G.; Equipe, U. M. R. C. Phosphorus-Containing Polymers : A Great Opportunity for the Biomedical Field. *Biomacromolecules* **2011**, *12*, 1973–1982.
- (93) Wu, J.; Liu, X.-Q.; Wang, Y.-C.; Wang, J. Template-Free Synthesis of Biodegradable Nanogels with Tunable Sizes as Potential Carriers for Drug Delivery. *J. Mater. Chem.* **2009**, *19*, 7856.
- (94) Chien, M.-P.; Rush, A. M.; Thompson, M. P.; Gianneschi, N. C. Programmable Shape-Shifting Micelles. *Angew. Chem., Int. Ed.* **2010**, *49*, 5076–5080.
- (95) Seeman, N. C. DNA in a Material World. *Nature* **2003**, *421*, 427–431.
- (96) Grabow, W. W.; Jaeger, L. RNA Self-Assembly and RNA Nanotechnology. *Acc. Chem. Res.* **2014**.
- (97) Rothmund, P. W. K. Folding DNA to Create Nanoscale Shapes and Patterns. *Nature* **2006**, *440*, 297–302.
- (98) Lu, C.-H.; Willner, B.; Willner, I. D. N. A.; Nanotechnology. From Sensing and DNA Machines to Drug-Delivery Systems. *ACS Nano* **2013**, *7*, 8320.
- (99) Peng, L.; Wu, C.; You, M.; Han, D.; Chen, Y.; Fu, T.; Ye, M.; Tan, W. Engineering and Applications of DNA-Grafting Polymer Materials. *Chem. Sci.* **2013**, *4*, 1928–1938.
- (100) Jakobsen, U.; Simonsen, A. C.; Vogel, S. DNA-Controlled Assembly of Soft Nanoparticles. *J. Am. Chem. Soc.* **2008**, *130*, 10462–10463.
- (101) Nussbaumer, A. L.; Studer, D.; Malinovskii, V. L.; Häner, R. Amplification of Chirality by Supramolecular Polymerization of Pyrene

-
- Oligomers. *Angew. Chem., Int. Ed.* **2011**, *50*, 5490–5494.
- (102) Malinovskii, V. L.; Nussbaumer, A. L.; Häner, R. Oligopyrenotides: Chiral Nanoscale Templates for Chromophore Assembly. *Angew. Chem., Int. Ed.* **2012**, *51*, 4905–4908.
- (103) Schöttler, S.; Becker, G.; Winzen, S.; Steinbach, T.; Mohr, K.; Landfester, K.; Mailänder, V.; Wurm, F. R. Protein Adsorption Is Required for Stealth Effect of Poly(ethylene Glycol)- and Poly(phosphoester)-Coated Nanocarriers. *Nat. Nanotechnol.* **2016**, *11*, 372–377.
- (104) Albert, S. K.; Thelu, H. V. P.; Golla, M.; Krishnan, N.; Varghese, R. Modular Synthesis of Supramolecular DNA Amphiphiles through Host-Guest Interactions and Their Self-Assembly into DNA-Decorated Nanovesicles. *Nanoscale* **2017**, *9*, 5355–5738.
- (105) Bousmail, D.; Amrein, L.; Fakhoury, J. J.; Fakh, H. H.; Hsu, J. C. C.; Panasci, L.; Sleiman, H. F. Precision Spherical Nucleic Acids for Delivery of Anticancer Drugs. *Chem. Sci.* **2017**, *8*, 6218–6229.
- (106) Krieg, E.; Bastings, M. M. C.; Besenius, P.; Rybtchinski, B. Supramolecular Polymers in Aqueous Media. *Chem. Rev.* **2016**, *116*, 2414–2477.
- (107) Aida, T.; Meijer, E. W.; Stupp, S. I. Functional Supramolecular Polymers. *Science* **2012**, *335*, 813–817.
- (108) Jones, M. R.; Seeman, N. C.; Mirkin, C. a. Programmable Materials and the Nature of the DNA Bond. *Science* **2015**, *347*, 1260901.
- (109) Schnitzler, T.; Herrmann, A. DNA Block Copolymers: Functional Materials for Nanoscience and Biomedicine. *Acc. Chem. Res.* **2012**, *45*, 1419–1430.
- (110) Carneiro, K. M. M.; Avakyan, N.; Sleiman, H. F. Long-Range Assembly of DNA into Nanofibers and Highly Ordered Networks. *WIREs Nanomed Nanobiotechnol* **2013**, *5*, 266–285.
- (111) Patwa, A.; Gissot, A.; Bestel, I.; Barthélémy, P. Hybrid Lipid Oligonucleotide Conjugates: Synthesis, Self-Assemblies and Biomedical

-
- Applications. *Chem. Soc. Rev.* **2011**, *40*, 5844–5854.
- (112) Yang, D.; Campolongo, M. J.; Nhi Tran, T. N.; Ruiz, R. C. H.; Kahn, J. S.; Luo, D. Novel DNA Materials and Their Applications. *Wiley Interdiscip. Rev. Nanomed. Nanobiotechnol.* **2010**, *2*, 648–669.
- (113) Tørring, T.; Voigt, N. V.; Nangreave, J.; Yan, H.; Gothelf, K. V. DNA Origami: A Quantum Leap for Self-Assembly of Complex Structures. *Chem. Soc. Rev.* **2011**, *40*, 5636–5646.
- (114) Wengel, J. Nucleic Acid Nanotechnology - towards Angstrom-Scale Engineering. *Org. Biomol. Chem.* **2004**, *2*, 277–280.
- (115) Heckel, A.; Famulok, M. Building Objects from Nucleic Acids for a Nanometer World. *Biochimie* **2008**, *90*, 1096–1107.
- (116) Endo, M.; Sugiyama, H. Chemical Approaches to DNA Nanotechnology. *ChemBioChem* **2009**, *10*, 2420–2443.
- (117) Liang, H.; Zhang, X. B.; Lv, Y.; Gong, L.; Wang, R.; Zhu, X.; Yang, R.; Tan, W. Functional DNA-Containing Nanomaterials: Cellular Applications in Biosensing, Imaging, and Targeted Therapy. *Acc. Chem. Res.* **2014**, *47*, 1891–1901.
- (118) Wang, F.; Liu, X.; Willner, I. DNA-Schalter: Grundlagen Und Anwendungen. *Angew. Chem., Int. Ed.* **2015**, *127*, 1112–1144.
- (119) Saccà, B.; Niemeyer, C. M. DNA Origami: The Art of Folding DNA. *Angew. Chem., Int. Ed.* **2012**, *51*, 58–66.
- (120) Alemdaroglu, F. E.; Herrmann, A. DNA Meets Synthetic Polymers-- Highly Versatile Hybrid Materials. *Org. Biomol. Chem.* **2007**, *5*, 1311–1320.
- (121) Schade, M.; Berti, D.; Huster, D.; Herrmann, A.; Arbuçova, A. Lipophilic Nucleic Acids — A Flexible Construction Kit for Organization and Functionalization of Surfaces. *Adv. Colloid Interface Sci.* **2014**, *208*, 235–251.
- (122) Stulz, E. DNA Architectonics: Towards the next Generation of Bio-Inspired Materials. *Chem.—Eur. J.* **2012**, *18*, 4456–4469.

-
- (123) Varghese, R.; Wagenknecht, H.-A. DNA as a Supramolecular Framework for the Helical Arrangements of Chromophores: Towards Photoactive DNA-Based Nanomaterials. *Chem. Commun.* **2009**, 2615.
- (124) Rudnev, A. V.; Malinovskii, V. L.; Nussbaumer, A. L.; Mishchenko, A.; Häner, R.; Wandlowski, T. Cooperative and Noncooperative Assembly of Oligopyrenotides Resolved by Atomic Force Microscopy. *Macromolecules* **2012**, *45*, 5986–5992.
- (125) Dohno, C.; Nakatani, K. Control of DNA Hybridization by Photoswitchable Molecular Glue. *Chem. Soc. Rev.* **2011**, *40*, 5718–5729.
- (126) Filichev, V. V.; Pedersen, E. B. DNA-Conjugated Organic Chromophores in DNA Stacking Interactions. In *Wiley Encyclopedia of Chemical Biology*; John Wiley & Sons, Inc.: Hoboken, NJ, USA, 2008; pp. 1–31.
- (127) Østergaard, M. E.; Hrdlicka, P. J. Pyrene-Functionalized Oligonucleotides and Locked Nucleic Acids (LNAs): Tools for Fundamental Research, Diagnostics, and Nanotechnology. *Chem. Soc. Rev.* **2011**, *40*, 5771–5788.
- (128) Singh, A.; Tolev, M.; Meng, M.; Klenin, K.; Plietzsch, O.; Schilling, C. I.; Müller, T.; Nieger, M.; Bräse, S.; Wenzel, W.; *et al.* Branched DNA That Forms a Solid at 95°C. *Angew. Chem., Int. Ed.* **2011**, *50*, 3227–3231.
- (129) Gompper, G.; Ihle, T.; Kroll, D. M.; Winkler, R. G. Multi-Particle Collision Dynamics -- a Particle-Based Mesoscale Simulation Approach to the Hydrodynamics of Complex Fluids. *Adv. Polym Sci* **2008**, *253*, 115–150.
- (130) Pu, F.; Ren, J.; Qu, X. Nucleic Acids and Smart Materials: Advanced Building Blocks for Logic Systems. *Adv. Mater.* **2014**, 5742–5757.
- (131) Langecker, M.; Arnaut, V.; Martin, T. G.; List, J.; Renner, S.; Mayer, M.; Dietz, H.; Simmel, F. C. Synthetic Lipid Membrane Channels Formed by Designed DNA Nanostructures. *Science* **2012**, *338*, 932–936.
- (132) Chen, X. J.; Sanchez-Gaytan, B. L.; Hayik, S. E. N.; Fryd, M.; Wayland, B. B.; Park, S. J. Self-Assembled Hybrid Structures of DNA Block-

-
- Copolymers and Nanoparticles with Enhanced DNA Binding Properties. *Small* **2010**, *6*, 2256–2260.
- (133) Edwardson, T. G. W.; Carneiro, K. M. M.; McLaughlin, C. K.; Serpell, C. J.; Sleiman, H. F. Site-Specific Positioning of Dendritic Alkyl Chains on DNA Cages Enables Their Geometry-Dependent Self-Assembly. *Nat. Chem.* **2013**, *5*, 868–875.
- (134) List, J.; Weber, M.; Simmel, F. C. Hydrophobic Actuation of a DNA Origami Bilayer Structure. *Angew. Chem., Int. Ed.* **2014**, *53*, 4236–4239.
- (135) Beales, P. a; Geerts, N.; Inampudi, K. K.; Shigematsu, H.; Wilson, C. J.; Vanderlick, T. K. Reversible Assembly of Stacked Membrane Nanodiscs with Reduced Dimensionality and Variable Periodicity. *J. Am. Chem. Soc.* **2013**, *135*, 3335–3358.
- (136) Kamps, A. C.; Cativo, M. H. M.; Chen, X. J.; Park, S. J. Self-Assembly of DNA-Coupled Semiconducting Block Copolymers. *Macromolecules* **2014**, *47*, 3720–3726.
- (137) Neelakandan, P. P.; Pan, Z.; Hariharan, M.; Zheng, Y.; Weissman, H.; Rybtchinski, B.; Lewis, F. D. Hydrophobic Self-Assembly of a Perylenediimide-Linked DNA Dumbbell into Supramolecular Polymers. *J. Am. Chem. Soc.* **2010**, *132*, 15808–15813.
- (138) Li, Z.; Zhang, Y.; Fullhart, P.; Mirkin, C. A. Reversible and Chemically Programmable Micelle Assembly with DNA Block-Copolymer Amphiphiles. *Nano Lett.* **2004**, *4*, 1055–1058.
- (139) Randolph, L. M.; Chien, M.-P.; Gianneschi, N. C. Biological Stimuli and Biomolecules in the Assembly and Manipulation of Nanoscale Polymeric Particles. *Chem. Sci.* **2012**, *3*, 1363.
- (140) Peng, L.; Wu, C. S.; You, M.; Han, D.; Chen, Y.; Fu, T.; Ye, M.; Tan, W.; Wu, S.; You, M.; *et al.* Engineering and Applications of DNA-Grafted Polymer Materials. *Chem. Sci.* **2013**, *4*, 1928–1938.
- (141) Averick, S.; Paredes, E.; Li, W.; Matyjaszewski, K.; Das, S. R. Direct DNA Conjugation to Star Polymers for Controlled Reversible Assemblies.

-
- Bioconjug. Chem.* **2011**, *22*, 2030–2037.
- (142) Lee, K.; Rouillard, J.-M. M.; Pham, T.; Gulari, E.; Kim, J. Signal-Amplifying Conjugated Polymer-DNA Hybrid Chips. *Angew. Chem., Int. Ed.* **2007**, *46*, 4667–4670.
- (143) Gibbs, J. M.; Park, S. J.; Anderson, D. R.; Watson, K. J.; Mirkin, C. a.; Nguyen, S. T. Polymer-DNA Hybrids as Electrochemical Probes for the Detection of DNA. *J. Am. Chem. Soc.* **2005**, *127*, 1170–1178.
- (144) De Greef, T. F. A.; Smulders, M. M. J.; Wolffs, M.; Schenning, A. P. H. J.; Sijbesma, R. P.; Meijer, E. W. Supramolecular Polymerization. *Chem. Rev.* **2009**, *109*, 5687–5754.
- (145) Häner, R.; Garo, F.; Wenger, D.; Malinovskii, V. L. Oligopyrenotides: Abiotic, Polyanionic Oligomers with Nucleic Acid-like Structural Properties. *J. Am. Chem. Soc.* **2010**, *132*, 7466–7471.
- (146) Nussbaumer, A. L.; Studer, D.; Malinovskii, V. L.; Häner, R. Amplification of Chirality by Supramolecular Polymerization of Pyrene Oligomers. *Angew. Chem., Int. Ed.* **2011**, *50*, 5490–5494.
- (147) Bittermann, H.; Siegemund, D.; Malinovskii, V. L.; Häner, R. Dialkynylpyrenes: Strongly Fluorescent, Environment-Sensitive DNA Building Blocks. *J. Am. Chem. Soc.* **2008**, *130*, 15285–15287.
- (148) Vybornyi, M.; Rudnev, A. V.; Langenegger, S. M.; Wandlowski, T.; Calzaferri, G.; Häner, R.; Oligomers, A. P. Formation of Two-Dimensional Supramolecular Polymers by Amphiphilic Pyrene Oligomers. *Angew. Chem., Int. Ed.* **2013**, *52*, 11488–114893.
- (149) Vybornyi, M.; Rudnev, A.; Häner, R. Assembly of Extra-Large Nanosheets by Supramolecular Polymerization of Amphiphilic Pyrene Oligomers in Aqueous Solution. *Chem. Mater.* **2015**, *27*, 1426–1431.
- (150) Jonkheijm, P.; van der Schoot, P.; Schenning, A. P. H. J.; Meijer, E. W. Probing the Solvent-Assisted Nucleation Pathway in Chemical Self-Assembly. *Science* **2006**, *313*, 80–83.
- (151) Fuks, G.; Mayap Talom, R.; Gauffre, F. Biohybrid Block Copolymers:

-
- Towards Functional Micelles and Vesicles. *Chem. Soc. Rev.* **2011**, *40*, 2475–2493.
- (152) Albert, S. K.; Thelu, H. V. P.; Golla, M.; Krishnan, N.; Chaudhary, S.; Varghese, R. Self-Assembly of DNA-Oligo(P -Phenylene-Ethynylene) Hybrid Amphiphiles into Surface-Engineered Vesicles with Enhanced Emission. *Angew. Chem., Int. Ed.* **2014**, *126*, 8492–8497.
- (153) Tang, L.; Tjong, V.; Li, N.; Yingling, Y. G.; Chilkoti, A.; Zauscher, S. Enzymatic Polymerization of High Molecular Weight DNA Amphiphiles That Self-Assemble into Star-like Micelles. *Adv. Mater.* **2014**, *26*, 3050–3054.
- (154) Dong, Y.; Sun, Y.; Wang, L.; Wang, D.; Zhou, T.; Yang, Z.; Chen, Z.; Wang, Q.; Fan, Q.; Liu, D. Frame-Guided Assembly of Vesicles with Programmed Geometry and Dimensions. *Angew. Chem., Int. Ed.* **2014**, *53*, 2607–2610.
- (155) Wang, L.; Feng, Y.; Yang, Z.; He, Y.-M.; Fan, Q.-H.; Liu, D. Reversibly Controlled Morphology Transformation of an Amphiphilic DNA–dendron Hybrid. *Chem. Commun.* **2012**, *48*, 3715.
- (156) Waybrant, B.; Pearce, T.; Kokkoli, E. Effect of Polyethylene Glycol, Alkyl, and Oligonucleotide Spacers on the Binding, Secondary Structure, and Self-Assembly of Fractalkine Binding FKN-S2 Aptamer-Amphiphiles. *Langmuir* **2014**, *30*, 7465–7474.
- (157) Vybornyi, M.; Bur-Cecilio Hechevarria, Y.; Glauser, M.; Rudnev, A. V.; Häner, R. Tubes or Sheets: Divergent Aggregation Pathways of an Amphiphilic 2,7-Substituted Pyrene Trimer. *Chem. Commun.* **2015**, *51*, 16191–16193.
- (158) Liu, M.; Zhang, L.; Wang, T. Supramolecular Chirality in Self-Assembled Systems. *Chem. Rev.* **2015**, *115*, 7304–7397.
- (159) Korevaar, P. A.; George, S. J.; Markvoort, A. J.; Smulders, M. M. J.; Hilbers, P. A. J.; Schenning, A. P. H. J.; Greef, T. F. A. De; Meijer, E. W. Pathway Complexity in Supramolecular Polymerization. *Nature* **2012**,

-
- 481, 492–496.
- (160) Vybornyi, M.; Rudnev, A. V.; Langenegger, S. M.; Wandlowski, T.; Calzaferri, G.; Häner, R. Formation of Two-Dimensional Supramolecular Polymers by Amphiphilic Pyrene Oligomers. *Angew. Chem., Int. Ed.* **2013**, *52*, 11488–11493.
- (161) Webber, M. J.; Appel, E. A.; Meijer, E. W.; Langer, R. Supramolecular Biomaterials. *Nat. Mater.* **2016**, *15*, 13–26.
- (162) Korevaar, P. A.; De Greef, T. F. A.; Meijer, E. W. Pathway Complexity in π -Conjugated Materials. *Chem. Mater.* **2014**, *26*, 576–586.
- (163) Ogi, S.; Sugiyasu, K.; Manna, S.; Samitsu, S.; Takeuchi, M. Living Supramolecular Polymerization Realized through a Biomimetic Approach. *Nat. Chem.* **2014**, *6*, 188–195.
- (164) Lutz, J.-F.; Lehn, J.-M.; Meijer, E. W.; Matyjaszewski, K. From Precision Polymers to Complex Materials and Systems. *Nat. Rev. Mater.* **2016**, *1*, 16024.
- (165) Lutz, J.-F.; Börner, H. G. Modern Trends in Polymer Bioconjugates Design. *Prog. Polym. Sci.* **2008**, *33*, 1–39.
- (166) Boekhoven, J.; Poolman, J. M.; Maity, C.; Li, F.; Mee, L. Van Der; Minkenberg, C. B.; Mendes, E.; Esch, J. H. Van; Eelkema, R. Catalytic Control over Supramolecular Gel Formation. *Nat. Chem.* **2013**, *5*, 433–437.
- (167) Cheng, C.; Mcgonigal, P. R.; Stoddart, J. F.; Astumian, R. D. Design and Synthesis of Nonequilibrium Systems. *ACS Nano* **2015**, *9*, 8672–8688.
- (168) Erbas-Cakmak, S.; Leigh, D. A.; McTernan, C. T.; Nussbaumer, A. L. Artificial Molecular Machines. *Chem. Rev.* **2015**, *115*, 10081–10206.
- (169) Ogi, S.; Stepanenko, V.; Thein, J.; Würthner, F. Impact of Alkyl Spacer Length on Aggregation Pathways in Kinetically Controlled Supramolecular Polymerization. *J. Am. Chem. Soc.* **2016**, *138*, 670–678.
- (170) Baram, J.; Weissman, H.; Rybtchinski, B. Supramolecular Polymer Transformation: A Kinetic Study. *J. Phys. Chem. B* **2014**, *118*, 12068–

12073.

- (171) Tantakitti, F.; Boekhoven, J.; Wang, X.; Kazantsev, R. V.; Yu, T.; Li, J.; Zhuang, E.; Zandi, R.; Ortony, J. H.; Newcomb, C. J.; *et al.* Energy Landscapes and Functions of Supramolecular Systems. *Nat. Mater.* **2016**, *15*, 469–476.
- (172) Henson, Z. B.; Müllen, K.; Bazan, G. C. Design Strategies for Organic Semiconductors beyond the Molecular Formula. *Nat. Chem.* **2012**, *4*, 699–704.
- (173) Seeman, N. C. Nanomaterials Based on DNA. *Annu. Rev. Biochem.* **2010**, *79*, 65–87.
- (174) Endo, M.; Sugiyama, H. Single-Molecule Imaging of Dynamic Motions of Biomolecules in DNA Origami Nanostructures Using High-Speed Atomic Force Microscopy. *Acc. Chem. Res.* **2014**, *47*, 1645–1653.
- (175) Yang, Y.; Wang, J.; Shigematsu, H.; Xu, W.; Shih, W. M.; Rothman, J. E.; Lin, C. Self-Assembly of Size-Controlled Liposomes on DNA Nanotemplates. *Nat. Chem.* **2016**, *8*, 476–483.
- (176) Li, J.; Mo, L.; Lu, C.; Fu, T.; Yang, H.; Tan, W. Functional Nucleic Acid-Based Hydrogels for Bioanalytical and Biomedical Applications. *Chem. Soc. Rev.* **2016**, *45*, 1410–1431.
- (177) de Rochambeau, D.; Barlóg, M.; Edwardson, T. G. W.; Fakhoury, J. J.; Stein, R. S.; Bazzi, H. S.; Sleiman, H. F. “DNA–Teflon” Sequence-Controlled Polymers. *Polym. Chem.* **2016**, *7*, 4998–5003.
- (178) Banga, R. J.; Chernyak, N.; Narayan, S. P.; Nguyen, S. T.; Mirkin, C. A. Liposomal Spherical Nucleic Acids. *J. Am. Chem. Soc.* **2014**, *136*, 9866–9869.
- (179) Rush, A. M.; Thompson, M. P.; Tatro, E. T.; Gianneschi, N. C. Nuclease-Resistant DNA via High-Density Packing in Polymeric Micellar Nanoparticle Coronas. *ACS Nano* **2013**, *7*, 1379–1387.
- (180) Luo, Q.; Shi, Z.; Zhang, Y.; Chen, X.-J.; Han, S.-Y.; Baumgart, T.; Chenoweth, D. M.; Park, S.-J. DNA Island Formation on Binary Block

-
- Copolymer Vesicles. *J. Am. Chem. Soc.* **2016**, *138*, 10157–10162.
- (181) Kwak, M.; Herrmann, A. Nucleic Acid Amphiphiles: Synthesis and Self-Assembled Nanostructures. *Chem. Soc. Rev.* **2011**, *40*, 5745.
- (182) Wu, F.; Song, Y.; Zhao, Z.; Zhang, S.; Yang, Z.; Li, Z.; Li, M.; Fan, Q. H.; Liu, D. Preparation and Self-Assembly of Supramolecular Coil-Rod-Coil Triblock Copolymer PPO-dsDNA-PPO. *Macromolecules* **2015**, *48*, 7550–7556.
- (183) Serpell, C. J.; Edwardson, T. G. W.; Chidchob, P.; Carneiro, K. M. M.; Sleiman, H. F. Precision Polymers and 3D DNA Nanostructures: Emergent Assemblies from New Parameter Space. *J. Am. Chem. Soc.* **2014**, *136*, 15767–15774.
- (184) Hernández-Ainsa, S.; Ricci, M.; Hilton, L.; Aviñó, A.; Eritja, R.; Keyser, U. F. Controlling the Reversible Assembly of Liposomes through a Multistimuli Responsive Anchored DNA. *Nano Lett.* **2016**, *16*, 4462–4466.
- (185) Knudsen, J. B.; Liu, L.; Bank Kodal, A. L.; Madsen, M.; Li, Q.; Song, J.; Woehrstein, J. B.; Wickham, S. F. J.; Strauss, M. T.; Schueder, F.; *et al.* Routing of Individual Polymers in Designed Patterns. *Nat. Nanotechnol.* **2015**, *10*, 892–898.
- (186) Ding, K.; Alemdaroglu, F. E.; Börsch, M.; Berger, R.; Herrmann, A. Engineering the Structural Properties of DNA Block Copolymer Micelles by Molecular Recognition. *Angew. Chem., Int. Ed.* **2007**, *46*, 1172–1175.
- (187) Kwak, M.; Gao, J.; Prusty, D. K.; Musser, A. J.; Markov, V. a; Tombros, N.; Stuart, M. C. a; Browne, W. R.; Boekema, E. J.; ten Brinke, G.; *et al.* DNA Block Copolymer Doing It All: From Selection to Self-Assembly of Semiconducting Carbon Nanotubes. *Angew. Chem., Int. Ed.* **2011**, *50*, 3206–3210.
- (188) Vyborna, Y.; Vybornyi, M.; Rudnev, A. V.; Häner, R. DNA-Grafted Supramolecular Polymers: Helical Ribbon Structures Formed by Self-Assembly of Pyrene-DNA Chimeric Oligomers. *Angew. Chem., Int. Ed.* **2015**, *54*, 7934–7938.

-
- (189) Peterson, A. W.; Wolf, L. K.; Georgiadis, R. M. Hybridization of Mismatched or Partially Matched DNA at Surfaces. *J. Am. Chem. Soc.* **2002**, *124*, 14601–14607.
- (190) Wang, F.; Lu, C.-H.; Willner, I. From Cascaded Catalytic Nucleic Acids to Enzyme-DNA Nanostructures: Controlling Reactivity, Sensing, Logic Operations, and Assembly of Complex Structures. *Chem. Rev.* **2014**, *114*, 2881–2941.
- (191) Zhang, F.; Nangreave, J.; Liu, Y.; Yan, H. Structural DNA Nanotechnology: State of the Art and Future Perspective. *J. Am. Chem. Soc.* **2014**, *136*, 11198–11211.
- (192) Yin, P.; Choi, H. M. T.; Calvert, C. R.; Pierce, N. a. Programming Biomolecular Self-Assembly Pathways. *Nature* **2008**, *451*, 318–322.
- (193) Douglas, S. M.; Dietz, H.; Liedl, T.; Högberg, B.; F, G.; Shih, W. Self-Assembly of DNA into Nanoscale Three-Dimensional Shapes. *Nature* **2009**, *18*, 29–32.
- (194) Bath, J.; Turberfield, A. J. DNA Nanomachines. *Nat. Nanotechnol.* **2007**, *2*, 275–284.
- (195) Nykypanchuk, D.; Maye, M. M.; van der Lelie, D.; Gang, O. DNA-Guided Crystallization of Colloidal Nanoparticles. *Nature* **2008**, *451*, 549–552.
- (196) Ke, Y.; Ong, L. L.; Sun, W.; Song, J.; Dong, M.; Shih, W. M.; Yin, P. DNA Brick Crystals with Prescribed Depths. *Nat. Chem.* **2014**, *6*, 994–1002.
- (197) Gong, P.; Levicky, R. DNA Surface Hybridization Regimes. *Proc. Natl. Acad. Sci.* **2008**, *105*, 5301–5306.
- (198) Randeria, P. S.; Jones, M. R.; Kohlstedt, K. L.; Banga, R. J.; Olvera de la Cruz, M.; Schatz, G. C.; Mirkin, C. A. What Controls the Hybridization Thermodynamics of Spherical Nucleic Acids? *J. Am. Chem. Soc.* **2015**, *137*, 3486–3489.
- (199) Aghebat Rafat, A.; Pirzer, T.; Scheible, M. B.; Kostina, A.; Simmel, F. C. Surface-Assisted Large-Scale Ordering of DNA Origami Tiles. *Angew. Chem., Int. Ed.* **2014**, *53*, 7665–7668.

-
- (200) Woo, S.; Rothmund, P. W. K. Self-Assembly of Two-Dimensional DNA Origami Lattices Using Cation-Controlled Surface Diffusion. *Nat. Commun.* **2014**, *5*, 4889.
- (201) Cutler, J. I.; Auyeung, E.; Mirkin, C. a. Spherical Nucleic Acids. *J. Am. Chem. Soc.* **2012**, *134*, 1376–1391.
- (202) Tjong, V.; Tang, L.; Zauscher, S.; Chilkoti, A. “Smart” DNA Interfaces. *Chem. Soc. Rev.* **2014**, *43*, 1612–1626.
- (203) Sassolas, A.; Leca-Bouvier, B. D.; Blum, L. J. DNA Biosensors and Microarrays. *Chem. Rev.* **2008**, *108*, 109–139.
- (204) Howorka, S.; Hesse, J. Microarrays and Single Molecules: An Exciting Combination. *Soft Matter* **2014**, *10*, 931–941.
- (205) Gour, N.; Kedracki, D.; Safir, I.; Ngo, K. X.; Vebert-Nardin, C. Self-Assembling DNA–peptide Hybrids: Morphological Consequences of Oligonucleotide Grafting to a Pathogenic Amyloid Fibrils Forming Dipeptide. *Chem. Commun.* **2012**, *48*, 5440.
- (206) Averick, S. E.; Dey, S. K.; Grahacharya, D.; Matyjaszewski, K.; Das, S. R. Solid-Phase Incorporation of an ATRP Initiator for Polymer-DNA Biohybrids. *Angew. Chem., Int. Ed.* **2014**, *53*, 2739–2744.
- (207) Peterson, A. M.; Heemstra, J. M. Controlling Self-Assembly of DNA-Polymer Conjugates for Applications in Imaging and Drug Delivery. *Wiley Interdiscip. Rev. Nanomedicine Nanobiotechnology* **2015**, *7*, 282–297.
- (208) Korri-Youssoufi, H.; Garnier, F.; Srivastava, P.; Godillot, P.; Yassar, A. Toward Bioelectronics: Specific DNA Recognition Based on an Oligonucleotide-Functionalized Polypyrrole. *J. Am. Chem. Soc.* **1997**, *119*, 7388–7389.
- (209) Lu, X.; Watts, E.; Jia, F.; Tan, X.; Zhang, K. Polycondensation of Polymer Brushes via DNA Hybridization. *J. Am. Chem. Soc.* **2014**, *136*, 10214–10217.
- (210) Watson, K. J.; Park, S.; Im, J.; Nguyen, S. T.; Mirkin, C. A. DNA - Block

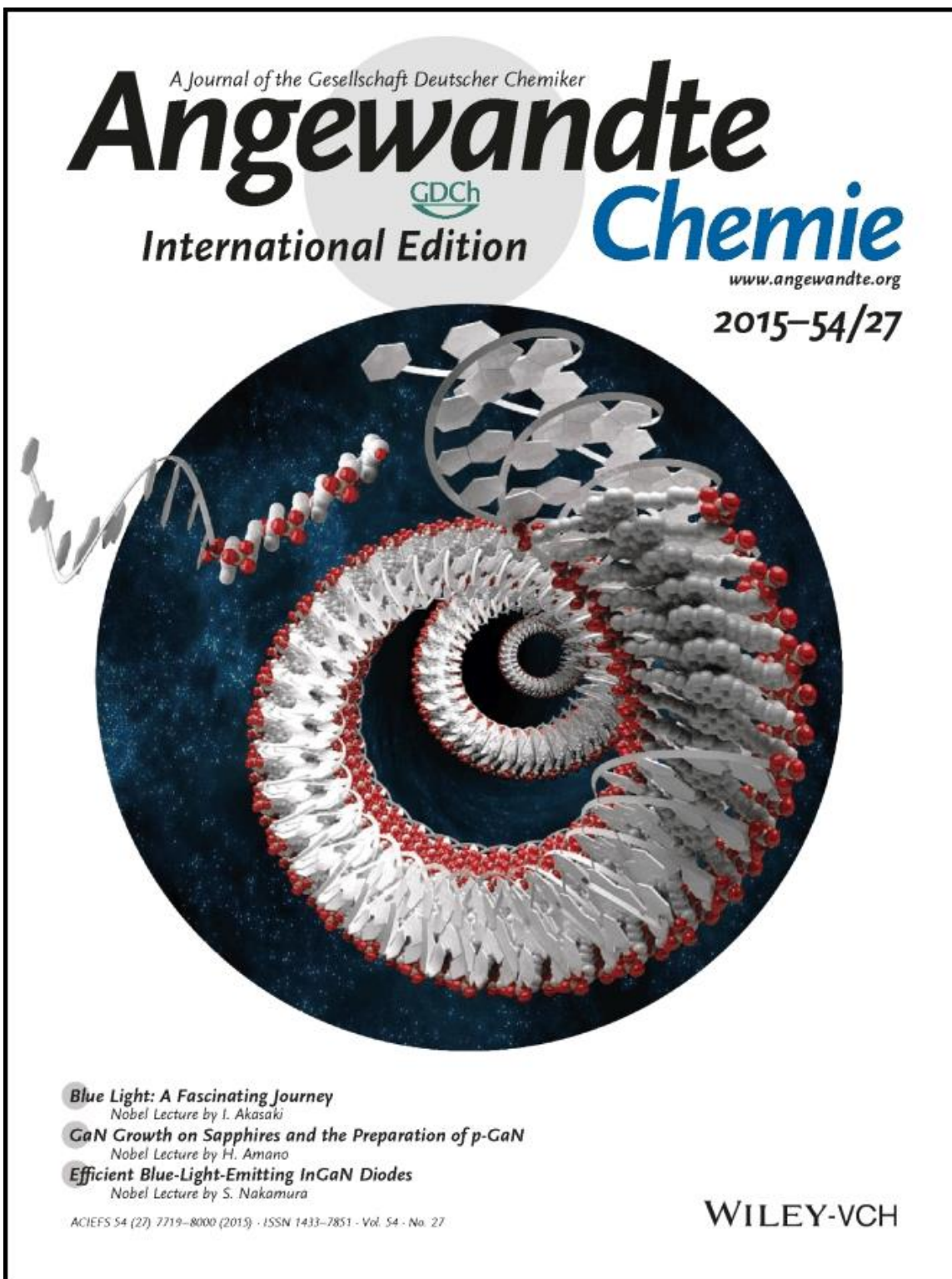
-
- Copolymer Conjugates. **2001**, 5592–5593.
- (211) Gibbs-Davis, J. M.; Schatz, G. C.; Nguyen, S. T. Sharp Melting Transitions in DNA Hybrids without Aggregate Dissolution: Proof of Neighboring-Duplex Cooperativity. *J. Am. Chem. Soc.* **2007**, *129*, 15535–15540.
- (212) Park, S. Y.; Gibbs-Davis, J. M.; Nguyen, S. T.; Schatz, G. C. Sharp Melting in DNA-Linked Nanostructure Systems: Thermodynamic Models of DNA-Linked Polymers. *J. Phys. Chem. B* **2007**, *111*, 8785–8791.
- (213) Lytton-Jean, A. K. R.; Gibbs-Davis, J. M.; Long, H.; Schatz, G. C.; Mirkin, C. A.; Nguyen, S. T. Highly Cooperative Behavior of Peptide Nucleic Acid-Linked DNA-Modified Gold-Nanoparticle and Comb-Polymer Aggregates. *Adv. Mater.* **2009**, *21*, 706–709.
- (214) Busseron, E.; Ruff, Y.; Moulin, E.; Giuseppone, N. Supramolecular Self-Assemblies as Functional Nanomaterials. *Nanoscale* **2013**, *5*, 7098–7140.
- (215) Yang, L.; Tan, X.; Wang, Z.; Zhang, X. Supramolecular Polymers : Historical Development , Preparation , Characterization , and Functions. *Chem. Rev.* **2015**, *115*, 7196–7239.
- (216) Zwaag, D. Van Der; Greef, T. F. A. De; Meijer, E. W. Programmable Supramolecular Polymerizations. *Angew. Chem., Int. Ed.* **2015**, *54*, 8334–8336.
- (217) Görl, D.; Zhang, X.; Stepanenko, V.; Würthner, F. Supramolecular Block Copolymers by Kinetically Controlled Co-Self-Assembly of Planar and Core-Twisted Perylene Bisimides. *Nat. Commun.* **2015**, *6*, 7009.
- (218) Vyborna, Y.; Vybornyi, M.; Rudnev, A. V.; Häner, R. DNA-Grafted Supramolecular Polymers: Helical Ribbon Structures Formed by Self-Assembly of Pyrene-DNA Chimeric Oligomers. *Angew. Chem., Int. Ed.* **2015**, *54*, 7934–7938.
- (219) Watson, K.; Park, S.; Im, J.; Nguyen, S. T.; Ca. DNA– Block Copolymer Conjugates. *J. Am. Chem. Soc.* **2001**, *123*, 5592–5593.
- (220) Micali, N.; Vybornyi, M.; Mineo, P.; Khorev, O.; Häner, R.; Villari, V.;

-
- Nanosheets, C. P.; Micali, N.; Vybornyi, M.; Mineo, P.; *et al.* Hydrodynamic and Thermophoretic Effects on the Supramolecular Chirality of Pyrene-Derived Nanosheets. *Chem. - A Eur. J.* **2015**, *21*, 9505–9513.
- (221) Gerling, T.; Wagenbauer, K. F.; Neuner, A. M.; Dietz, H. DNA Devices and Assemblies Formed by Shape-Complementary, Non-Base Pairing 3D Components. *Science* **2015**, *347*, 1446–1452.
- (222) Endo, M.; Sugita, T.; Katsuda, Y.; Hidaka, K.; Sugiyama, H. Programmed-Assembly System Using DNA Jigsaw Pieces. *Chem. - A Eur. J.* **2010**, *16*, 5362–5368.
- (223) Wang, R.; Kuzuya, A.; Liu, W.; Seeman, N. C. Blunt-Ended DNA Stacking Interactions in a 3-Helix Motif. *Chem. Commun. (Camb)*. **2010**, *46*, 4905–4907.
- (224) Nakata, M.; Zanchetta, G.; Chapman, B. D.; Jones, C. D.; Cross, J. O.; Pindak, R.; Bellini, T.; Clark, N. a. End-to-End Stacking and Liquid Crystal Condensation of 6 to 20 Base Pair DNA Duplexes. *Science* **2007**, *318*, 1276–1279.
- (225) SantaLucia, J.; Hicks, D. The Thermodynamics of DNA Structural Motifs. *Annu. Rev. Biophys. Biomol. Struct.* **2004**, *33*, 415–440.
- (226) Protozanova, E.; Yakovchuk, P.; Frank-Kamenetskii, M. D. Stacked-Unstacked Equilibrium at the Nick Site of DNA. *J. Mol. Biol.* **2004**, *342*, 775–785.
- (227) Pescitelli, G.; Di Bari, L.; Berova, N. Application of Electronic Circular Dichroism in the Study of Supramolecular Systems. *Chem. Soc. Rev.* **2014**, *43*, 5211–5233.
- (228) Ma, X.; Tian, H. Stimuli-Responsive Supramolecular Polymers in Aqueous Solution. *Acc. Chem. Res.* **2014**, *47*, 1971–1981.
- (229) Yashima, E.; Ousaka, N.; Taura, D.; Shimomura, K.; Ikai, T.; Maeda, K. Supramolecular Helical Systems: Helical Assemblies of Small Molecules, Foldamers, and Polymers with Chiral Amplification and Their Functions.

-
- Chem. Rev.* **2016**, *116*, 13752–13990.
- (230) Bakker, M. H.; Lee, C. C.; Meijer, E. W.; Dankers, P. Y. W.; Albertazzi, L. Multicomponent Supramolecular Polymers as a Modular Platform for Intracellular Delivery. *ACS Nano* **2016**, *10*, 1845–1852.
- (231) Engelen, W.; Janssen, B. M. G.; Merkx, M. DNA-Based Control of Protein Activity. *Chem. Commun.* **2016**, *52*, 3598–3610.
- (232) Pearce, T. R.; Kokkoli, E. DNA Nanotubes and Helical Nanotapes via Self-Assembly of ssDNA-Amphiphiles. *Soft Matter* **2014**, *11*, 109–117.
- (233) Albert, S. K.; Thelu, H. V. P.; Golla, M.; Krishnan, N.; Chaudhary, S.; Varghese, R. Self-Assembly of DNA-Oligo(P -Phenylene-Ethynylene) Hybrid Amphiphiles into Surface-Engineered Vesicles with Enhanced Emission. *Angew. Chem., Int. Ed.* **2014**, *53*, 8352–8357.
- (234) Lin, Y.; Pashuck, E. T.; Thomas, M. R.; Amdursky, N.; Wang, S.; Chow, L. W.; Stevens, M. M. Plasmonic Chirality Imprinting on Nucleobase-Displaying Supramolecular Nanohelices by Metal-Nucleobase Recognition. *Angew. Chem., Int. Ed.* **2017**, *56*, 2361–2365.
- (235) Noteborn, W. E. M.; Zwagerman, D. N. H.; Talens, V. S.; Maity, C.; van der Mee, L.; Poolman, J. M.; Mytnyk, S.; van Esch, J. H.; Kros, A.; Eelkema, R.; *et al.* Crosslinker-Induced Effects on the Gelation Pathway of a Low Molecular Weight Hydrogel. *Adv. Mater.* **2017**, *29*, 1603769.
- (236) Roh, Y. H.; Lee, J. B.; Kiatwuthinon, P.; Hartman, M. R.; Cha, J. J.; Um, S. H.; Muller, D. A.; Luo, D. DNAsomes: Multifunctional DNA-Based Nanocarriers. *Small* **2011**, *7*, 74–78.
- (237) Lu, C. H.; Willner, B.; Willner, I. DNA Nanotechnology: From Sensing and DNA Machines to Drug-Delivery Systems. *ACS Nano* **2013**, *7*, 8320–8332.
- (238) Li, J.; Mo, L.; Lu, C.; Fu, T.; Yang, H.; Tan, W. Functional Nucleic Acid-Based Hydrogels for Bioanalytical and Biomedical Applications. *Chem. Soc. Rev.* **2016**, *45*, 1410–1431.
- (239) Li, C.; Chen, P.; Shao, Y.; Zhou, X.; Wu, Y.; Yang, Z.; Li, Z.; Weil, T.; Liu,

-
- D. A Writable Polypeptide-DNA Hydrogel with Rationally Designed Multi-Modification Sites. *Small* **2015**, *11*, 1138–1143.
- (240) Wilks, T. R.; Bath, J.; de Vries, J. W.; Raymond, J. E.; Herrmann, A.; Turberfield, A. J.; O'Reilly, R. K. “Giant Surfactants” created by the Fast and Efficient Functionalization of a DNA Tetrahedron with a Temperature-Responsive Polymer. *ACS Nano* **2013**, *7*, 8561–8572.
- (241) Al Ouahabi, A.; Kotera, M.; Charles, L.; Lutz, J.-F. Synthesis of Monodisperse Sequence-Coded Polymers with Chain Lengths above DP100. *ACS Macro Lett.* **2015**, *4*, 1077–1080.
- (242) Al Ouahabi, A.; Charles, L.; Lutz, J.-F. Synthesis of Non-Natural Sequence-Encoded Polymers Using Phosphoramidite Chemistry. *J. Am. Chem. Soc.* **2015**, *137*, 5629–5635.
- (243) Adeyemi, O. O.; Malinovskii, V. L.; Biner, S. M.; Calzaferri, G.; Häner, R. Photon Harvesting by Excimer-Forming Multichromophores. *Chem. Commun.* **2012**, *48*, 9589.
- (244) Kim, Y.; Macfarlane, R. J.; Jones, M. R.; Mirkin, C. A. Transmutable Nanoparticles with Reconfigurable Surface Ligands. *Science* **2016**, *351*, 579–582.
- (245) Samanta, A.; Medintz, I. L. Nanoparticles and DNA - a Powerful and Growing Functional Combination in Bionanotechnology. *Nanoscale* **2016**, 9037–9095.
- (246) Randeria, P. S.; Jones, M. R.; Kohlstedt, K. L.; Banga, R. J.; Olvera De La Cruz, M.; Schatz, G. C.; Mirkin, C. A. What Controls the Hybridization Thermodynamics of Spherical Nucleic Acids? *J. Am. Chem. Soc.* **2015**, *137*, 3486–3489.
- (247) D. A. Handley, in *Colloidal Gold: Principles, Methods and Applications*, 1, Ed.: M. A. Hayat, Academic Press, San Diego 1989, pp. 13-22

APPENDICES



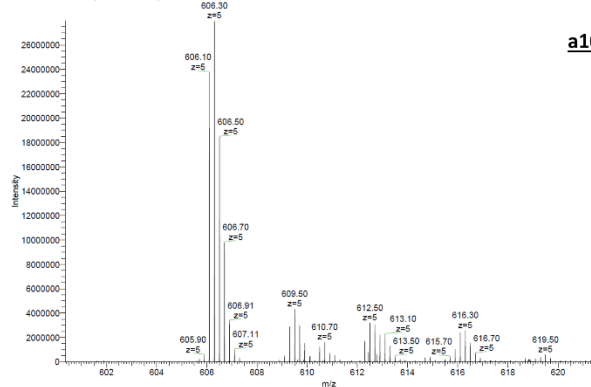
Appendix B. MS and HPLC characterization of the synthesized oligomers used in the current study.

Table 6-1. Molecular weight of the synthesized DNA block copolymers.

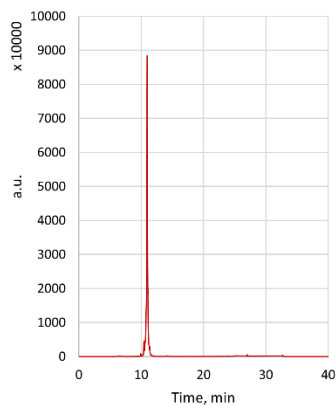
Name	Sequence	Mass theor.	Mass found
a10	CTC ACG GAA G - 3'	3035.6	3034.5
b10	CTT CCG TGA G - 3'	3017.5	3017.5
Py1a10	Py - CTC ACG GAA G - 3'	3463.7	3463.7
Py1b10	Py - CTT CCG TGA G - 3'	3445.7	3445.6
Py4a10	(Py) ₄ - CTC ACG GAA G - 3'	4749.0	4748.0
Py4b10	(Py) ₄ - CTT CCG TGA G - 3'	4728.8	4728.8
Py7a10	(Py) ₇ - CTC ACG GAA G - 3'	6032.4	6032.2
Py7b10	(Py) ₇ - CTT CCG TGA G - 3'	6014.4	6014.3
Py10b10	(Py) ₁₀ - CTT CCG TGA G - 3'	7298.8	7298.6
²⁷Py7b10	(2,7-Py) ₇ - CTT CCG TGA G - 3'	6014.4	6014.3
S-a10	(Thiol-Modifier C6 S-S) -CTC ACG GAA G - 3'	3365.5	3264.6
Py7c10	(Py) ₇ - CTT CCG TGG A - 3'	6014.9	6014.3
d10	TCC ACG GAA G - 3'	3035.6	3035.6

Name	Sequence	Mass theor.	Mass found
a30	(CTC ACG GAA G) ₃ - 3'	9230.6	9230.5
a20	(CTC ACG GAA G) ₂ - 3'	6133.08	6132.8
a8	C ACG GAA G - 3'	2442.5	2442.5
a9	TC ACG GAA G - 3'	2746.5	2746.4
8a	CTC ACG GA - 3'	2393.5	2393.3
9a	CTT CCG TGA - 3'	2706.5	2705.9
Py7b1G	(Py) ₇ - G - 3'	3263.1	3263.9
Py7b1T	(Py) ₇ - T - 3'	3238.1	3238.8
Py7b1A	(Py) ₇ - A - 3'	3247.1	3247.9
Py7b1C	(Py) ₇ - C - 3'	3223.1	3223.8
Py7b2CG	(Py) ₇ - CG - 3'	3552.3	3552.9
Py7b2AG	(Py) ₇ - AG - 3'	3576.3	3576.9
Py7b2TG	(Py) ₇ - TG - 3'	3567.3	3567.9
Py7b2GG	(Py) ₇ - GG - 3'	3592.3	3592.9
Py7b3	(Py) ₇ - CTG - 3'	3856.5	3856.9
Py7b4	(Py) ₇ - CTT G - 3'	4160.7	4161.0
Py7b5	(Py) ₇ - CTT CG - 3'	4449.9	4450.0
Py7b14	(Py) ₇ - CTT CCG TGA G - 3'	7259.7	7258.5
Py7b20	(Py) ₇ - (CTT CCG GAA G) ₂ - 3'	9095.8	9095.8

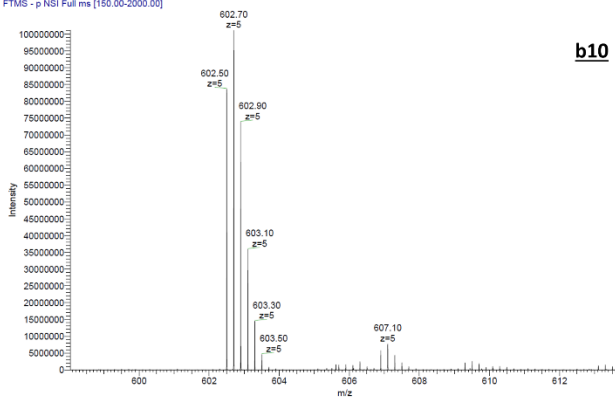
Vybarna 1050_141113081421 #2-8 RT: 0.1-0.3 AV: 5 NL: 2.80E7
T: FTMS - p NSI Full ms [150.00-2000.00]



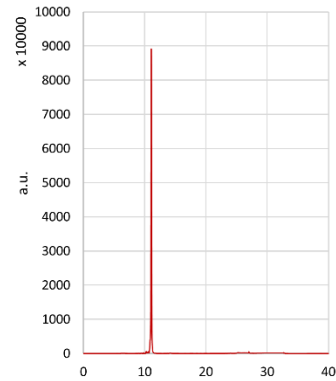
a10



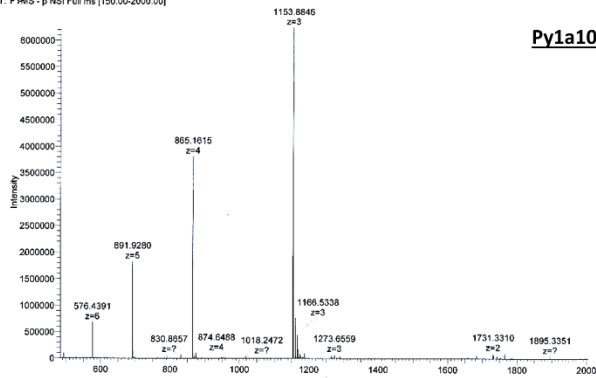
Vybarna 1030_150202080700 #5-13 RT: 0.2-0.4 AV: 9 NL: 1.01E8
T: FTMS - p NSI Full ms [150.00-2000.00]



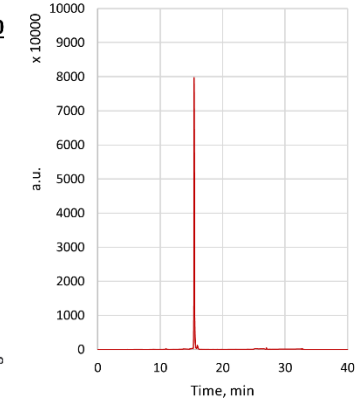
b10



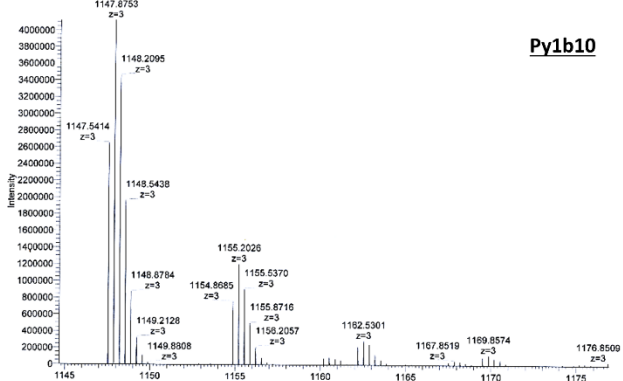
Vybarna 1030_150202080700 #5-13 RT: 0.2-0.4 AV: 9 NL: 1.01E8
T: FTMS - p NSI Full ms [150.00-2000.00]



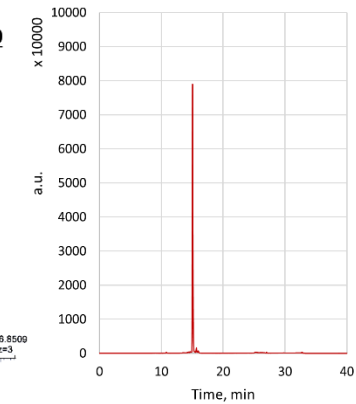
Py1a10

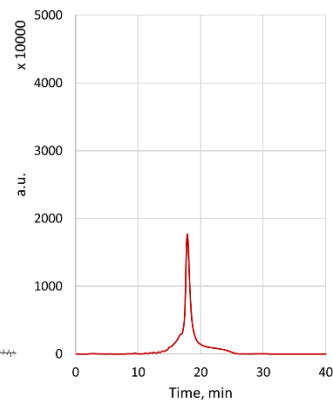
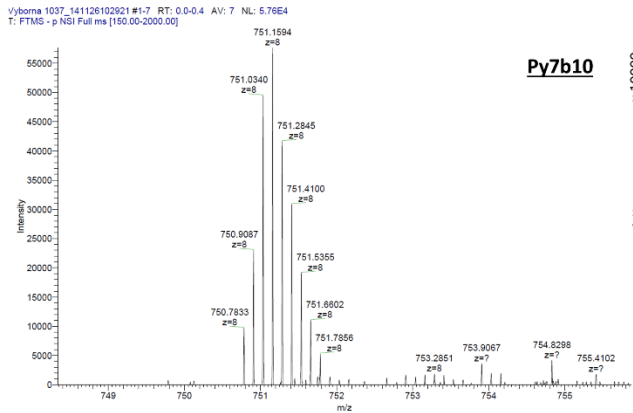
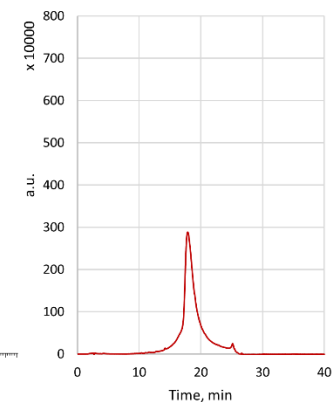
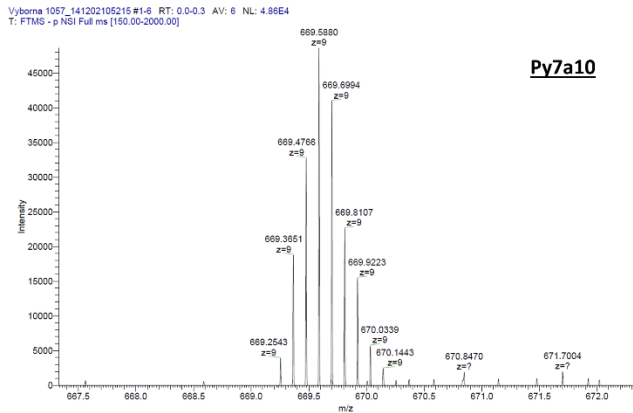
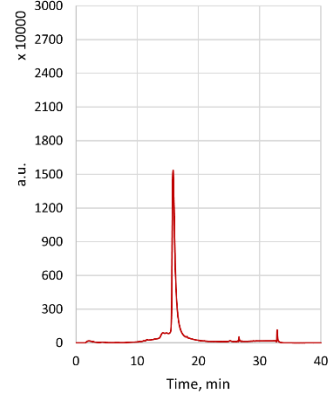
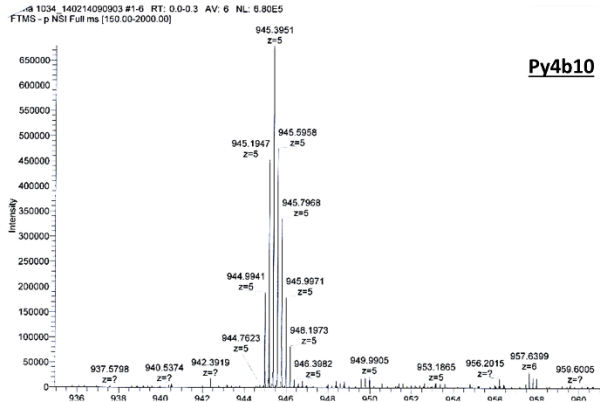
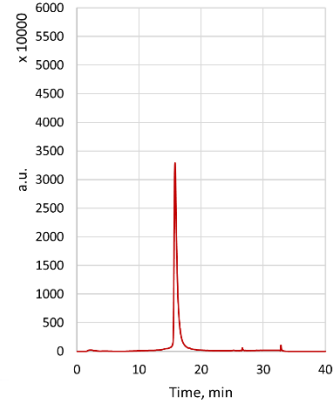
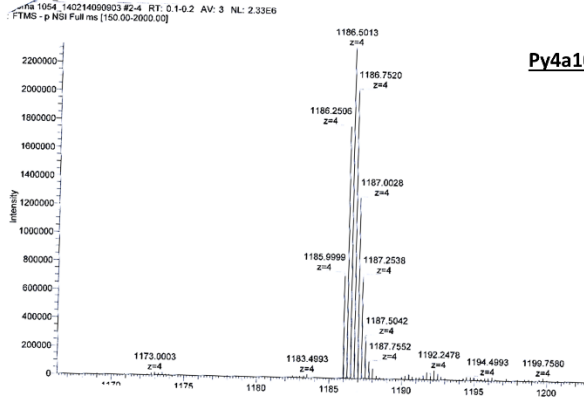


Vybarna 1030_150202080700 #5-13 RT: 0.2-0.4 AV: 9 NL: 1.01E8
T: FTMS - p NSI Full ms [150.00-2000.00]

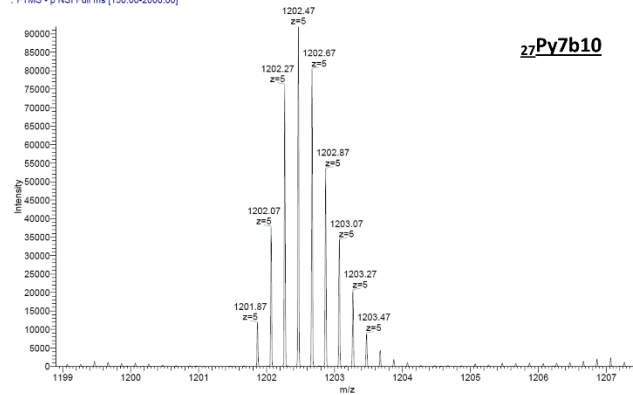


Py1b10

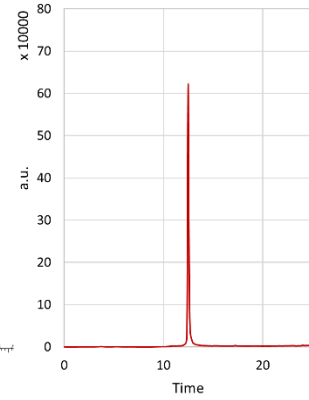




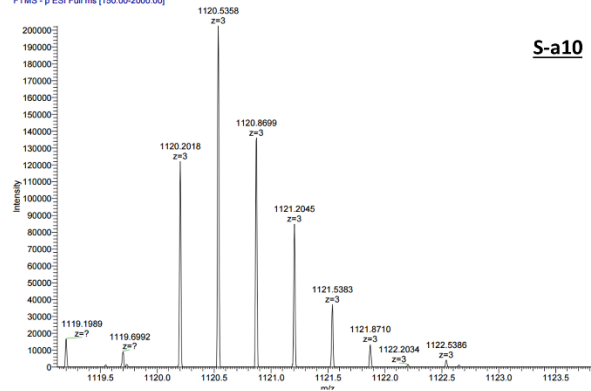
/yboma 1037_27_160314144457 #4-20 RT: 0.1-0.6 AV: 17 NL: 9.19E4
T: FTMS - p NSI Full ms [150.00-2000.00]



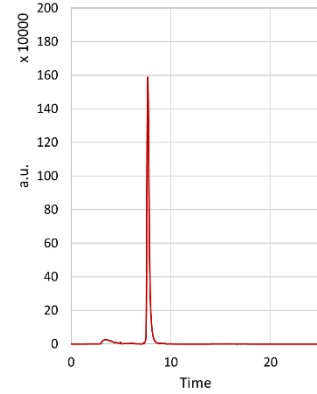
27Py7b10



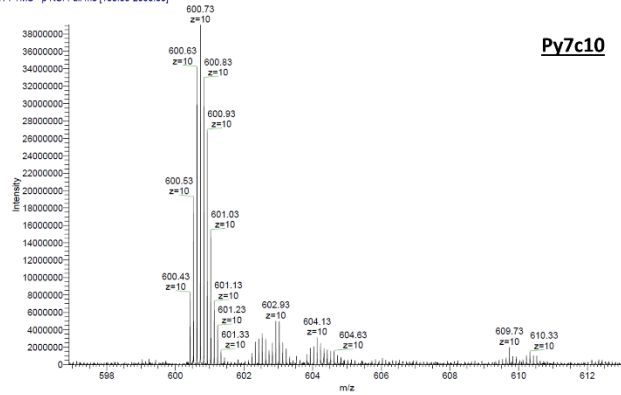
FTMS - p ESI Full ms [150.00-2000.00]



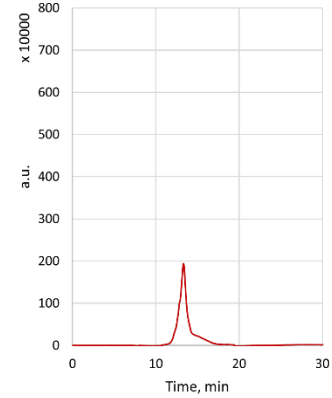
S-a10



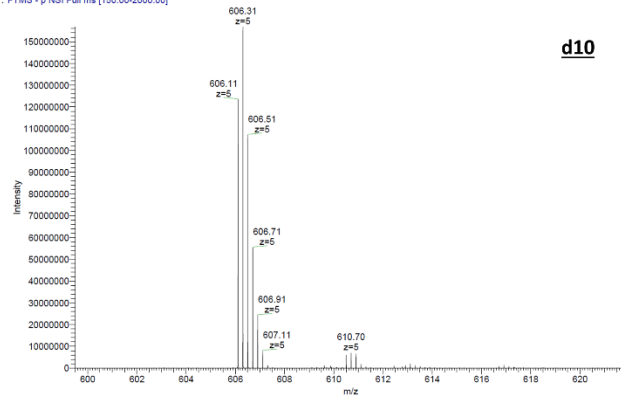
Yboma 1027_150510132559 #1-7 RT: 0.0-0.2 AV: 7 NL: 3.90E7
T: FTMS - p NSI Full ms [150.00-2000.00]



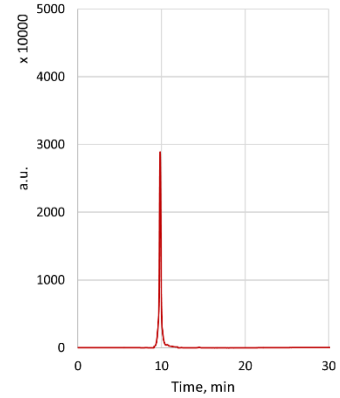
Py7c10



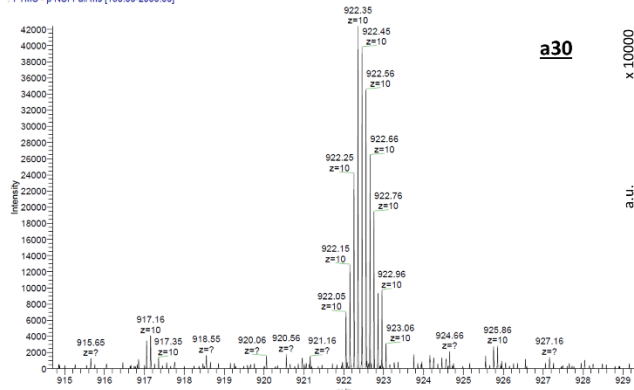
Yboma 1027_150510132559 #1-7 RT: 0.0-0.2 AV: 7 NL: 3.90E7
T: FTMS - p NSI Full ms [150.00-2000.00]



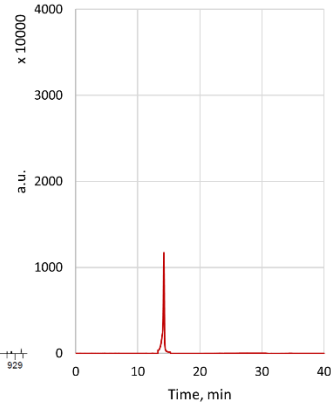
d10



yboma 3090_150202080700 #5-22 RT: 0.240.7 AV: 17 NL: 4.24E4
FTMS - p NSI Full ms [150.00-2000.00]

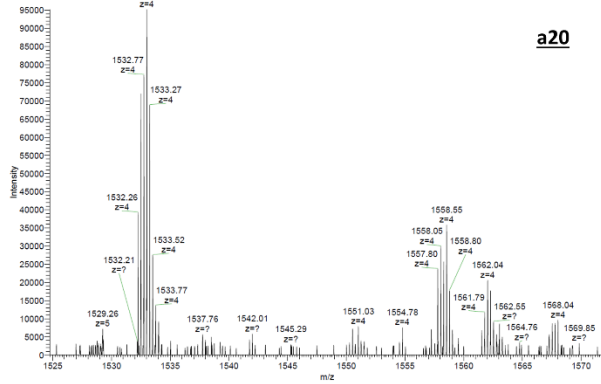


a30

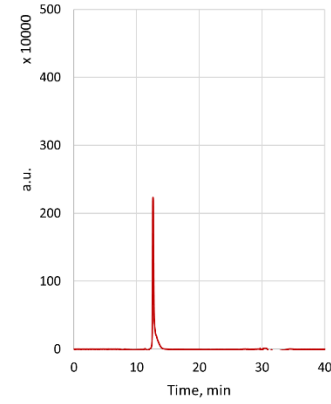


V: FTMS - p NSI Full ms [150.00-2000.00]

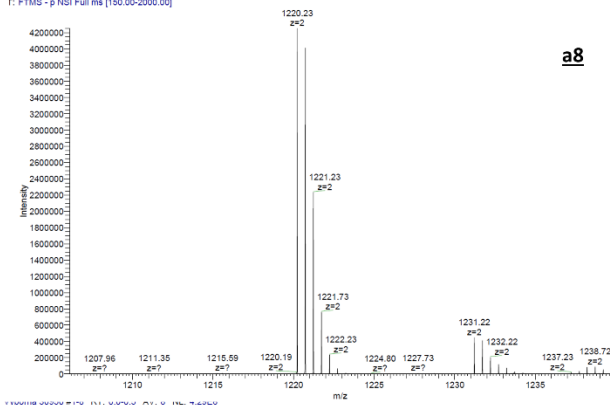
T: FTMS - p NSI Full ms [150.00-2000.00]



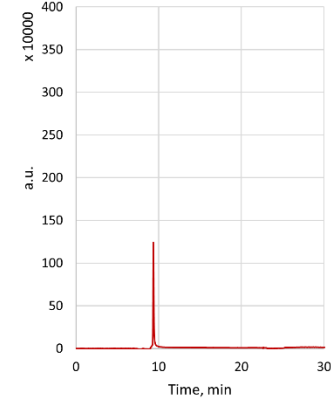
a20



yboma 30950 #1-8 RT: 0.0-0.5 AV: 8 NL: 4.20E5
FTMS - p NSI Full ms [150.00-2000.00]

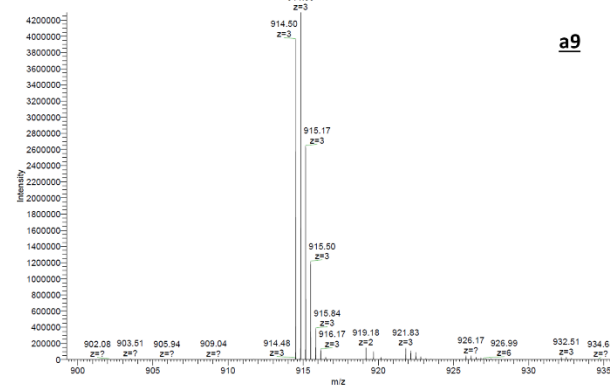


a8

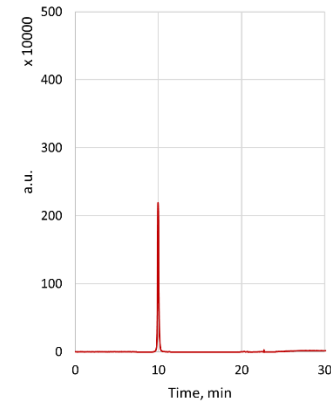


V: FTMS - p NSI Full ms [150.00-2000.00]

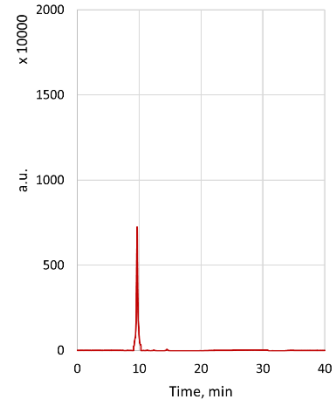
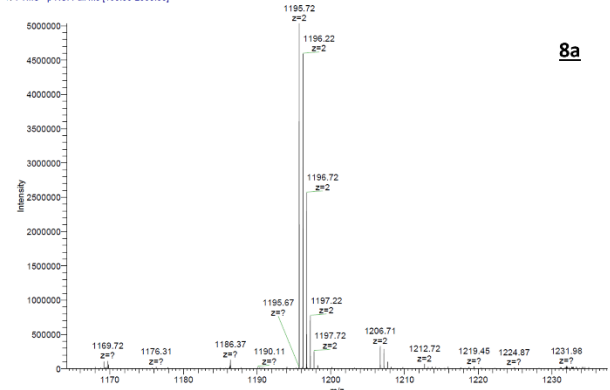
T: FTMS - p NSI Full ms [150.00-2000.00]



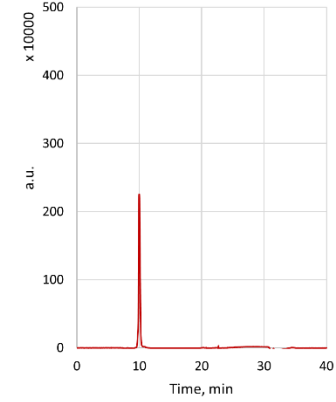
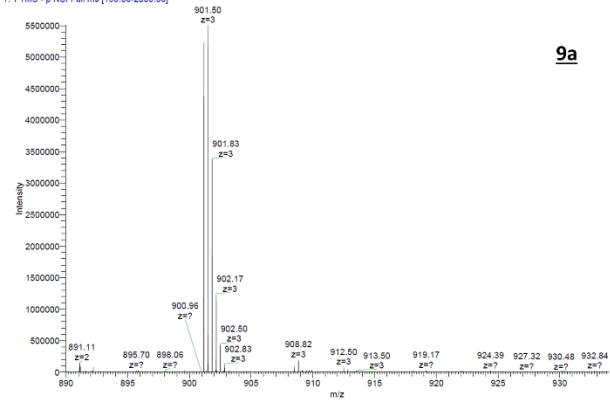
a9



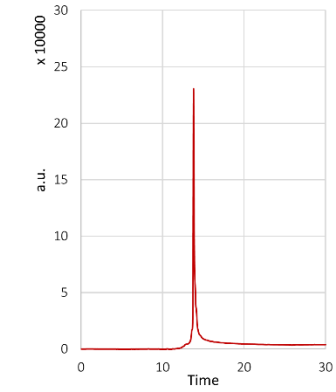
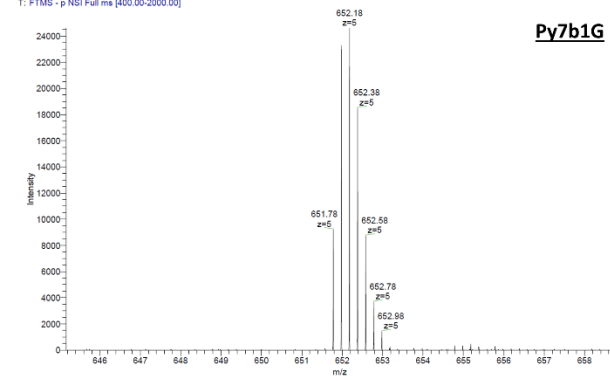
ypbma 00909 #4-0 K1: 0.340.0 AV: 0 NL: 5.0UE6
FTMS - p NSI Full ms [150.00-2000.00]



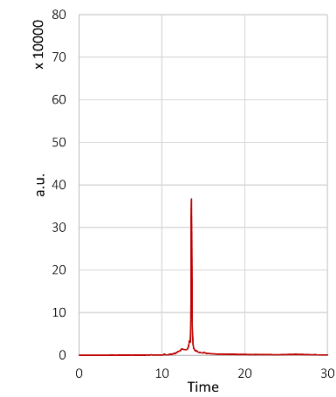
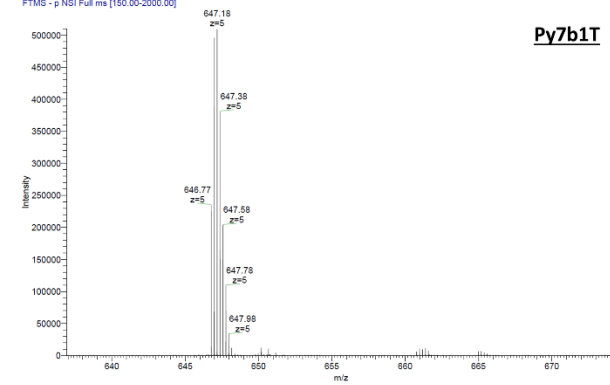
ypbma 00909 #4-0 K1: 0.340.0 AV: 0 NL: 5.0UE6
FTMS - p NSI Full ms [150.00-2000.00]

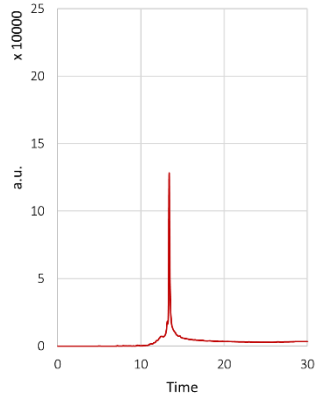
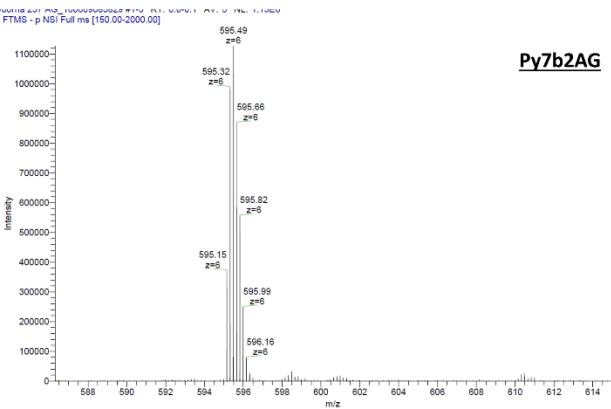
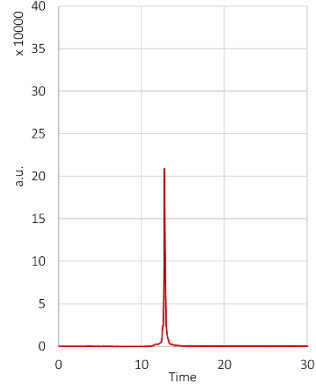
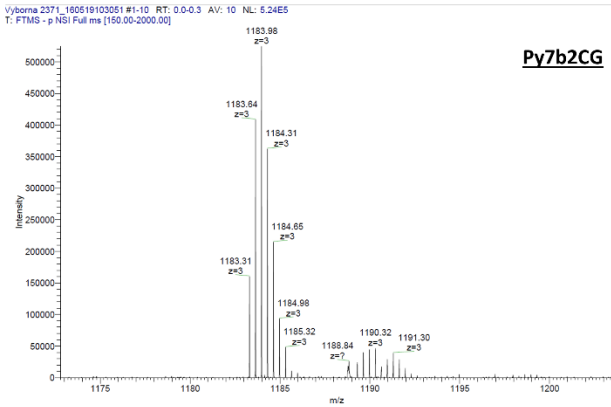
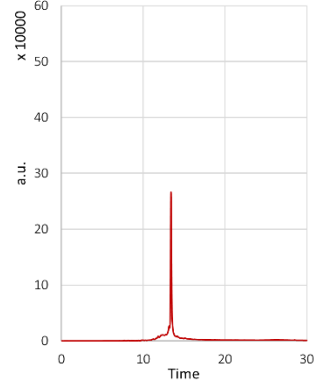
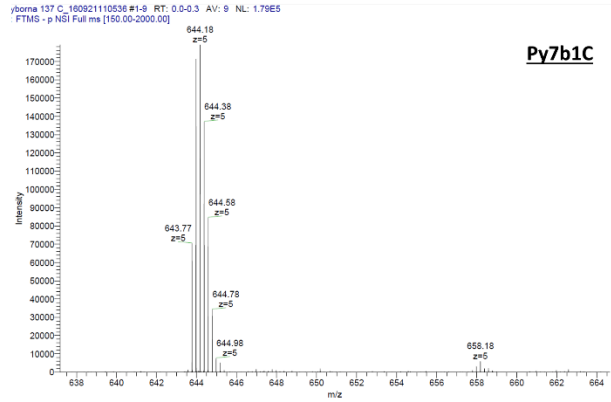
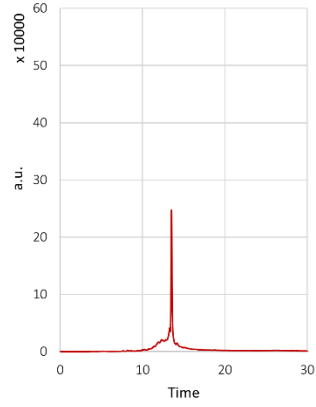
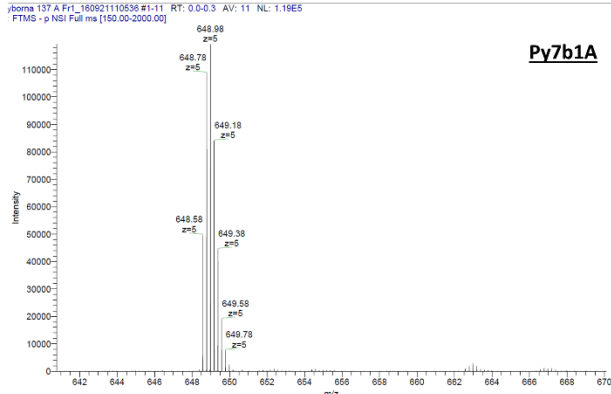


ypbma 137_160921110536 #1-8 RT: 0.0-0.3 AV: 0 NL: 5.10E5
FTMS - p NSI Full ms [400.00-2000.00]

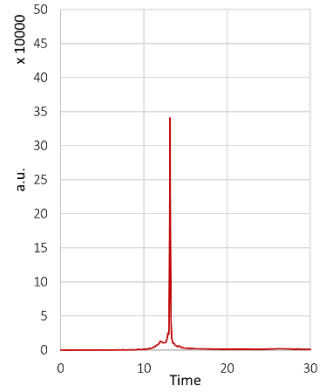
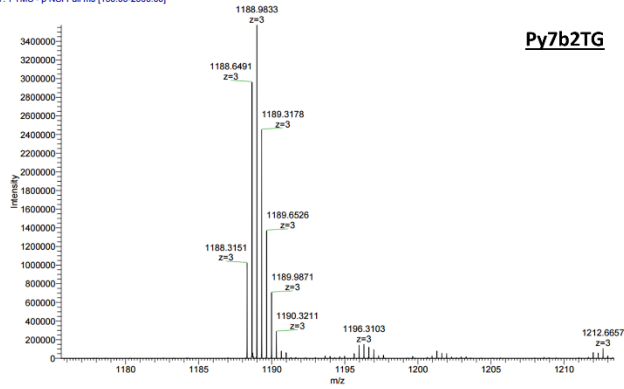


ypbma 137_160921110536 #1-8 RT: 0.0-0.3 AV: 0 NL: 5.10E5
FTMS - p NSI Full ms [150.00-2000.00]

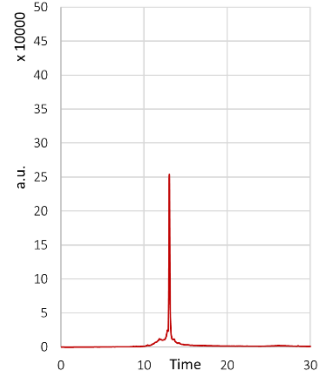
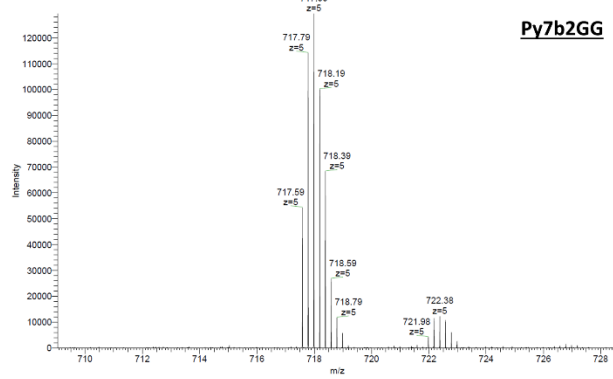




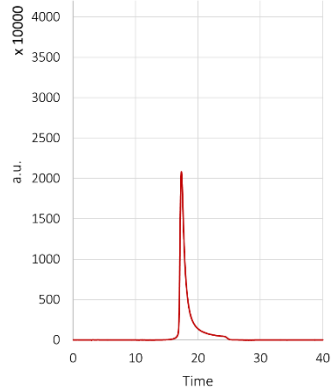
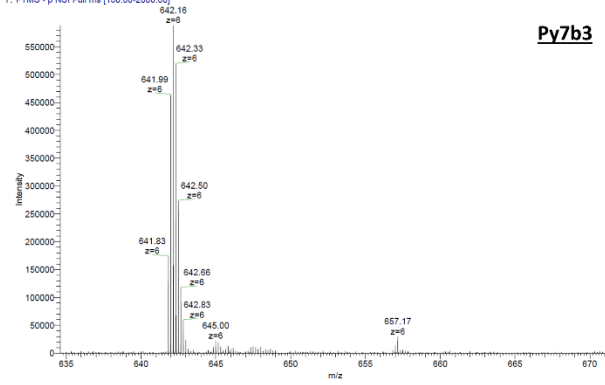
Vyborna 237 TG_160928142630 #1-3 RT: 0.0-0.1 AV: 3 NL: 3.57E6
 T: FTMS - p NSI Full ms [150.00-2000.00]



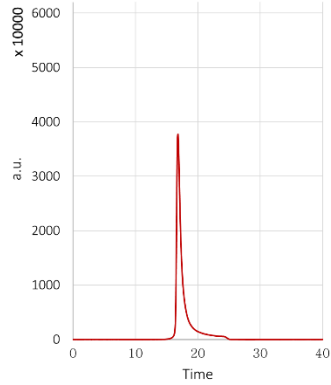
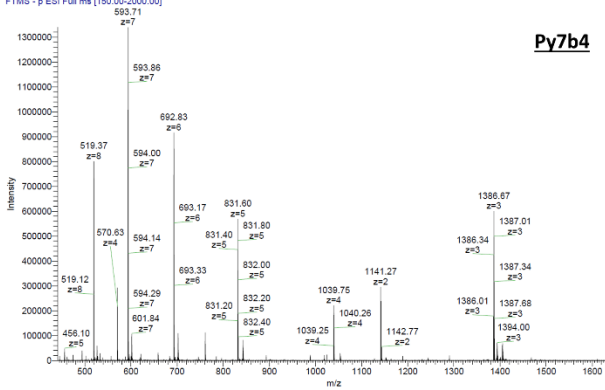
Vyborna 237 TG_160928142630 #1-3 RT: 0.0-0.1 AV: 3 NL: 3.57E6
 T: FTMS - p NSI Full ms [150.00-2000.00]



Vyborna 337_160928065629 #1-6 RT: 0.0-0.1 AV: 6 NL: 5.88E6
 T: FTMS - p NSI Full ms [150.00-2000.00]



Vyborna 437_160520080530 #5-19 RT: 0.2-0.5 AV: 12 NL: 1.34E6
 T: FTMS - p ESI Full ms [150.00-2000.00]



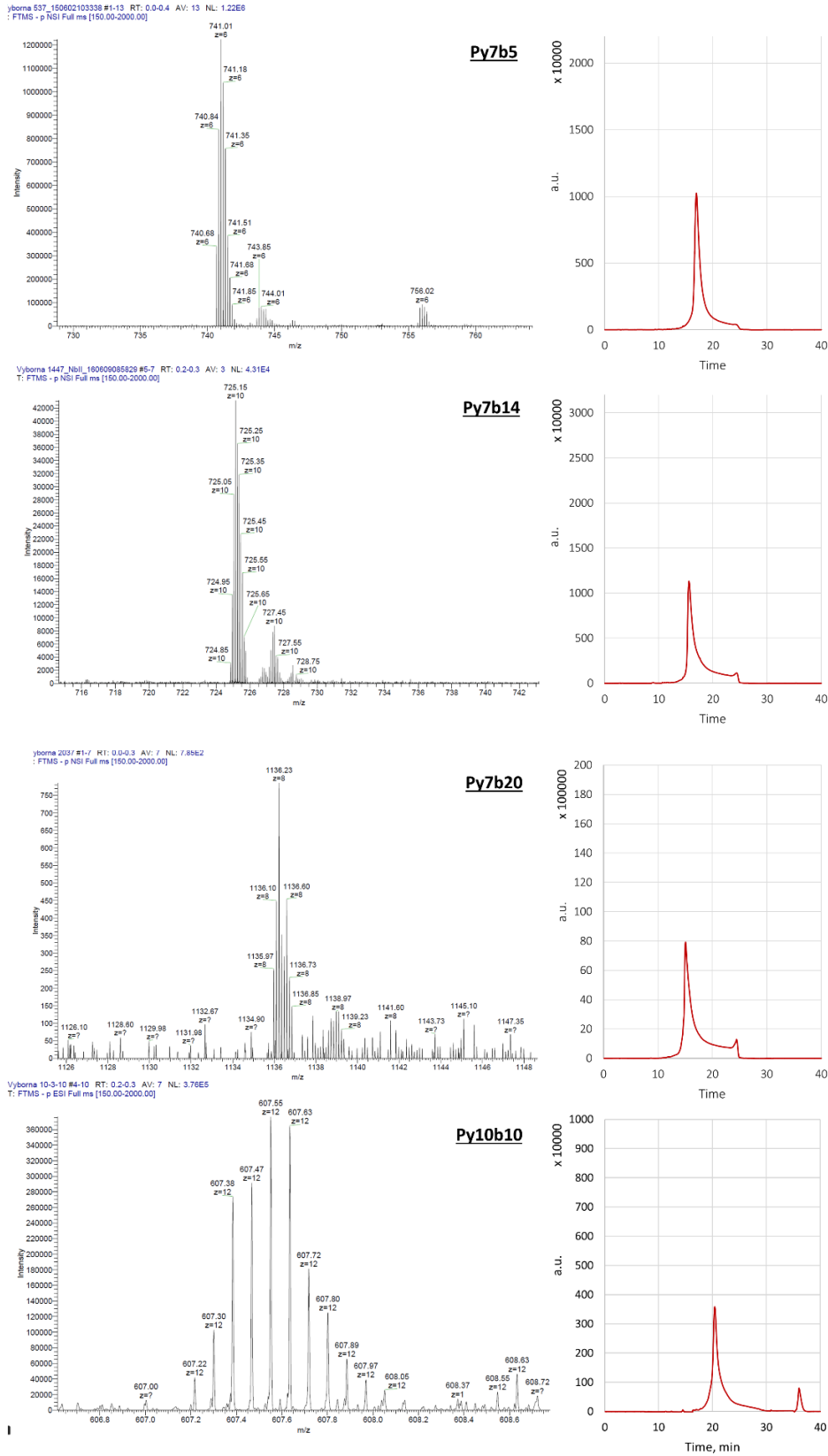


Figure 6-1. MS analysis and HPLC traces for the synthesized oligomers.

Declaration of consent

on the basis of Article 28 para. 2 of the RSL05 phil.-nat.

Name/First Name: Yuliia Vyborna
Matriculation Number: 13-135-496/320691
Study program: Chemistry and Molecular Science

Bachelor Master Dissertation

Title of the thesis:

Supervisor: Prof. Dr. Robert Häner

I declare herewith that this thesis is my own work and that I have not used any sources other than those stated. I have indicated the adoption of quotations as well as thoughts taken from other authors as such in the thesis. I am aware that the Senate pursuant to Article 36 para. 1 lit. r of the University Act of 5 September, 1996 is authorised to revoke the title awarded on the basis of this thesis. I allow herewith inspection in this thesis.

Place/Date

Signature

CURRICULUM VITAE

Vyborna Yuliia

Date of birth 21 December 1987
Address Freiestrasse 3, Bern CH-3012, Switzerland
Phone +41788961454
E-mail yuliia.vyborna@dcb.unibe.ch



EDUCATION

2014 – present *Ph.D. student*, the group of Prof. Robert Häner, Department of Chemistry and Biochemistry, University of Bern, Switzerland
2009 – 2011 *M.Sc. in Analytical Chemistry*, Faculty of Chemistry, Taras Shevchenko National University of Kyiv, Ukraine
2005 – 2009 *B. Sc. in General and Analytical Chemistry*, Faculty of Chemistry, Taras Shevchenko National University of Kyiv, Ukraine

HONORS AND AWARDS

2017 “Chemistry Travel Award” SCNAT, SCS, Switzerland
2016 CEMS Rising Star Award at CEMS International Symposium on Supramolecular Chemistry and Functional Materials, Tokyo, Japan
2015 Best oral talk at the First Year Graduate Student Symposium, Bern, Switzerland
2015 Travel Grant - Nachwuchsförderung, Switzerland
2014 Poster Prize at 7th International Meeting on Molecular Electronics, Strasbourg, France

PEER-REVIEWED PUBLICATIONS

- 1) **Y. Vyborna**, S. Altunbas, M. Vybornyi, R. Häner, *Morphological diversity of supramolecular polymers of DNA-containing oligopyrenes – Formation of chiroptically active nanosheets*, Chem. Commun. 2017, accepted.
- 2) M. Vybornyi, **Y. Vyborna**, R. Häner, *Silica mineralization of supramolecular polymers in aqueous environment*, ChemistryOpen, 2017, 6, 488.
- 3) **Y. Vyborna**, M. Vybornyi, R. Häner, *Functional DNA-grafted supramolecular polymers – chirality, cargo binding and hierarchical organization*, Chem. Commun. 2017, 53, 5179.
- 4) **Y. Vyborna**, M. Vybornyi, R. Häner, *Pathway Diversity in the Self-Assembly of DNA-Derived Bioconjugates*, Bioconjugate Chem. 2016, 27, 2755.
- 5) **Y. Vyborna**, M. Vybornyi, R. Häner, *From Ribbons to Networks: Hierarchical Organization of DNA-Grafted Supramolecular Polymers*, J. Am. Chem. Soc. 2015, 137, 14051 (This paper was featured in JACS Spotlights).
- 6) **Y. Vyborna**, M. Vybornyi, A. Rudnev, R. Häner, *DNA-Grafted Supramolecular Polymers – Helical Ribbon Structures Formed by Self-Assembly of Pyrene-DNA Chimeric Oligomers* Angew. Chem. Int. Ed. 2015, 54, 7934-7938 (This paper was highlighted as Cover image).

